
Oxidation State Ambiguities in Cerium Organometallics- A Computational Approach

Rosemary Coates

UCL

PhD in Chemistry

I, Rosemary Coates, confirm that the work presented in this thesis is my own. Where information has been derived for other sources, I confirm that this has been indicated in the thesis.

A handwritten signature in black ink, appearing to read 'Coates', with a long horizontal flourish underneath.

Abstract

Seven cerium organometallic systems are studied using both density functional theory and multiconfigurational techniques in order to better understand the oxidation state of the metal in each of these systems. These calculations show that in formally Ce(IV) organometallic systems with electron-rich, carbon-based ligands the total number of Ce 4f electrons is closer to the formal value of a Ce(III) system, rather than that of a Ce(IV) system. However, there remains a clear distinction between the Ce(III) and Ce(IV) f electron density: a localised f electron being found for Ce(III) system a delocalised f density is identified for the formally Ce(IV) systems.

The calculations carried out have been used to rationalise the apparently contradictory experimental data on the oxidation state of Ce in cerocene, to analyse the claims that cerocene might represent a molecular Kondo system, to rationalise the variable energy photoelectron spectrum of CeCp₃ and to speculate about the possibility of synthesising CeCp₂X compounds.

Contents

Abstract	- 3 -
Contents	- 4 -
Acknowledgements	- 9 -
1. Introduction	- 10 -
1.1. Chemical Introduction.....	- 10 -
1.1.1 General considerations for the lanthanide series.....	- 10 -
1.1.1.1 Relativity	- 10 -
1.1.1.2 Chemical accessibility of the valence electrons.....	- 12 -
1.1.2 Chemical Context.....	- 14 -
1.1.2.1 Conceptual considerations	- 14 -
1.1.2.2 Cerocene.....	- 16 -
1.1.2.3 Cerium tris-cyclopentadiene	- 18 -
1.1.2.4 Cerium bis-cyclopentadiene oxo, imido and methylene	- 19 -
1.2 Computational Introduction	- 19 -
1.2.1 The Schrödinger equation	- 20 -
1.2.1.1 Simplifying the solving of the Schrödinger equation	- 20 -
1.2.1.1.1 The Variation Principle	- 20 -
1.2.1.1.2 The Born-Oppenheimer approximation	- 21 -
1.2.1.1.3 The Orbital Approximation and the Slater Determinant.....	- 22 -
1.2.1.2 Hartree Fock Method	- 22 -
1.2.1.3 SCF.....	- 23 -
1.2.1.3.1 LCAO	- 24 -
1.2.1.4 Correlation.....	- 25 -
1.2.1.5 Post Hartree-Fock Methods.....	- 28 -
1.2.1.5.1 MP2	- 29 -
1.2.1.5.2 CASSCF.....	- 32 -
1.2.1.5.3 CASPT2	- 34 -
1.2.1.5.4 Other Methods.....	- 35 -
1.2.1.5.4.1 CISD.....	- 35 -
1.2.1.5.4.2 Coupled Cluster (CC).....	- 35 -
1.2.2 Density Functional Theory.....	- 36 -
1.2.2.1 The Density Approach	- 36 -

1.2.2.2 Types of functional	- 39 -
1.2.2.2.1 Local spin density approximation (LSDA).....	- 39 -
1.2.2.2.2 Generalised gradient approximation (GGA).....	- 39 -
1.2.2.2.3 Hybrid	- 40 -
1.2.2.3 Time-Dependent Density Functional Theory.....	- 40 -
1.2.3 Geometry Optimisations	- 41 -
1.2.3.1 Methods for optimisation	- 41 -
1.2.3.2 Transition states and imaginary frequencies	- 41 -
1.2.3.3 The effect of symmetry to geometry optimisations.....	- 42 -
1.2.4 Basis Sets	- 42 -
1.2.4.1 STOs.....	- 43 -
1.2.4.2 GTOs	- 43 -
1.2.4.3 Use of basis sets in calculation	- 44 -
1.2.4.3.1 Pople Style Basis Sets	- 46 -
1.2.4.3.2 ANO Basis Sets.....	- 46 -
1.2.4.3.3 Correlation Consistent Basis Sets	- 47 -
1.2.4.3.4 Pseudopotentials.....	- 47 -
1.2.5 Relativity	- 48 -
1.2.5.1 Scalar Effects	- 49 -
1.2.5.1.1 ZORA.....	- 49 -
1.2.5.1.2 DKH	- 50 -
1.2.5.1.3 RECPs	- 51 -
1.2.5.2 Spin-Orbit Coupling.....	- 51 -
1.2.6 Symmetry Considerations	- 52 -
1.2.7 Level of theory	- 53 -
1.2.8 Some notes on convergence	- 53 -
1.2.9 Software packages used	- 54 -
1.2.9.1 Gaussian	- 54 -
1.2.9.2 Amsterdam Density Functional (ADF).....	- 54 -
1.2.9.3 Molcas	- 55 -
2. Cerocene.....	- 56 -
2.1 Previous studies.....	- 56 -
2.1.1 Experimental Approach	- 56 -
2.1.1.1 Photoelectron spectroscopy.....	- 56 -

2.1.1.2 X-Ray Absorption Near Edge Structure (XANES)	- 57 -
2.1.1.3 Cyclic Voltametry	- 57 -
2.1.1.4 Magnetic Measurements	- 58 -
2.1.2 Previous Calculations.....	- 60 -
2.2 Aims	- 60 -
2.2.1 Broader context of calculations.....	- 61 -
2.3 Computational and Experimental details	- 61 -
2.3.1 Experimental Details- XANES	- 61 -
2.3.2 Computational Details.....	- 62 -
2.3.2.1 Symmetry considerations and active spaces	- 63 -
2.3.2.2 Note	- 66 -
2.4 Results	- 67 -
2.4.1 XANES results	- 67 -
2.4.2 Full geometry optimisations using Gaussian03	- 68 -
2.4.3 Partial geometry optimisations using Molcas	- 69 -
2.4.3.1 Orbital Analysis	- 70 -
2.4.3.2 Calculation of n_f values using MOLCAS.....	- 73 -
2.4.3.2.1 RHF Results	- 73 -
2.4.3.2.2 B3LYP Results.....	- 73 -
2.4.3.2.3 CASSCF (8,14) Results	- 74 -
2.4.3.3 Energies of excited states	- 75 -
2.4.3.3.1 Spin-orbit coupling free (SOF) energies	- 75 -
2.4.3.3.2 Spin-orbit coupled (SOC) energies	- 77 -
2.4.3.3.3 Comparison with experimental data	- 78 -
2.4.3.4 Density difference plots	- 78 -
2.5 Discussion	- 80 -
2.5.1 Comparison of results with other theoretical work.....	- 80 -
2.5.2 XANES	- 83 -
2.5.3 UV-Vis	- 84 -
2.5.4 Magnetic measurements.....	- 84 -
2.5.5 Chemical implications.....	- 86 -
2.5.6 Theoretical implications.....	- 87 -
2.5.7 Further work.....	- 87 -
2.6 Conclusions	- 88 -

3. Cerium tris-cyclopentadiene	- 90 -
3.1 Experimental Approach	- 90 -
3.1.1 Photoelectron spectroscopy.....	- 90 -
3.1.1.1 Delayed Maxima and Giant Resonances.....	- 91 -
3.1.1.2 Experimental Results	- 92 -
3.2 Computational Approach	- 94 -
3.2.1 Computational Details.....	- 94 -
3.2.2 Results	- 97 -
3.2.2.1 Natural Orbital Analysis	- 98 -
3.2.2.1.1 Rationale for Natural Orbital Analysis	- 98 -
3.2.2.1.2 Performing the analysis.....	- 100 -
3.2.2.1.2.1 Symmetry Considerations	- 100 -
3.2.2.1.2.2 Visualising the Orbitals.....	- 101 -
3.2.2.1.2.3 Comparison with Experiment	- 105 -
3.2.2.1.2.4 Oxidation State.....	- 107 -
3.2.2.2 Summary of CASPT2 results for CeCp ₃ and CeCp ₃ ⁺	- 108 -
3.2.2.3 TD-DFT approach.....	- 109 -
3.2.3 Anion calculations.....	110
3.2.3.1 Ground state analysis	111
3.2.3.1.1 LaCp ₃ ⁻	111
3.2.3.1.2 CeCp ₃ ⁻	112
3.2.4 Conclusions	113
4. Bis-cyclopentadienyl complexes.....	114
4.1 Previous work	114
4.2 Computational details	115
4.2.1 Geometry Optimisation.....	115
4.2.2 Electronic Structure.....	116
4.3 Results	116
4.3.1 Geometry Optimisations	116
4.3.2 Natural Orbital Analysis	121
4.3.2.1 CeCp ₂ O	121
4.3.2.2 CeCp ₂ NH	123
4.3.2.3 CeCp ₂ CH ₂	125
4.3.2.3.1 Perpendicular Methylene Results.....	126

4.3.2.3.2 Parallel Methylene Results.....	128
4.3.2.3.3 Twisted Methylene Results.....	131
4.3.2.3.4 Summary.....	134
4.3.2.4 HfCp ₂ O.....	134
4.3.2.5 HfCp ₂ CH ₂	136
4.3.2.6 ThCp ₂ O.....	137
4.3.2.7 ThCp ₂ CH ₂	139
4.4 Conclusions.....	140
5. General Conclusions.....	142
6. Bibliography.....	144

Acknowledgements

This project was funded by a UCL Teaching Assistantship in Inorganic and Physical Chemistry for which I am grateful to UCL. I would also like to thank the Department of Chemistry for awarding me this position and for its continued interest in my professional development.

The last four years have been enhanced both scientifically and personally by all the occupants, past and present, of delightful room G19 as well as Drs Jelfs, Knapp, Nunn and Potts.

Most importantly I am enormously indebted to Prof. Nikolas Kaltsoyannis, Dr Andrew Kerridge and Dr Andrea Sella for their wisdom, knowledge and enthusiasm.

1. Introduction

1.1. Chemical Introduction

1.1.1 General considerations for the lanthanide series

The lanthanide elements, lanthanoids or rare earths (Ln) may be considered to comprise the series from lanthanum to lutetium, or this group plus scandium and yttrium, but can generally be assumed to be the 4f block, i.e. cerium to lutetium. It is appropriate that there is a preponderance of lanthanide names originating from Sweden as this nation has perhaps contributed the most to the discoveries of these elements, with major contributions from A.F. Cronstedt, J.J. Berzelius and C.G. Mosander. Despite these elements having been identified from 1839 (Ce) to 1907 (Lu) and being easily isolable from monazite and bastnaesite, with abundances ranging from 5 times greater than lead (Pb) to close to that of iodine (I)ⁱ, they have not been the subjects of the variety and number of studies as either their transition metal or actinide cousins¹.

There are certain characteristics demonstrated by the lanthanide elements which are imperative to consider when undertaking a computational study of the properties of their compounds. The first is that with such heavy elements the effects of relativity are non-negligible. The second is that in the cations the valence electrons exclusively populate the 4f orbitals. Let us consider each of these characteristics in turn.

1.1.1.1 Relativity

For the heavy elements in the periodic table it is important to consider the effects of relativity, both direct and indirect. As the value of Z (the nuclear charge) increases the velocity of the 1s electrons also increases. The velocity of the 1s electrons is approximately equal to Z when the velocity of light is expressed in atomic units

($137 \alpha^{-1}$). Atomic units in this case is defined by the classical speed of the 1s electrons being equivalent to Z in a one nucleus, one electron system. For the heavy elements the velocity of the 1s electrons becomes a significant fraction of the velocity of light and the mass of these electrons correspondingly increases according to the following expression, eq. 1.1:

$$m = \frac{m_0}{\sqrt{1 - \left(\frac{v}{c}\right)^2}}$$

Equation 1.1- Relativistic mass increase

where m is the mass of the electron, m_0 is the rest mass of the electron, v is the velocity of the electron and c is the velocity of light. This mass increase subsequently leads to a reduction in the Bohr radius. Thus, the direct effect of relativity is to contract and stabilise the s orbitals for $n \geq 2$ (where n is the principle quantum number) in order to ensure that the s orbitals retain orthogonality with the contracted 1s orbital. The p electrons experience a similar phenomenon, but to a lesser degree. This contraction and stabilisation leads to expansion and destabilisation of the d and f-orbitals, known as the indirect relativistic effect, occurring as the stabilised s and p orbitals screen the d and f orbitals more completely from the nucleus.

The 4f orbitals do not have a radial node and penetrate the core to a greater extent than the 5f orbitals, making the former more contracted. This is exacerbated by the indirect effect of relativity which, due to the greater core penetration of the 4f orbitals, is much less pronounced. In fact, the 4f orbitals of the lanthanides are generally considered to be core-like.

Spin orbit coupling also becomes an increasingly important effect with increasing Z . This is the effect by which the orbital angular momentum (l) and the spin angular momentum (s) of an electron couple to give the total angular momentum (j) and occurs in all cases for all bound electrons with $l \geq 1$. The increase in spin-orbit coupling with increasing Z occurs due to the dependence of the mass of the electron on Z , shown in equation 1 to vary with Z due to relativity. This means that spin-orbit coupling may be

ⁱ The epithet 'rare earths' is a significant misnomer.

significant for lanthanide compounds and consideration of this effect must be taken for a thorough electronic structure investigation. Spin-orbit coupling, whilst proportional to Z^4 , is also inversely proportional to l^2 and may not play such an important role for the valence electrons ($f, l = 3$) as might be expected given the effect on the valence for e.g. iodine. The effect of spin-orbit coupling is to increase the number of non-degenerate electronic states of a system, each state having the same values for angular momentum of the state (L) and total spin of the state (S) but different total angular momentum for the state (J), where $J = L+S, L+S-1, \dots, L-S$, according to the Russell-Saunders scheme. Thus the $L=3$ state for a Ce(III) system is split into two levels: $L\pm S$, i.e. $J = 5/2$ and $J = 7/2$.

1.1.1.2 Chemical accessibility of the valence electrons

As described above, the 4f orbitals of the lanthanides are generally considered to be core-like and are therefore typically assumed not to be involved in covalent bonding. The core-like nature of the f-electrons also results in a smaller range of oxidation states for the lanthanides than are observed for the actinides, with their more radially extended, diffuse and thus accessible 5f orbitals.

Most of the lanthanides are generally found in the 3+ oxidation state with electronic configuration $[\text{Xe}]4f^{n-1}$, where n is the place of the lanthanide in the series. This is due to the fact that the fourth ionisation energy is extremely high (greater than the sum of the first three ionisation energies). This arises as a result of the fact that the first three ionisations correspond to removal of 5d and 6s electrons. Once these electrons have been removed the remaining electrons occupy the 4f orbitals. This occurs because the 4f orbitals are stabilised by the nuclear charge to a greater extent than the 5d and 6s due to greater core penetration by the 4f orbitals, which have no radial nodes, whilst the 5d have 2 radial nodes and the 6s 5. The 4f orbitals are in fact so stabilised that the electrons occupying them are generally considered to be chemically inaccessible¹. These properties mean that lanthanide compounds are expected to be largely ionic with very little covalent character. The largely ionic character of lanthanide compounds serves to explain their characteristic pale colours, as there is little relaxation of the

selection rules governing forbidden $f \rightarrow f$ transitions via vibronic coupling (which acts considerably in many transition metal and, to a lesser extent, actinide, compounds).

Whilst the fourth ionisation energy of all the lanthanides is larger than the sum of the first three ionisation energies, for cerium this difference is just 24 kJmol^{-1} (this compares with an average difference for the series of 209 kJmol^{-1}) and the barrier to ionisation is not insurmountable. Cerium can therefore form compounds in the 4+ oxidation state. The behaviour of cerium differs from that of the rest of the lanthanide series because the 4f orbitals are less stabilised at the start of the series and thus all four valence electrons ($6s^2 5d^1 4f^1$) can be ionised yielding the electronic configuration $[\text{Xe}]4f^0$.

The low 3+/4+ oxidation potential of Ce (1.61 V)³ and thus its ability to exhibit both the 3+ and 4+ oxidation states lead to some important consequences. Compounds containing Ce(IV) are often good oxidising agents. This means that Ce(IV) chemistry is industrially important, for example ceria (CeO_2) is used as an oxidation catalyst in car exhausts as well as being used as a pigment⁴. Ceric ammonium nitrate $[(\text{NH}_4)_2\text{Ce}(\text{NO}_3)_6]$ is a widely used stoichiometric oxidant in organic chemistry. It is part of the aim of this work to establish the oxidation state in some cerium compounds in which it is disputed.

1.1.2 Chemical Context

1.1.2.1 Conceptual considerations

This section may seem a little esoteric, or indeed philosophical. However, it is included in order to clarify some ontological features both of the subject being investigated and the mode of investigation.

Oxidation state in the context of cerium organometallics is an unresolved and important question. An understanding of oxidation state is important in order to develop applications of molecular cerium systems, as well as for a more fundamental understanding of the bonding of lanthanides. It is commonly quoted and rarely questioned that lanthanide bonding is almost exclusively ionic, in fact the f-electrons are considered by some researchers to be of such little consequence that they can be modelled as part of the core electrons, using a pseudopotential.ⁱⁱ However, if this rule of thumb were to be broken, the most likely candidate for such disobedience would be cerium. This is because the f-electron of cerium experiences a reduced effective nuclear potential relative to the later members of the series, which suffer from the poor self-screening of the f-electrons and are thus pulled closer to nucleus, ever more core-like.

One might suggest that a well-known heuristic is best mentioned in passing and then accepted. However, not only is this not in the spirit of the scientific method (any good Aristotelian knows the well-known heuristic that heavy things fall faster than light things) but it also rules out the possibilities of some interesting chemistry and may lead to serious misunderstandings. In terms of interesting chemistry, if we hold that the bonding in the cerium organometallics is purely ionic we discount the possibility of low lying electronic states with occupied orbitals having both metal and ligand character. The presence of such states could result in lanthanide organometallics with, for

ⁱⁱ Note, however, that these pseudopotentials do allow for a change in f-density. This will be discussed more fully in 1.2.4.3.4

example, tuneable colours.ⁱⁱⁱ More importantly, I would argue that much of the confusion around the oxidation state of cerium in the molecules introduced below arises as a result of the assumption of purely ionic bonding.

Let us therefore first consider what an oxidation state is. An oxidation state is the nominal charge on an atom. It does not necessarily correspond to a charge density, however. It is important to note that whilst both oxidation potential and charge density are observables, the oxidation state is merely a useful chemical concept. As such it cannot be deduced directly from experiment but must rather be inferred with reference to theoretical assumptions surrounding the experiment purporting to measure it. Such experiments are heavily theory-laden^{iv} and great care must be taken in disentangling their meaning.

Such theory-laden experiments to probe oxidation state exist in many forms for good reasons. However, oxidation state is an extremely useful guide to aid us in predicting the reactivity of compounds, as well as other physical properties, including colour and magnetism. Thus, being confident that the oxidation state of manganese in the manganate ion, MnO_4^- is 7+ enables us to make predictions regarding this ion's capabilities as an oxidising agent. However, we would be stretching the concept beyond what would be reasonable if we were then to argue that, our predictions having been shown to be correct, there must consequently be no d-electron density around the manganese. This distinction between oxidation state and charge density is a crucial one, which will be returned to in subsequent chapters.

Finally, it is, I believe, important to state explicitly the role of the computationalist in elucidating these problems. The computationalist has the benefit of being able to probe 'directly' the electronic structure of molecules under investigation without recourse to theory-laden experiment (though of course the computational methods involve their

ⁱⁱⁱ Indeed, the fact that the electronic absorption spectra of Ce^{3+} compounds are strongly dependent on the environment of the metal ion would seem to lend weight to the argument for not holding to this heuristic rigorously.

^{iv} Alas, all experiments are theory laden (see Kuhn, T.S *The Structure of Scientific Revolutions* 1967) and we can never believe ourselves, as Newton did, to be '*hypothesis non fingo*', working without any hypothesis.

own assumptions and approximations, discussed below.) This means that the computationalist has the opportunity to rationalise surprising or contradictory experimental work and in doing so propose further experiments. However, it is easy to become distracted by the desire to perform ever more perfect calculations. Whilst this is a noble goal it must be balanced against what I consider to be the two imperatives of computational chemistry.

- 1) The calculations should consider genuine experimental problems.
- 2) The results of calculations should be expressed in a language meaningful to experimentalists.

In the words attributed to Eugene Wigner ‘it is nice to know that the computer understands the problem. But I would like to understand it too.’

It seems appropriate at this point to include a brief introduction to each of the systems studied in order to understand how they relate to each other and to the overall aims of this work. More detailed introductions for each project are included in the relevant chapters.

1.1.2.2 Cerocene

One of the most well recorded examples of oxidation state ambiguity in cerium organometallics is that of cerocene (CeCOT_2 , $\text{COT}=\text{C}_8\text{H}_8$). A ball and stick diagram of cerocene, a D_{8h} symmetry molecule, is shown in fig. 1.1

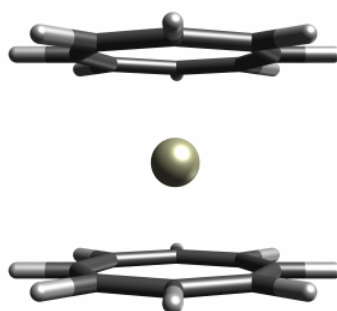


Figure 1.1- A ball and stick representation of cerocene

Cerocene was first synthesized serendipitously in 1976⁵. This synthesis was then replicated by Streitweiser et al. in 1985⁶ and the molecule was studied using He I/II photoelectron spectroscopy and computational methods, both of which indicated a 4+ oxidation state. However this result is somewhat surprising as it indicates a highly oxidizing Ce⁴⁺ sandwiched between two highly reducing COT²⁻ rings, a rather counter-intuitive situation. It is also important to note that it is unlikely that even if a 4f electron were localized on the cerium (i.e. if the Ce was Ce(III)) this would be apparent in the photoelectron spectrum unless variable energy photoelectron spectroscopy (VEPES) was performed.^v

Dolg and Fulde and co-workers subsequently carried out more advanced computational work in the 1990s⁷⁻⁹. The results of these calculations suggested a ground state dominated by the +3 oxidation state of cerium. This characterisation was supported by experimental work using X-ray absorption spectroscopy¹⁰. XANES K- and L_{III}-edges were determined for a range of cerium compounds, including ring-substituted cerocene, yielding absorption energies typical of Ce(III) rather than Ce(IV) systems.

Magnetic measurements have shown cerocene to be diamagnetic¹¹. This might be seen as evidence in support of the Ce(IV) model as there is no magnetic moment in this case, where there are no metal-based valence electrons. Typical Ce(III) compounds are paramagnetic with μ_{eff} of ~ 2.5 Bohr Magnetons³. However, the ambiguity in the oxidation state remains as the diamagnetism of cerocene might also be achieved if an open shell singlet was formed¹².

Although most of the recent work has suggested that Ce is in the 3+ oxidation state in cerocene there has additionally been NMR and cyclic voltammetry data collected for K[Ce(*tert*-butylC₈H₇)₂] and Ce(*tert*-butylC₈H₇)₂ which indicate that Ce in the substituted cerocene is in the 4+ oxidation state¹³.

Each of these methods will be discussed in more detail in chapter 2. However, it is apparent that after more than 30 years of research, employing a wide range of different

^v The necessity of using VEPES to determine whether f-electrons are present in a lanthanide system is discussed at length in chapter 3.

techniques, there remains little consensus regarding the oxidation state of cerium in cerocene. Cerocene therefore still represents an exemplar of oxidation state ambiguity in cerium organometallics.

1.1.2.3 Cerium tris-cyclopentadiene

Cerium tris-cyclopentadienyl (CeCp_3) consists of a Ce(III) ion surrounded by three cyclopentadienyl (Cp^- , C_5H_5^-) rings with near trigonal, C_{3v} symmetry, fig. 1.2

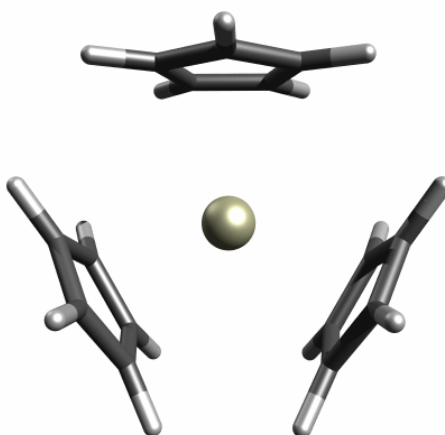


Figure 1.2- A ball and stick representation of CeCp_3

The electronic structure of this molecule is expected to be the most simple example of a lanthanide tris-cyclopentadienyl (LnCp_3) system, as it has just one f-electron. Consequently it was used as a benchmarking molecule to begin to rationalise the electronic structure of the series of LnCp_3 molecules in a variable energy photoelectron spectroscopy study. However, the results of this experiment were startling. Instead of identifying one f-ionisation, two such ionisations were observed, with an energy difference of 3.2 eV¹⁴. Such an energy difference between the two ionisations could not be explained in terms of spin-orbit coupling, (i.e. the $J=5/2$ and $J=7/2$ states) as this would be expected to result in a state-splitting of much smaller magnitude, as suggested in 1.1.1.1 and discussed further in chapter 3.

It therefore became necessary to investigate the origin of this effect and whether, in the context of oxidation state ambiguity in cerocene, CeCp_3^+ could really be considered to be a Ce(IV) system.

1.1.2.4 Cerium bis-cyclopentadiene oxo, imido and methylene

This group of molecules form an isoelectronic series of C_{2v} symmetry with the general structure given below, fig. 1.3.

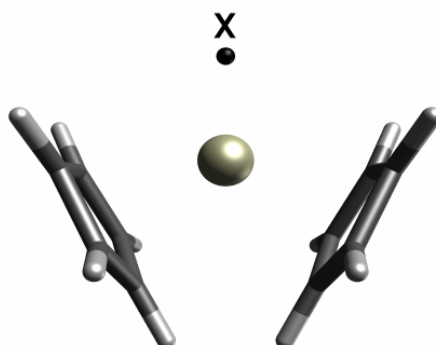


Figure 1.3- A ball and stick representation of $CeCp_2X$ ($X=O, NH, CH_2$)

They represent an interesting subject of study for a number of reasons. They would be expected to consist of Ce(IV) with two Cp^- rings and an X^{2-} group. As such, they offer an interesting comparison with the other formally Ce(IV) systems studied. The variation in the electronegativity of the X group allows for a comparison of the effects of the ligand on the oxidation state of Ce, extending the scope of the systems investigated. They also offer an opportunity for consideration of the interplay between computational and synthetic chemistry: none of this series has been successfully synthesised, however, computational studies have suggested that this should be possible¹⁵.

1.2 Computational Introduction

This work uses various *ab initio* techniques to model the electronic structure of the systems under consideration. In order to understand the merits and drawbacks of these techniques and thus to understand the reliability of any conclusions drawn from their results one must first consider their basis and the underlying assumptions.

1.2.1 The Schrödinger equation

At the heart of electronic structure theory is the Schrödinger equation:

$$\hat{H}\psi = E\psi$$

Equation 1.2- The Schrödinger equation¹⁶. Where \hat{H} is the Hamiltonian (the energy operator) for the system under investigation and ψ is the wavefunction of the system

The choice of Hamiltonian will be discussed below. The wavefunction, when squared, yields the electronic density, an observable.

1.2.1.1 Simplifying the solving of the Schrödinger equation

To solve the Schrödinger equation exactly for a many body system is generally unachievable. Hence, use is often made of a number of different assumptions. It is imperative to understand the assumptions that have to be made to solve the Schrödinger equation in order to be able to identify situations in which they are inappropriate and modify them accordingly.

1.2.1.1.1 The Variation Principle

The Variation Principle states that the energy of any trial wavefunction cannot be more negative (more favourable) than the energy of the true wavefunction. This means that if ansatz ψ_a when acted upon by the Hamiltonian results in an energy lower than ansatz ψ_b then ψ_a should be considered a better representation of the system.

1.2.1.1.2 The Born-Oppenheimer approximation

The non-relativistic Hamiltonian for a many-body system is:

$$\hat{H} = -\sum_a \frac{1}{2m_a} \nabla_a^2 + \sum_{a<b} \frac{q_a q_b}{r_a - r_b}$$

Equation 1.3- Non-relativistic Many Body Hamiltonian. a and b are indices for any charged particles (i.e. both nuclei and electrons), r the position, q the charge and m the mass.

The first part of the expression is the kinetic energy of the charged particle and the second part the potential energy. This is a complicated Hamiltonian but can be simplified by consideration of the relative size of nuclei and electrons.

The kinetic energy of the nuclei can be separated from the other parts of the Hamiltonian, forming an electronic Hamiltonian at fixed nuclear positions. This assumption of fixed nuclear positions is the Born-Oppenheimer approximation. The assumption is generally a reasonable one. This is because, due to their much greater mass relative to the electrons, the nuclei in a system will tend to move much more slowly than the electrons and therefore, to a good approximation, the electrons experience the effect of the nuclei at their instantaneous position.

Thus, we can write the electronic Hamiltonian decoupled from nuclear motion. This is simply the total Hamiltonian with the nuclear kinetic energy operator removed.

$$\hat{H}_{el} = \sum_i \frac{1}{2} \nabla_i^2 - \sum_{\mu,i} \frac{Z_\mu}{|r_\mu - r_i|} + \sum_{i<j} \frac{1}{|r_i - r_j|} + \sum_{\mu<\nu} \frac{Z_\mu Z_\nu}{|r_\mu - r_\nu|}$$

Equation 1.4- Electronic Hamiltonian using the Born-Oppenheimer Approximation

Greek indices represent nuclei and Roman indices electrons, Z is the nuclear charge, and r the position.

The Born-Oppenheimer approximation simplifies the problem of determining the electronic structure of a many body system. However, this is still a differential equation in $3n$ coordinates (where n is the number of electrons) due to the electronic kinetic energy term and, even using the Variation Principle, further approximations become necessary to make the problem tractable.

1.2.1.1.3 The Orbital Approximation and the Slater Determinant

A significant and extremely useful approximation is the orbital approximation. This holds that the total wavefunction of the many-body system can be written as the product of one electron orbitals, φ . And thus can be used to yield:

$$\psi(n) = \varphi_1(1)\varphi_2(2)\dots\varphi_n(n)$$

Equation 1.5- The Hartree product

One electron orbitals (which are exact for one electron systems but not so for many-electron systems) can be a powerful heuristic and are sufficiently entrenched through chemical pedagogy that it may be difficult to remember that they arise as a result of a major assumption and are not real. Their formation involves decoupling the electron degrees of freedom which greatly reduces computational demand but neglects some electron-electron interactions. This has some important consequences which will be discussed at length below.

In order for the total wavefunction for the system to abide by the Pauli Exclusion Principle it must be antisymmetric with respect to the interchange of two electrons (as is the case for any fermion). This is not necessarily the case for the Hartree product. A simple way of ensuring this is to write the total wavefunction as a single Slater determinant, which is a linear combination of Hartree products. The nature of determinants means that this is automatically antisymmetric and that no two of the one electron orbitals can be identical, ensuring compliance with the Pauli Exclusion Principle.

1.2.1.2 Hartree Fock Method

The Hartree-Fock Method employs the Slater determinant and the Born-Oppenheimer approximation to give an approximate solution to the Schrödinger equation which, whilst approximately modelling the total wavefunction as the product of non-interacting one-electron wavefunctions (Hartree), does account for electron-electron interactions in part (Fock).

The Hartree Fock energy thus incorporates *exactly* 0 electron (nuclear-nuclear), 1 electron ($\sum_i \frac{1}{2} \nabla_i^2 - \sum_{\mu,i} \frac{Z_\mu}{|r_\mu - r_i|}$) and two components of the 2 electron contributions to the energy of the system. These latter are termed the Coulomb (J_{ij}) and Exchange (K_{ij}) interactions. The Coulomb interaction is akin to that observed macroscopically between charged particles whilst the exchange interaction arises from necessity for an antisymmetric wavefunction.

The Hartree-Fock equations are commonly expressed:

$$\hat{F}_i \phi_i = \sum_j^N \lambda_{ij} \phi_j$$

Equation 1.6- Hartree-Fock equation. Where λ_{ij} is the ij^{th} element of a Hermitian matrix.

Once these equations are solved, the energy of each orbital determined in this way (known as the Canonical Orbitals) is:

$$\hat{F}_i \phi_i = \varepsilon_i \phi_i$$

Equation 1.7- Expression for energies of canonical orbitals.

The total energy of the system is calculated using the orbital energies but is not equal to their sum as this would mean double counting of the Coulomb and Exchange terms (J_{21} and K_{21} as well as J_{12} and K_{12}).

1.2.1.3 SCF

Self-Consistent Field Theory (SCF) is used in order to solve the Hartree-Fock equations. This is necessary as, in order to determine the i^{th} orbital, all other orbitals must be known, to some degree. This method uses an initial set of molecular orbitals to construct a new, improved set of orbitals, each one constructed using the $N-1$ other initial molecular orbitals. The cycle continues until there is little or no energy change between successive sets of molecular orbitals, making use of the Variation Principle (1.2.1.1.1). The energy of the system is calculated from the Slater determinant constructed from the molecular orbitals. Switching the position of the molecular orbitals in the Slater determinant doesn't change the determinant and thus the energy is

independent of unitary transformations of the occupied molecular orbitals. This characteristic can be useful for developing quantifiable analyses but can be misleading if one is trying to gain information from inspection of the orbitals directly.

1.2.1.3.1 LCAO

Until this point it has been tacitly assumed that it is possible to have a starting set of molecular orbitals (MOs) from which to begin the SCF process. This is made possible as a result of the Linear Combination of Atomic Orbitals (LCAO) approach. Chemically when we form a molecule we combine atoms and computationally we take the same approach. The initial molecular orbitals which are the input for the SCF process are a combination of atomic orbitals (or atomic basis functions, described more fully in **1.2.4**) with variable coefficients, c , describing their weight in each molecular orbital.

$$\varphi_i = \sum_a c_{ai} \phi_a$$

Equation 1.8- Linear Combination of Atomic Orbitals. a indexes the atomic orbital and i indexes the molecular orbital.

It is, in fact, these coefficients which are varied in the SCF procedure, thus modifying the molecular orbitals by reducing or increasing the contribution from a particular atomic orbital in order to reduce the total energy of the system, using the Fock operator. For the whole system this set of equations can be written in matrix form:

$$\mathbf{FC} = \mathbf{SC}\boldsymbol{\varepsilon}$$

Equation 1.9- Roothaan Equations, which are solved in the Hartree-Fock method. F is the Fock matrix, C the coefficient matrix, S the overlap matrix and $\boldsymbol{\varepsilon}$ the diagonal MO energy matrix.

The Fock matrix is constructed from one electron integrals, two electron integrals and the density matrix. The density matrix is the only part of the Fock matrix which is dependent on the coefficients of the atomic orbitals. Thus, the SCF procedure previously described occurs in the order:

-
1. Initial guess for density matrix obtained.
 2. One electron integrals calculated (For a system of M basis functions there are $\sim M^2$ such integrals).
 3. Two electron integrals calculated (For a system of M basis functions there are $\sim M^4$ such integrals).
 4. Fock matrix formed and used to determine improved molecular orbitals.
 5. New density matrix obtained and used to construct new Fock matrix.
 6. Repeat steps 4-5 until little or no variation in the energy of the system^{vi}.

1.2.1.4 Correlation

As stated in **1.2.1.2**, the HF method yields all of the components of the energy which it considers exactly. However, it ignores an important contribution to the energy as a result of the orbital approximation. There are only two 2-electron contributions to the HF energy, arising from the Coulomb and the Exchange terms, both of which involve the one electron wavefunction under the influence of a distributed potential arising from all the other electrons in the system, rather than an instantaneous interaction with each of the other electrons. This distributed potential arises from the demarcation of the total wavefunction into discrete one electron orbitals which results in the calculation of interactions between one electron densities (J and K) rather than between discrete electrons.

The neglected instantaneous interactions of the electrons, known as correlation, would tend to make the electrons avoid each other more effectively than is possible in the HF system (thus varying the kinetic energy), and in doing so reducing the electron-electron repulsions (thus varying the potential energy). The overall effect is a system with a lower energy. The correlation energy is difficult to describe qualitatively as it is merely the energy neglected by employing the gross, but extremely useful, orbital approximation. The formal definition of the correlation energy is the energy difference

^{vi} Many codes may, in fact, repeat steps 2-5 until there is no variation in the energy of the system. It may be significantly more efficient to calculate these 'on the fly' at each step rather than storing any large files generated.

between the true total energy of the system and the HF result. Typically, this is a tiny fraction of the total energy of the system $\sim 1\%$ ¹⁷. However, in chemistry we are rarely interested in total energies but rather energy differences and, as correlation may contribute differently to different excited states, ion states or geometries of a system, it can be of crucial chemical significance.

Correlation is very important in many different situations and, depending on the situation, different post-Hartree-Fock methods can be used to attempt to include as much of the important correlation energy as possible. All these methods use the HF result as a basis and thus retain the orbital approximation but include additional terms to approach the result that would be generated without this approximation.

If we use the extremely loose definition of correlation as the energy reduction due to electrons avoiding one another we can quickly build up a picture of the situations in which correlation will be important and different possible approaches to including it. Electrons may particularly avoid each other when:

1. There are a large number of electrons in different orbitals which occupy a similar spatial region.
2. There are several possible arrangements of the electrons in different orbitals, all of which have similar energies. Why this results in electrons avoiding each other is explained below.

The first case is generally termed ‘dynamic’ correlation and should be considered for all many electron systems. It is normally the largest component of the correlation energy. Dynamic correlation can be visualised by considering the $2p_x$ and $2p_z$ orbitals, shown in fig. 1.4. These occupy a similar spatial region, thus if the $2p_x$ electron approaches one of the regions marked *a* the $2p_z$ electron will tend to move away from that region, thus reducing the overall Coulomb interaction experienced by the two electrons. The more electrons in a system the more significant will be the dynamic correlation. Dynamic correlation should therefore ideally be modelled by a relatively inexpensive method which scales well with system size.

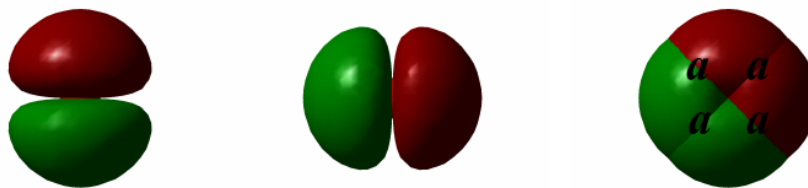


Figure 1.4- From left to right: p_z orbital, p_x orbital, p_x and p_z orbitals displayed together.

The second case, often termed ‘static’ correlation, is not so intuitively a result of electrons avoiding each other. That it is correlation is best illustrated with an example. Let us imagine we have two near degenerate states which have the same electronic structure with the exception of one electron. In both cases, orbitals A and B are occupied but in state 1 orbital C is also occupied whilst in state 2 the third electron is in orbital D. When orbital C is occupied there is repulsion between this electron and that in orbital A, when orbital D is occupied there is repulsion between this electron and that in orbital B. One possible way of minimising these repulsions is for the electron to partially occupy both orbital C and D, thus partially avoiding both the electrons in orbital A and B.

Static correlation is generally a smaller component of the correlation energy but can have significant consequences for an understanding of the electronic structure of the system. Static correlation may be important when considering a variety of common situations, all of which require consideration of more than one Slater determinant (or configuration). Two of these are illustrated below:

a) Bond Dissociation

The simplest example of the importance of static correlation in bond dissociation is that of the dissociation of H_2 . If we imagine the electronic configurations we would expect at different points in the dissociation of H_2 we can quickly understand the correlation problem. At equilibrium bond distance we would expect the two electrons to be located in the σ_g MO. At infinite bond distance we would expect one electron to be located in the $1s$ orbital of H_a and one to be located in the $1s$ orbital of H_b , this corresponds to a 50:50 linear combination of the σ_g and σ_g^* MOs. However, this cannot be represented using a single Slater determinant of MOs. This may not be a problem when considering complete dissociation, however, it is problematic when we try to consider intermediate bond distances. In this case the HF method can generate erroneous results with elevated

energies. The energies at extended bond lengths are overestimated as a result. This occurs because each electron only experiences the average potential of the other, not the instantaneous interaction, if the electrons were to experience the instantaneous interaction there would be a greater probability of finding one electron nearer to one of the H nuclei and one nearer to the other. This, like the fully dissociated H₂, can only be represented by a linear combination of the σ_g and σ_g^* MOs. Correlation must be included in order to generate the correct H₂ dissociation curve, and indeed all investigations of dissociation require a consideration of ‘static’ correlation.

b) High Density of States

In some systems a high density of states means that several configurations may need to be considered for an accurate representation of the system. For example, in a high symmetry cerium(III) compound the seven f-orbitals will be degenerate or near degenerate. It may therefore be necessary to consider seven different configurations, one with each of the f-orbitals as the HOMO in order to properly represent the real wavefunction of the system.

Static correlation tends to be important only in specific circumstances and only generally for the valence electrons, or indeed, a subset of the valence electrons. However, any method for treating static correlation should be as rigorous as possible as inclusion of different electrons can have dramatic consequences for the chemistry of the system under investigation. Thus methods for the inclusion of static correlation may be more costly than those employed for dynamic correlation.

1.2.1.5 Post Hartree-Fock Methods

The requirement for post Hartree-Fock methods arises as a result of the neglect of correlation due to the orbital approximation. The use of the orbital approximation allows the total wavefunction to be written as a single Slater determinant. Thus, in order to mitigate the effects of this approximation, further determinants may be included to better represent the wavefunction. These will appear as excited configurations relative to the HF determinant, i.e. one or more orbitals which were occupied in the HF determinant will now be virtual and, correspondingly, one or more orbitals which were

virtual in the HF determinant will now be occupied. If an excited determinant has one such excitation it is known as a single, if two a double and so forth. In order to include correlation fully all excitations (up to N tuple) should be included and the coefficients of the determinants optimised. This is full Configuration Interaction (CI). Most post-HF methods can be considered in some way as truncated CI, and the choice of where to make the truncation depends on the nature of the correlation in the system. Thus, if dynamic correlation is most significant in a system it may be best to consider correlation for all electrons to a low order (i.e. singles and doubles); whilst if static correlation is more important it may be better to focus solely on the electrons contributing to the static correlation, but to high order.

A consideration of whether dynamic or static correlation is likely to be more significant for a particular problem is often imperative; however, other factors may also be important. Ideally all post-HF methods would be size consistent, size extensive, variational and cheap. Alas, this is not the case and these factors must also be considered when selecting a computational approach.

Size consistent means that the same energy will be obtained for the energy of two fragments at large separation as for the sum of the individual fragments. Size extensivity is similar but the fragments may be interacting (it is thus a measure of whether the method scales properly with system size). The Variational Principle has been mentioned previously but it is worth recalling that if a method is non-variational the energy may have the propensity to tend to $-\infty$! The cost of a calculation, always a consideration and sometimes determining whether or not a calculation is viable, depends on how the computational time scales with the number of basis functions, M .

1.2.1.5.1 MP2

A common and popular post-HF method which includes largely dynamic correlation is Møller-Plesset Perturbation Theory, in particular to the second order (MP2), as this is the most inexpensive way of including a reasonable amount of correlation, in cases where static correlation is not significant.

All perturbation theories rely on the assumption that it is possible to improve an inexact Hamiltonian with a perturbation Hamiltonian. For the theory to be effective the perturbation must be small relative to the original Hamiltonian, i.e. the reference wavefunction is reasonable.

In Møller-Plesset perturbation theory (MP) the inexact, original Hamiltonian chosen is the sum of the Fock operators i.e. the sum of the orbital energies. It is important to recall that this is not the same as the HF energy, which, as noted above avoids the double counting of J and K that occurs in this approach. The perturbation is therefore to remove this double counting.

$$W_1 = \langle \Phi_0 | \mathbf{H}' | \Phi_0 \rangle = \langle \mathbf{V}_{ee} \rangle - 2 \langle \mathbf{V}_{ee} \rangle = - \langle \mathbf{V}_{ee} \rangle$$

Equation 1.10- MP1 energy correction where \mathbf{H}' is the zeroth order Hamiltonian.

This yields the HF energy as the energy to 1st order using the 0th order wavefunction. It is important to note that correlation is only included at MP2 and higher perturbations as correlation is the difference in energy between the HF result and the true result. Thus MP1, being equivalent to HF is uncorrelated and MP theory is only a post-HF method at 2nd and higher orders.

MP allows calculation of the (2n+1)th order energy from the nth order wavefunction. Thus the first order correction to the wavefunction is required to calculate the second order correction to the energy. This first order correction to the wavefunction arises from the inclusion of double excitations. Thus the second order energy correction is:

$$W_2 = \sum_{i < j}^{\text{occ}} \sum_{a < b}^{\text{vir}} \frac{\langle \Phi_0 | \mathbf{H}' | \Phi_{ij}^{ab} \rangle \langle \Phi_{ij}^{ab} | \mathbf{H}' | \Phi_0 \rangle}{E_0 - E_{ij}^{ab}}$$

Equation 1.11- MP2 energy correction

From which the expression for the second order energy can be determined to be:

$$E(\text{MP2}) = \sum_{i < j}^{\text{occ}} \sum_{a < b}^{\text{vir}} \frac{[\langle \phi_i \phi_j | \phi_a \phi_b \rangle - \langle \phi_i \phi_j | \phi_b \phi_a \rangle]^2}{\epsilon_i + \epsilon_j - \epsilon_a - \epsilon_b}$$

Equation 1.12- MP2 energy

Up to MP3, there is no need for the second order wavefunction and the perturbation acts merely as an energy correction. This means that, up to MP3, the method is tractable, scaling as M^5 or M^6 . MP4 represents a big jump in accuracy as it uses the second order wavefunction, but scales more like M^7 due to the inclusion of singles, triples and quadruples in addition to double excitations, and is therefore not so attractive in terms of resource. MP2 is generally the preferred method as MP3 often only gives comparable accuracy and MP4 is considerably more costly. However, MP2 tends to overestimate correlation and a more accurate result typically lies between that determined by MP3 and that from MP4. This is because the estimation of correlation, and thus of any calculated property, tends to oscillate with increasing perturbation order, as shown below.

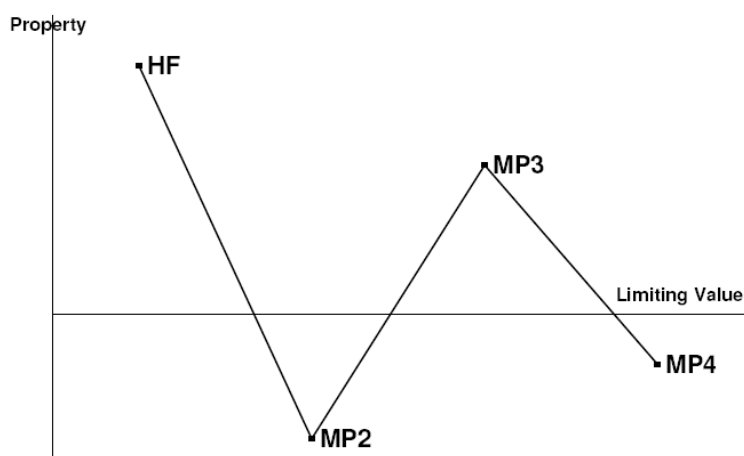


Figure 1.5- Schematic variation of calculated properties with increasing levels of perturbation theory.^{xv}

The MP2 method is non-variational, hence the possibility of calculating an energy lower than the true energy of the system, as shown in figure 1.5, but is size extensive, and is therefore reasonably reliable for energy differences. The caveat here is that the reference wavefunction must be reasonable, if this is not the case (i.e. if there is significant static correlation) there will not be convergence with increasing levels of perturbation theory. A continued oscillation and variation without apparent convergence with increasing order of perturbation theory is a good indicator that the reference (HF) wavefunction is not a good one and another approach needs to be taken. Such an alternative approach is offered by the Complete Active Space Self-Consistent Field (CASSCF) method.

1.2.1.5.2 CASSCF

The MP_n approach to correlation correlates all the electrons in the system but typically only includes double excitations (MP2) and is thus best suited to systems with mostly dynamic correlation. In systems with more static correlation a better approach is often to treat a subset of the electrons, those involved in contributing largely to the static correlation of the system, more thoroughly. The CASSCF method involves carrying out full CI on such a subset of electrons and orbitals, known as the active space. CASSCF is thus based on including additional Slater determinants in the wavefunction and, as it is based on CI, is variational. However, in an attempt to improve the result using this method the orbitals are also simultaneously optimised. This means that not only are the coefficients of the determinants arising from the active space orbitals optimised during the CASSCF procedure (as with CI) but also the coefficients of the atomic orbitals that contribute to all the molecular orbitals (as with SCF). This approach means that, if the active space is sufficiently well chosen, the vast majority of the static correlation is included as well as some dynamic correlation.

The choice of active space for a CASSCF calculation is crucial but, due to the intensive nature of full-CI may be quite severely limited, typically an active space of around 18 electrons in 20 orbitals, given the notation (18,20), represents the limit of computational viability. If it is necessary to correlate a larger number of electrons the Restricted Active Space (RASSCF) method may be utilised. This involves including the most important orbitals in the CAS-space (or RAS2 space), additional occupied orbitals in the RAS1 space and additional virtual orbitals in the RAS3 space. Full-CI is performed in the RAS2 space whilst the excitations from RAS1 (into RAS2 or RAS3) and the excitations into RAS3 (from RAS1 or RAS2) are limited, typically to doubles or triples. Even so, this can be a very resource-demanding method.

The CASSCF wavefunction can be difficult to interpret as it is a many determinant or multiconfigurational wavefunction. A unitary transformation may be performed on the optimised active space orbitals without varying the total wavefunction therefore, whilst it may be tempting to inspect the configurations and their coefficients, this is not a

reliable way to characterise the wavefunction. A better approach is the use of natural orbitals and their occupancies.

As is well known, the wavefunction is not an observable, however, the square of the wavefunction is the electron density, from which all observables can be derived. The wavefunction can thus be used to calculate the reduced density matrices. The first order reduced density matrix can be diagonalised to generate the Natural Orbitals (NOs) and their Natural Occupancies (NOOs), the eigenvectors and eigenvalues, respectively. Whilst the natural orbitals may be transformed to another set of orbitals according to any number of criteria (such as maximising charge localisation), any such transformation will necessarily be less connected to the observables and hence of less use when trying to compare the results of the calculation with experimental data.

The literature on CASSCF calculations on organometallic systems is rather slight. This is in part due to the relative difficulty of these calculations. In particular these difficulties arise due to the physical limitations of these calculations in terms of the size of the calculations. Organometallic systems may involve a large number of atoms; the systems investigated in this work are 33, 31 and 22 atom systems with over 200 electrons. In addition, in order to properly model the valence region many active space orbitals may need to be included, for example, some or all of the d and/or f orbitals as well as ligand-based orbitals. This can result in very large active spaces with many possible configurations. For example, a (12,16) calculation results in 4,013,380 possible configurations whilst an (8,14) calculation results in a more feasible 63,251, the former calculation may take several days to perform whilst the latter could be completed within 24 hours.

In some systems there may be several degenerate or near-degenerate electronic states close to the ground state. In these cases, a single state calculation may yield a misleading wavefunction, or fail to converge as first one and then the other state is optimised, known as 'root flipping'. If several states are optimised concurrently these root-flipping problems can be eliminated. This is known as state averaging.

1.2.1.5.3 CASPT2

If a system is studied using the CASSCF method static correlation may be well modelled. However, little dynamic correlation will have been included. This can be rectified in part by applying the MP2 method to the CASSCF wavefunction, an approach known as CASPT2 which is the least resource-demanding method of including dynamic correlation to a multiconfigurational wavefunction.

In this case MP2 is performed but with the CASSCF wavefunction as the 0th order wavefunction. In the limit of orbital occupations exclusively 2 or 0 in the CASSCF part the result will be identical to the MP2 result. As mentioned in section 1.2.1.5.2, the choice of active space for a CASSCF calculation can have a pronounced effect on the results of the calculation and is far from a black-box technique. Whilst CASPT2 can act as an energy correction for dynamic correlation, if the active space chosen is not a good one the results may be misleading, as is found to be the case in MP2 when the HF wavefunction is not a good representation of the system. Fortunately, when using the CASPT2 method we can get a good indication of whether or not our CASSCF wavefunction is reasonable based on the reference weight, ω . The reference weight is a measure of the contribution of the CASSCF wavefunction to the 1st order wavefunction. For a reasonable CASSCF wavefunction the reference weight scales approximately as $k^{-n/2}$, where k is a constant empirically found to be ~ 1.015 ¹⁸ and n is the number of electrons in the system. This is a consequence of the size-extensivity of the CASPT2 method. Thus, transition metal organometallics typically have $\omega \sim 0.7-0.8$ and lanthanide organometallics can be expected to have somewhat lower values of ω , between 0.5 and 0.6. If a CASPT2 calculation yields a much lower reference weight this is an indication of the presence of one or more intruder states.

Intruder states arise due to orbitals outside the active space having zeroth order energies close to orbitals in the active space, i.e. intruder states have CASSCF energies close to the CASSCF energy of the state under investigation¹⁹. This may mean that one or more orbitals which should be treated in the active space have been omitted (resulting in a strong intruder state) or alternatively that a weak intruder state is involved. A weak intruder state has little interaction with the reference state and therefore has little effect

on the energy. Weak intruder states are fairly common in the CASPT2 method due to the smaller energy gap between the occupied and unoccupied, inactive orbitals than is usual for MP2. In the case of a strong intruder state the only solution is to change the active space however, in the case of a weak intruder state an imaginary shift may be employed, moving the energy of the intruder state to prevent interaction.

1.2.1.5.4 Other Methods

1.2.1.5.4.1 CISD

As noted above, full-CI, whilst exact, is unfeasible for almost all chemically interesting systems. Other methods of inclusion tend, therefore, to involve different methods of truncating CI. CISD is probably the best known form of truncation. This is configuration interaction only involving single and double excitations. CISD is not size-consistent or size-extensive, the latter of which means that it becomes increasingly inaccurate for larger numbers of electrons. Also, because only single and double excitations are included, CISD accounts reasonably well for dynamical correlation but less so for static correlation. Consequently, Multireference CI (MR-CI) was developed, performing CISD on each of the configurations from a CASSCF method, and thus including both static and dynamic correlation in a more theoretically robust manner than by using perturbative methods. However, MR-CI is generally used only on small molecules due to its computational demands.

1.2.1.5.4.2 Coupled Cluster (CC)

Perhaps the most accurate way of including dynamic correlation is the coupled cluster method. This is a reformulation of CI in terms of a Taylor expansion. The truncations of CC are more rigorous than those of CI as they involve exact termination of the Hausdorff expansion²⁰ to defined order. This has the consequence of ensuring that CCSD is size-extensive and size-consistent unlike CISD, whilst scaling similarly. This seeming inconsistency in behaviour occurs because, whilst CISD includes only the

single and double excitations, CCSD also includes the coefficients of quadruple excitations, which can be expanded purely in terms of the coefficients of double excitations. CCSD therefore offers considerable benefits over CISD however, there is a drawback as the calculations cannot be performed variationally. CCSD, whilst an excellent and accurate method for systems with little static correlation, is not suitable for describing multiconfigurational systems. Efforts have been made to develop multireference coupled cluster methods, which would enable the inclusion of static correlation, but thus far they have proved too resource-demanding for all but the smallest molecules. It is therefore important to be able to tell the point at which CCSD is not appropriate for a system with some static correlation. Fortunately a test is available which does this, known as the T_1 diagnostic²¹. The T_1 diagnostic should be no more than 0.02 for a CCSD and no more than 0.04 for CCSD(T) calculation to ensure that correlation is properly accounted for.

1.2.2 Density Functional Theory

1.2.2.1 The Density Approach

In later life Schrödinger is purported to have said of quantum mechanics ‘I don’t like it and I’m sorry I had anything to do with it’ and those of us who feel more comfortable with the tangible and observable than the esoteric and mathematical may feel we have cause to agree with him. Fortunately, however, in 1964, two men with a foot in both camps formulated a proof that fits more easily with the observable world. The Hohenberg-Kohn theorems²² show that there is a one-to-one correspondence between the electron density and the ground state energy and that the density approach is variational. The first theorem is most easily formulated by recalling that the density is the square of the wavefunction integrated over $N-1$ coordinates and then considering the following:

Let there be two external potentials, $v_1(\mathbf{r})$ and $v_2(\mathbf{r})$ arising from the same density, $\rho(\mathbf{r})$. Thus there will be two Hamiltonians, H_1 and H_2 with the same (ground state) density, but different wavefunctions, Ψ_1 and Ψ_2 . The variational principle is then invoked:

$$\begin{aligned}
 E_1^0 < \langle \Psi_2 | H_1 | \Psi_2 \rangle &= \langle \Psi_2 | H_2 | \Psi_2 \rangle + \langle \Psi_2 | H_1 - H_2 | \Psi_2 \rangle \\
 &= E_2^0 + \int \rho(\mathbf{r}) [v_1(\mathbf{r}) - v_2(\mathbf{r})] d\mathbf{r}
 \end{aligned}$$

Equation 1.13- Two energies from the same density

The subscripts may be interchanged to give a second inequality. Addition of the two inequalities yields:

$$E_1^0 + E_2^0 < E_2^0 + E_1^0$$

Equation 1.14- False statement arising from equation 1.13

which is contradictory, thus proving the one-to-one correspondence between electron density and energy.

Following from this is the Bright Wilson Observation²³, that knowledge of the electron density yields not only the electronic structure but also the nuclear positions (the cusps of the density) and the nuclear charges (Laplacian of the density at the nuclear positions) and, furthermore, the asymptotic behaviour of the ground state electron density gives the 1st ionisation potential. Consequently, to have full understanding of the ground state all that remains is to find the functional linking the electron density to the energy.

Early attempts to determine the exact density functional modelled systems as a uniform non-interacting electron gas, as described by Thomas and Fermi in 1927^{24, 25}. Unfortunately this model was not promising for chemistry as it does not predict bonding and thus the existence of molecules is forbidden! The major step towards a useable theory arrived with the introduction of a method to determine the energy using density functional theory by Kohn and Sham in 1965²⁶.

The Kohn-Sham formalism imagines the simplistic situation of non-interacting electrons and then gradually builds up to a situation where the electrons do interact. In the non-interacting system the energy is simply the kinetic energy:

$$E_{\text{nonint}}(\rho) = T_{\text{nonint}}(\rho)$$

Equation 1.15- Density functional for the energy of the non-interacting system

If interactions are now included we will need to consider the Coulombic interaction, $J(\rho)$, the electron-nuclear interaction (E_{ne}) and the other terms ignored due to interacting electrons. These last are collected together as the exchange-correlation energy (E_{xc}), giving:

$$E(\rho) = T_{\text{nonint}}(\rho) + J(\rho) + E_{ne}(\rho) + E_{xc}(\rho)$$

Equation 1.16- Density functional for the energy of the interacting system.

This formulation appears very similar to the HF approach and can be solved using orbitals, known as Kohn-Sham orbitals, using a single Slater Determinant. Unlike HF theory, however, the Kohn-Sham method is exact, providing the exact exchange-correlation functional is known. This is the drawback of density functional theory. Not only is the exchange-correlation functional unknown, but there is no systematic way of searching for it. This has proven the Holy Grail of DFT: promising much to the successful seeker, though few seeking it do so with any real hope of success.

There are two final general points to make about DFT. The first concerns the Kohn-Sham orbitals. It may be tempting to compare these with the Hartree-Fock orbitals but this could be misleading. The eigenvalues of the HF orbitals have meaning, corresponding to ionisation energies of the respective electrons, with associated errors arising from the assumptions of the HF method, described by Koopmans' theorem²⁷. The Kohn-Sham orbital eigenvalues do not have the same property, although it is possible to determine ionisation energies in the Kohn-Sham formalism. This is done making use of Janak's theorem²⁸ and the Slater transition state²⁹.

Perhaps the most important general comment regarding DFT relates to correlation. If the exact functional were known correlation would be perfectly accounted for using DFT and there would be no problem in using it to model systems such as those described in **1.2.1.4**. However, the exact functional being unknown, correlation, though accounted for in part, is not necessarily treated adequately using DFT and, more importantly, is not treated consistently. DFT, like HF is a single determinant method, with no possibility of adding determinants to better model the system. Thus, if a system is likely to be highly multiconfigurational in the HF scheme, DFT may also not be a good approach.

1.2.2.2 Types of functional

Because the exact density functional is not known different schools have developed in an attempt to approach it. Some methods for developing functionals make use of empirical parameterisation, others try to avoid this and follow a heuristic that demands that the result is accurate in the extreme of a uniform electron density³⁰. This may leave the chemist with the choice between a pragmatic approach that may yield better results but is theoretically unsatisfactory and a more systematic approach, which may be less cost-effective and often produces results which are less in agreement with experiment. There are three commonly used ‘flavours’ of DFT. These are:

1.2.2.2.1 Local spin density approximation (LSDA)

This is the method favoured by the purist. Locally the electron density is assumed to be modeled by a uniform gas. This method does not take any fitting parameters from experiment and consequently often yields results differing significantly from the observed data. However, it is rigorously consistent with the axioms of DFT.

1.2.2.2.2 Generalised gradient approximation (GGA)

These methods require both the electron density at a given point and the gradient (derivative) of the electron density at that point. Use of the derivative of the electron density tends to give a substantial improvement over LSDA calculations. In general the exchange and correlation are separated and different functionals used for each. Commonly used GGA functionals include PW91³¹ and B88³² for exchange, PBE^{33, 34} for exchange and correlation and LYP³⁵ for correlation. Following on from this improvement to LSDA a ‘Jacob’s ladder’³⁰ has been determined leading to the heaven of chemical accuracy, with ever improved functionals on higher rungs, though it is also increasingly costly to climb the rungs. TPSS³⁶ is an example of a meta-GGA functional and is described as being on the third rung of ‘Jacob’s Ladder’, using the local density and both the first and second derivatives of the local density as well as the kinetic energy density.

1.2.2.2.3 Hybrid

These methods take the exact part of the exchange energy (K) from Hartree-Fock theory. This is combined, using suitable parameters (determined by a process of fitting calculated data to experimental quantities such as ionisation energies as well as electron affinities and bond dissociation energies), with exchange from LSDA and correlation from GGA. The use of HF exchange and experimental parameters means that these methods are even less 'pure' DFT than GGA. The most frequently used hybrid functional is B3LYP which uses B88 and HF for exchange and LYP for correlation. The contributions of LSDA, HF, B88 and LYP are determined using three parameters, hence the '3' in the name.

1.2.2.3 Time-Dependent Density Functional Theory

DFT is, as described above, purely a ground state method, the electron density providing the ground state energy. This means that if excited states are required, for example for comparison with UV-Vis spectra, another approach must be taken. The approach taken invokes response theory, determining the response to a perturbation in an electric field which varies with time. This inclusion of time dependence results in Time-Dependent Density Functional Theory (TDDFT) and enables the calculation of excited states. A full description of TDDFT is given elsewhere³⁷⁻³⁹. The most important factors to be aware of are that TDDFT is the most robust method to use when considering excited states in DFT and that the best functionals for time-independent DFT may not be the best functionals in TDDFT. This is because TDDFT requires functionals which are asymptotically correct in order to properly model the potential of the system and thus obtain accurate excitation energies. An asymptotically correct functional models the exchange-correlation potential behaviour correctly at large values of r , LSDA and most GGAs fail to do this. If the potential is not well modelled at large r , the density will be poorly described for excited states, for which the wavefunction has larger values at larger r than is the case for the ground state. An example of an asymptotically correct functional is SAOP⁴⁰.

1.2.3 Geometry Optimisations

It is often important to find the optimum geometry for a structure. This is done by selecting an initial geometry, calculating the energy and then determining whether or not this is an energy minimum. In order to determine this both the first and second derivatives of the energy with respect to position (the latter of which is the Hessian) are calculated. If the first derivative is zero the structure is either an energy minimum or maximum (i.e. a transition state or higher order saddlepoint). The eigenvalues of the Hessian determine which of these the structure is (all of which will be positive if the structure is a minimum and one of which will be negative if it is a transition state). If, on the other hand, the first derivative of the energy is non-zero the geometry must be further optimised.

1.2.3.1 Methods for optimisation

The first derivative of the energy with respect to position is greatest furthest away from the minimum and reduces as the minimum is approached. Therefore following the line of steepest descent is guaranteed to approach a minimum¹⁷. However, this method will only locate minima and it is sometimes advantageous to determine transition states or saddle points. One very popular approach, which does enable the location of saddle points is the Newton-Raphson method. This method uses the value of the Hessian to determine the direction to follow to reach a stationary point as well as the step size. The step size taken to reach the minimum is critical to avoid 'overshooting' the optimum geometry, resulting in a continuously oscillating calculation.

1.2.3.2 Transition states and imaginary frequencies

At a transition state the eigenvalues of Hessian will be positive in all directions but one. A structure which is not a global minimum will exhibit imaginary frequencies. These can be used to identify a local minimum or transition state. Additionally, the nature of

the imaginary frequency can offer guidance for structural changes required to reach a minimum, i.e. in some cases the path from the transition state to a minimum.

1.2.3.3 The effect of symmetry to geometry optimisations

In the case of a highly symmetric initial starting structure it may be difficult for the energy of the structure to be minimised, if this minimum results from a reduction in the symmetry. This is because there are no forces acting on the molecule to force the structure from the symmetry initially imposed. It may be necessary in these cases for a deviation from the symmetric system to be imposed in order for such forces to act during the geometry optimisation.

1.2.4 Basis Sets

As was discussed in the section **1.2.1.3.1**, it is necessary to have a starting set of orbitals with which to begin the SCF procedure. These are constructed from the atomic basis sets. It is clearly of importance that these basis sets model the atoms well in order to provide a good starting point for the calculation. The basis sets are therefore often selected to be functions of a mathematical form which both closely model the behaviour of the atomic orbitals and which are easy to manipulate computationally. The most computationally demanding part of the SCF procedure is the calculation of the one- and two-electron integrals (steps 2 and 3 in **1.2.1.3.1**) and thus the most efficient basis sets will be those which are of a form which can be easily integrated. As was described in section **1.2.2.1** the nuclei in a system are marked by a cusp in the electron density (and hence in the wavefunction), and this behaviour should therefore be modelled by a basis set, as should the decay in the wavefunction far from the nucleus. This decay is particularly important as it represents the bonding region.

The two main categories of basis sets are Slater Type Orbitals (STOs) and Gaussian Type Orbitals (GTOs).

1.2.4.1 STOs

Slater Type Orbitals have the form:

$$\chi_{\zeta,n,l,m}(r,\theta,\varphi) = NY_{l,m}(\theta,\varphi)r^{n-1}e^{-\zeta r}$$

Equation 1.17- Polar coordinate representation of the form of STOs. N is the normalisation constant, $Y_{l,m}$ are the spherical harmonics, r is the distance between the electron and the nucleus and ζ is the exponent.

STOs have the advantage that the exponential dependence on the distance between nucleus and the electron mirrors the exact orbitals for the hydrogen atom but the lack of radial nodes means that it is necessary to make linear combinations of STOs. As is often the case, there is a balance between accurate representation of the atomic structure and computational feasibility and the use of STOs has the consequence that three and four centre two-electron integrals cannot be performed analytically. This increases the computational demand as numerical methods must be employed. However, it should be recalled that steps 2 and 3 (the integration steps) of the SCF procedure need only to be carried out once and this initial investment may therefore be worthwhile if it allows a better representation of the system.

1.2.4.2 GTOs

Gaussian Type Orbitals have the form:

$$\chi_{\zeta,n,l,m}(r,\theta,\varphi) = NY_{l,m}(\theta,\varphi)r^{(2n-2-l)}e^{-\zeta r^2}$$

Equation 1.18- Polar coordinates representation of the form of GTOs. N is the normalisation constant, $Y_{l,m}$ are the spherical harmonics, r is the distance between the electron and the nucleus and ζ governs the decay of the function

It is immediately apparent that this form does not well represent the cusp in the electron density at the nucleus, as at this point the slope is zero. Not only is this a problem but a perhaps more serious one exists in the representation of the valence regions. Here the basis function decays too rapidly. However, several GTOs can be combined to approximate the correct behaviour. This means that, for the same degree of accuracy,

more GTOs are required than STOs. However, the form of GTOs is much easier to integrate than STOs and thus can be done analytically.

1.2.4.3 Use of basis sets in calculation

In practice the choice between STOs and GTOs comes down to the electronic structure code being used, some have been written with efficient numerical integration modules whilst others have been optimised for a larger throughput of analytical integration. Typically, most users select their code and then work within its limitations rather than choosing a type of basis set and then finding an appropriate code. User choice takes a much greater effect when it comes to the size and type of contraction scheme of a basis set. It is these, more subtle choices which will now be considered.

The simplest way of forming an atomic basis set is to form the minimum basis. This is just one function for each of the occupied orbitals. So, for Ce this would be 5 s-functions, 3 sets of p-functions, 2 sets of d-functions and 1 set of f-functions. However, this gives very little flexibility. This is of particular importance in the valence region in order to properly model the chemically active electrons, and therefore more functions are generally included here. If the number of valence functions are doubled this is called Valence Double Zeta (VDZ), if tripled, Valence Triple Zeta (VTZ) and so forth. Whilst this increase in the valence basis functions improves the modelling of bonding interactions this can be further improved by adding polarisation functions. These are higher angular momentum basis functions that can act to polarise an occupied atomic orbital, more accurately representing the bonding situation. Polarisation functions are particularly important when considering correlation and electronic excitations.

Basis sets are devised based on variational calculations, typically HF, to determine the value of the exponents. Whatever the method employed to do this a problem arises. Because the 1s orbital of Ce, for example, contributes more to the energy than a 4f orbital, the optimised basis set will describe this orbital better than the much more chemically interesting 4f orbital. In order to get a good representation of the valence region very many core functions may therefore be required in generating the basis set but be of little value for most calculations. It is therefore common practice to contract

the basis set, combining many core functions to a more reasonable number by means of a linear combination with fixed contraction coefficients. There are two ways of contracting GTOs (known as Primitive GTOs, PGTOs), by means of either a segmented or general contraction scheme. The terminology now changes a little such that a basis set labelled DZP has a double zeta valence with single polarisation in the contracted GTOs (CGTOs) and thus may be formed from very many more PGTOs.

Segmented contraction schemes follow the rule that each PGTO is used by only one CGTO whilst in a General contraction scheme all the PGTOs are used to form all the CGTOs, as shown below in fig. 1.6.

	SEGMENTED CONTRACTION				GENERAL CONTRACTION			
	CGTO1	CGTO2	CGTO3	CGTO4	CGTO1	CGTO2	CGTO3	CGTO4
PGTO1	X				X	X	X	X
PGTO2	X				X	X	X	X
PGTO3	X				X	X	X	X
PGTO4	X				X	X	X	X
PGTO5	X				X	X	X	X
PGTO6	X				X	X	X	X
PGTO7		X			X	X	X	X
PGTO8		X			X	X	X	X
PGTO9		X			X	X	X	X
PGTO10			X		X	X	X	X
PGTO11				X	X	X	X	X

Figure 1.6– Schematic for Segmented and General Contraction. Segmented scheme is of 6-311G form.

The choice of basis set is crucial for a calculation: performing a high level calculation is of little value if using a minimum basis set and similarly there is likely to be little value in using a quadruple zeta polarised basis set to perform a Hartree-Fock calculation. A basis adequate for the method employed is always required, as described by the Pople-square paradigm, a schematic of which is shown below, fig. 1.7.

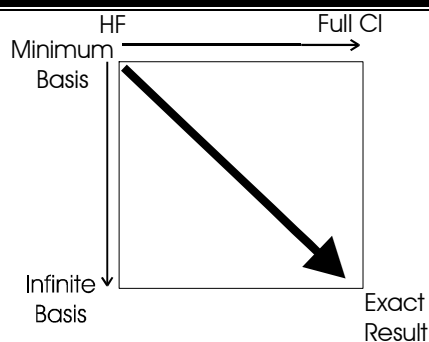


Figure 1.7- Schematic of the Pople-square paradigm

1.2.4.3.1 Pople Style Basis Sets

These basis sets are of the split valence type. This means that the valence is split into two or more sub-spaces with different contractions. The naming guide for these basis sets is $k-nlmG$, where k is the number of PGTOs contracted to form each core orbital, n is the number of PGTOs contracted to form each of the first set of valence orbitals, l the second and m the third. G stands for Gaussian. Polarisation is represented by one or more asterisks after the G. Thus the segmented contraction scheme in figure 1.6 is a 6-311G basis set. Inclusion of one set of orbitals of higher angular momentum would result in a 6-311G* basis set.

1.2.4.3.2 ANO Basis Sets

Atomic Natural Orbital basis sets use a general, rather than segmented contraction scheme. The contraction scheme is determined by means of a correlated calculation on the atom, generally at the CISD level. The natural orbitals generated and their occupancies (see section 1.2.1.5.2 for a description) determine the combinations of PGTOs. Different quality contractions may be determined by varying the natural occupancy threshold. This approach has two major advantages: the basis sets are well designed for correlated calculations and all the basis sets for an atom use the same set of primitive functions and thus genuinely form a set which can be systematically improved if required.

1.2.4.3.3 Correlation Consistent Basis Sets

These have been developed by the research group of Dunning and are similar to ANO basis sets in that they use a general contraction scheme and can be systematically improved. They have the advantage, however, that they require fewer PGTOs and are thus less computationally demanding. The name correlation consistent (cc) is used to describe these basis sets as they include correlating orbitals in a consistent manner, according to the impact on energy. Thus, as the first f-function added to a basis set will give a similar contribution to the energy as a second d-function, the first f-function and second d-function should be added concurrently. The basis set cc-pVDZ is a correlation consistent polarised valence double zeta basis which, for carbon, has 9s, 4p and 1d PGTOs contracted to 3s, 2p and 1d CGTOs by a general contraction scheme. This contraction is generally expressed as (9s4p1d/3s2p1d). The Correlation Consistent Basis sets of Dunning gives results of comparable accuracy to those of ANO basis sets, however, the ANOs remain a benchmark due to their less empirical formulation of contraction coefficients.

1.2.4.3.4 Pseudopotentials

As described above much of the energy contribution to the basis set arises from the core orbitals, whilst much of the chemical interest lies in the valence. Part of the solution to this problem is to use a contraction scheme to form the basis set, however, for very heavy elements, such as the lanthanides, the large number of integrals required for the core orbitals may make some calculations difficult if not unfeasible. A solution to this problem is provided by pseudopotentials. These model the core orbitals (or a significant proportion of the core) by means of a potential and model only the valence orbitals explicitly using basis functions. The functions used must be specially designed to be nodeless in the core region but have the correct radial nodality in the valence region. This is done using pseudo-orbitals. Pseudopotentials may be generated from an all-electron HF calculation or, as is often the case for heavy atoms, a Dirac-Hartree-Fock (DHF) calculation, thus enabling the inclusion of scalar relativistic effects (see section 1.2.4). Whilst it may often be necessary to use pseudopotentials when investigating lanthanide systems, especially if they are large and with little symmetry (see section

1.2.5), care must be taken in selecting an appropriately sized ‘core’. For example, whilst the 4f orbitals are generally considered ‘core-like’ including them in the core could be problematic in some cases. This is because, whilst functions are included to allow for additional occupation of the f orbitals, no reduction in the formal number of f-electrons is possible in this case, this being fixed by the core potential. Thus, such pseudopotentials cannot correctly model a lanthanide system where the f density is reduced from the formal value. However, including the 4f orbitals in the core may be very useful in calculations on some lanthanides systems. Complexes of the later lanthanides are very unlikely to involve the f-orbitals in bonding and representing them in the valence may make convergence of the SCF very difficult, especially in low symmetry systems where there is likely to be a large degree of f-orbital degeneracy. In these cases, the SCF may ‘flip’ between configurations with an f-electron in one of two or more, near-degenerate orbitals. Including the f-orbitals in the core of a pseudopotential avoids these convergence problems.

1.2.5 Relativity

The Schrödinger equation does not include the effects of special relativity, for which all four dimensions must be treated even-handedly. Dirac reformulated the Schrödinger equation in 1928 to do this and thus incorporate relativity⁴¹. The Dirac equation yields four-component wavefunctions, with spin now explicit in the wavefunction. The other two components of the wavefunction are the positron results, which were first predicted by the Dirac equation.

$$\left[c\boldsymbol{\alpha} \cdot \mathbf{p} + \beta mc^2 \right] \Psi = i \frac{\partial \Psi}{\partial t}$$

Equation 1.19- Time-dependent Dirac Equation, where $\boldsymbol{\alpha}$ and β are 4x4 matrices and \mathbf{p} is the momentum operator

The two electron spin components to the wavefunction are known as the large components and the positron components the small components. The small components contribute the lowest-order corrections to the electron-electron interactions but also result in the most two-electron integrals, and thus the most computational demand⁴².

The time-independent Dirac equation forms the basis of the implementation of relativity into calculation.

$$\left[c\boldsymbol{\alpha} \cdot \mathbf{p} + \beta mc^2 + \hat{V} \right] \Psi = E\Psi$$

Equation 1.20- Time-independent Dirac Equation, \hat{V} is the potential operator.

The computational cost of implementing this four-component equation as the Dirac-Fock equation is so severe that most electronic structure programmes utilise approximations to incorporate relativity more feasibly. These approximations involve removal of the small, positronic components.

The Foldy-Wouthuysen transformation⁴³ can be used to reduce the four-component wavefunction to two components. However, this must be approximated when a general potential is used. In this work two approximations are used. The first is the Douglas-Kroll-Hess (DKH)⁴⁴⁻⁴⁶ approximation. Alternative to the Foldy-Wouthuysen transformation, the Breit-Pauli approximation, may be employed and can be expanded to different orders. The other approximation used is the zeroth order regular approximation (ZORA)^{47, 48}. Both of these implementations exclude spin-orbit coupling and are said to include scalar relativistic effects.

1.2.5.1 Scalar Effects

As mentioned in section **1.1.1.1** scalar relativistic effects must be included in any serious consideration of lanthanide chemistry in order to properly account for the behaviour of the valence electrons. Three different methods for the inclusion of scalar relativity, all of a comparable accuracy, are referred to in this work. They are:

1.2.5.1.1 ZORA

ZORA derives from the Breit-Pauli approach in which the small component of the wavefunction is eliminated by assuming no magnetic fields and thus deriving a relation between the small and large components which is used subsequently. This relation is:

$$\begin{aligned}\psi^S(\mathbf{r}) &= \left(1 + \frac{E-V}{2mc^2}\right)^{-1} \frac{\boldsymbol{\sigma} \cdot \mathbf{p}}{2mc} \psi^L(\mathbf{r}) \\ &= K(E, \mathbf{r}) \frac{\boldsymbol{\sigma} \cdot \mathbf{p}}{2mc} \psi^L(\mathbf{r})\end{aligned}$$

Equation 1.21- Breit-Pauli relation between the small component and the large component, where $\boldsymbol{\sigma}$ are the Pauli spin matrices and K a local multiplicative operator which depends on the energy of the electron.

K is then expanded with $\frac{E}{2mc^2 - V}$ as the expansion parameter. Using only the first term of the expansion yields the Zeroth Order Regular Approximation, and by application of the Dirac relation, the scalar relativistic ZORA.

$$\left\{ \frac{1}{2m} \mathbf{p} \cdot \left(1 - \frac{V}{2c^2}\right)^{-1} \mathbf{p} + V \right\} \psi^{scZORA}(\mathbf{r}) = E^{scZORA} \psi^{scZORA}(\mathbf{r})$$

Equation 1.22- Scalar Relativistic ZORA equation

ZORA is a widely used approach and is generally adequate for most calculations. However it does suffer from not being gauge invariant. This means that in the presence of an external potential the energy of all the orbitals will not be shifted equally. This can lead to problems in the calculation of ionisation energies.

1.2.5.1.2 DKH

The basis of the Douglas-Kroll-Hess method is the Foldy-Wouthuysen transformation⁴³ which attempts to iteratively decouple the small components of the relativistic wavefunction from the large components and then discard them by means of a unitary operator. This can be done exactly in the absence of a potential but is not possible in the presence of a potential and thus additional transformations must be defined, in order to reduce the coupling in a step-wise manner. Two such additional transformations yield the second-order DKH or DKH2 Hamiltonian. This is the most common implementation of DKH and that which has been used in this work.

DKH is gauge invariant and therefore does not suffer the same problems as ZORA is liable to. However, it is subject to the picture change error. The picture change error arises when relativity is accounted for differently for different aspects of the system-

yielding a change in ‘picture’. In the case of DKH this is due to the fact that generally the transformation is applied only to one-electron matrix elements, not two-electron interactions, which is inconsistent. There is therefore an error in the electron-electron interaction which generally mitigates against the advantage of using DKH Hamiltonians of greater than DKH2.

1.2.5.1.3 RECPs

When employing either the DKH or ZORA Hamiltonian appropriate basis sets must be used. These basis sets are optimised for relativistic Hamiltonians as using non-relativistic basis sets will generate unreliable results. An alternative approach is to use Relativistic Effective Core Potentials. These are atomic basis sets of the same form as the pseudopotentials described in 1.2.4.3.4 but they model relativistic atoms. This enables the inclusion of relativity using a non-relativistic Hamiltonian. This is because direct relativity is most significant for the core electrons. If these are treated with a RECP, which also provides the indirect relativistic effects to the valence electrons, a non-relativistic Hamiltonian is suitable for the treatment of the valence electrons. The results generated using RECPs are often very accurate and it has been argued that they may be not only undemanding of resources but also more accurate than the most common implementations of scalar relativity⁴⁹. However, as for the pseudopotentials, they must be used with care to ensure an appropriately sized core is selected.

1.2.5.2 Spin-Orbit Coupling

Spin-orbit coupling is less likely to be significant for lanthanide systems than is the case for the actinides but should be included in a thorough treatment. As mentioned in 1.1.1.1, spin-orbit coupling arises from the coupling of the spin angular momentum of an electron with its orbital angular momentum, s and l respectively. Spin orbit coupling becomes particularly important when considering the ordering of electronic states of a system, the energy splittings of those states and the allowed transitions between them. This is because spin-orbit coupling acts to reduce the degeneracy of terms with a given L and S resulting in different values of J . This occurs for all states with $L > 0$.

Spin-orbit coupling is included in a complete treatment of relativity. Four-component implementations are still very rare and it is normally accounted for either by spin-orbit coupled two-component methods or by coupling together electronic states which are treated at the scalar relativity level.

Having considered approaches to the inclusion of relativity in calculations, we can now expand the Pople square, fig. 1.7 to a third dimension, including relativistic effects such that ideally calculations should line along the line $x=y=z$, treating basis set, method and relativity to a similar degree of accuracy, as shown in fig. 1.8, below.

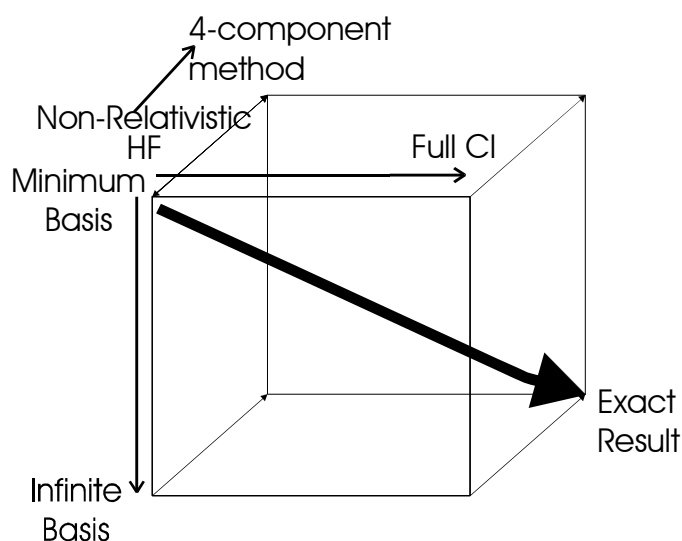


Figure 1.8- Schematic of the "Visscher-cube" paradigm⁵⁰

1.2.6 Symmetry Considerations

Many organometallic molecules are pleasingly symmetric. Not only is this aesthetically satisfying, it can be very useful both for the rationalisation of experimental results and the computational feasibility of calculations. Experimentally a highly symmetric molecule will tend to have fewer allowed electronic transitions than one of lower symmetry, which can be very helpful in identifying the nature of the transitions involved. This is similarly useful for calculations, especially in cases with a high density of states. Furthermore, the inclusion of symmetry in calculations can reduce computational time as some matrix elements can automatically be set to zero and thus need not be calculated. However, most electronic structure codes are not able to properly enforce symmetry for all point groups. This means that a calculation may have

to be run in a lower symmetry point group to that of the molecule. In theory this should be no problem, the computational time will increase but matrix elements which would be zero in the correct point group will be calculated at near-zero values. Unfortunately this is not always the case and orbitals which are not formally allowed to mix may do so, giving erroneous results. It is especially important to be aware of symmetry lowering problems when carrying out CASSCF calculations as the symmetry lowering can lead to an unbalanced active space. This problem and some of the possible solutions to it will be discussed further in chapter 3.

1.2.7 Level of theory

Figures 1.7 and 1.8 show a change in level of theory from the lowest level calculations along the optimum arrow of calculation improvement to the highest level possible calculation. There are well-known points along this line for which the errors are well known and well documented. This arises from a large body of work from which these errors have been established. For example, the B3LYP functional in conjunction with the 6-31G* is a well established level of theory which is suitable for many organic systems but which is known not to be able to appropriately account for dispersion. In the field of inorganic chemistry calculations there is no such well established level of theory. This means that currently many published calculations initially involve significant method-testing components.

1.2.8 Some notes on convergence

The word convergence can be used in several different contexts. In a geometry optimisation convergence is achieved when a structure is obtained with a gradient of the energy with respect to the atom positions of zero (within pre-determined limits). In an SCF calculation convergence means that the further changes to the molecular orbitals makes no difference to the energy of the system (within pre-determined limits). Convergence of basis set may also be achieved. This occurs when further enlargement of the basis set for an atom does not lead to further energy lowering for the system.

1.2.9 Software packages used

A pragmatic approach has been taken throughout this work and consequently several different software packages have been used, depending on their relative strengths for solving different problems. The three packages used have been Gaussian03⁵¹, Molcas 6.4/7.2⁵² and ADF2008⁵³. Gaussian has been used for geometry optimisations, Molcas for CASSCF/CASPT2 calculations and ADF for TD-DFT calculations and some geometry optimisations.

1.2.9.1 Gaussian

The Gaussian software package uses Gaussian-type basis sets and effective core potentials. This enables analytical integration to be carried out. Gaussian is a multi-purpose software package which means that a variety of techniques can be employed, using the same basis sets. In this work Gaussian geometry optimisations have been performed at the HF, MP2, B3LYP and TPSS levels of theory. Gaussian accounts for relativity using relativistic effective core potentials as well as through the Douglas-Kroll formalism.

1.2.9.2 Amsterdam Density Functional (ADF)

The ADF software package mainly uses Slater-type basis sets. This means that numerical integration must be performed, which can be somewhat slower than a method using analytical integration. ADF is well developed for carrying out density functional calculations and is a good tool for TD-DFT. In this work ADF has been used for TD-DFT calculations using the SAOP functional, as well as PBE for geometry optimisations. ADF accounts for relativity using ZORA. Spin-orbit coupling can also be included within this formalism.

1.2.9.3 Molcas

The Molcas software package mainly uses Atomic Natural Orbitals. These basis sets are specially designed to be used for CASSCF calculations, for which this software package is developed. In this work Molcas has been used for CASSCF and CASPT2 calculations. Molcas accounts for relativity using relativistic ANOs in conjunction with the Douglas-Kroll formalism. Spin-orbit coupling can be included using the RASSI⁵⁴ module of the code, which computes the spin-orbit interaction matrix elements from a set of spin-free states and the resulting spin-orbit eigenstates.

2. Cerocene

2.1 Previous studies

As mentioned previously, cerium exists in both the 3+ and 4+ oxidation states in its compounds¹. A well known example of disputed Ce oxidation state in a molecular system is that of cerocene and it is this compound which will be the subject of this chapter. The cerocene molecule is formed of two cyclooctatetraenyl rings sandwiching a cerium ion, a motif which is only found in the f-block⁵⁵ and may alternatively be termed di- π -cyclooctatetraene(COT) cerium or bis(π -[8]annulene)cerium.

2.1.1 Experimental Approach

Cerocene was first synthesized serendipitously in 1976⁵. This synthesis was then replicated by Streitweiser et al. in 1985⁶ who investigated the oxidation state using experimental and theoretical methods. There are several different ways of establishing the oxidation state of a metal in an organometallic system experimentally.

2.1.1.1 Photoelectron spectroscopy

Streitweiser et al.⁶ studied the molecule using He I/II photoelectron spectroscopy and scattered wave X_α computational methods, both of which indicated a 4+ oxidation state. However, it is also important to note that it is unlikely that even if a 4f electron was localized on the cerium (i.e. if the Ce was Ce(III)) this would not be apparent in the photoelectron spectrum unless variable energy photoelectron spectroscopy (VEPES) was performed. VEPES is required to get a more accurate idea of whether or not an electron occupies an f-orbital in a molecule because such electrons display a delayed maximum in their photoelectron cross-section such that they exhibit significant intensities only at incident photon energies much higher than are achievable using a He discharge lamp. This behaviour, which contrasts with that for s and p orbital electrons

but is exhibited to some extent by those occupying d orbitals, arises due to the high angular momentum of the f orbitals and is explained in more detail in chapter 3⁵⁶. Thus, as the energy of the incident photons in either He I or He II PES is not typically sufficient to easily observe f-electron ionisations this method would not be expected to yield conclusive results regarding Ce f-orbital population.

2.1.1.2 X-Ray Absorption Near Edge Structure (XANES)

XANES is a very useful technique for investigating oxidation state as it probes the absorption of X-rays by an atom at energies near to the core binding energies. The probability of absorption is modulated by the chemical environment of the atom and is therefore extremely susceptible to the formal oxidation state of the atom⁵⁷. Additionally, because of the penetrating ability of hard X-rays XANES can be used for crystals, disordered solids and solutions and is not surface sensitive. Ce(III) cerocene is supported by experimental work using X-ray absorption spectroscopy^{10, 11}. XANES K- and L_{III}-edges were determined for a range of cerium compounds, including ring-substituted cerocene. However, there remains some dispute over the oxidation state, largely due to skepticism regarding the interpretation of the XANES data. This is because the oxidation state of cerium is determined with reference to 3+ and 4+ oxidation state standards, and the edge position relative to these, as well as the edge shape are considered in assigning an oxidation state. The edge position data are more reliable for K-edge XANES as this results in a more significant difference between 3+ and 4+ standard edge positions. However, the L_{III} edge data appear to show features characteristic of 4+ standards. It is this characteristic in particular which could be viewed with some skepticism.

2.1.1.3 Cyclic Voltametry

This method involves cyclically ramping and reducing the voltage applied to a solution and measuring the resulting current. This yields very reliable data regarding the redox potential of the solute. In practical terms the greatest motivation for determining the oxidation state of a metal in a complex is in order to be able to make redox predictions.

In this case, cyclic voltametry provides the most reliable experimental measure of oxidation state. However, it does not necessarily offer information regarding metal electron density and thus cannot yield information about the nature of the metal-ligand bonding in a specific complex. Cyclic voltammetry data collected for $\text{K}[\text{Ce}(\text{tert-butylC}_8\text{H}_7)_2]$ and $\text{Ce}(\text{tert-butylC}_8\text{H}_7)_2$ indicate that Ce in the substituted cerocene is in the 4+ oxidation state¹³.

2.1.1.4 Magnetic Measurements

From a single-configurational perspective, cerium in the 3+ oxidation state has one unpaired (f) electron and is therefore paramagnetic with typical μ_{eff} of ~ 2.5 Bohr Magnetons³ whilst cerium in the 4+ oxidation state has no unpaired electrons and is therefore diamagnetic.

Magnetic measurements⁶ have shown diamagnetism in cerocene. This might be seen as evidence in support of the Ce(IV) model as there is no magnetic moment in this case, where there are no metal-based valence electrons. However, the apparent diamagnetism of cerocene might also be achieved if an open shell singlet is formed¹².

In 1989 Fulde and Neumann⁵⁸ proposed the existence of a molecular Kondo singlet state and suggested cerocene as a possible candidate. The Kondo effect was described in 1964 by Jun Kondo in his seminal paper⁵⁹. The effect is displayed by some solid state systems and can be explained in terms of the Anderson Impurity Model. In this model an unpaired electron in a localized impurity orbital couples to an unpaired electron in the conduction band, thus forming a singlet. This results in characteristic properties such as increased resistivity below the Kondo temperature in bulk materials. The Kondo temperature is the temperature below which the localized impurity electron polarises an electron in the conduction band. In recent years the effect has been observed in nanoscale materials⁶⁰⁻⁶³ but if cerocene does indeed represent a molecular Kondo system it will be the first to have been identified. In 2005 Booth et al. suggested that this was indeed the case¹¹, the major justification being the magnetic data which, on detailed analysis and the removal of the diamagnetic contribution from the COT ligands, show van Vleck temperature independent paramagnetism (TIP), which the

authors suggest is a manifestation of the Kondo effect. The weight of the experimental evidence is somewhat lessened by the fact that the diamagnetic correction is six times larger than the measured magnetic susceptibility and the resultant TIP therefore approximately equal magnitude but of opposite sign to the diamagnetic correction. Van Vleck TIP is expected to be small (typically of the order of 10^{-5} emu mol⁻¹)⁶⁴ but this does leave the results open to the suggestion that a small error in the calculation of the diamagnetic correction could lead to significant errors in the TIP calculated.

In summary, the experimental evidence which any successful computational study would hope to be consistent with is:

- i) *n_f value obtained from XANES* – The Ce f orbital population, *n_f*, can be calculated with reference to the weights of different configurations in a multiconfigurational method, or, for greater reliability, the f-character of the occupied orbitals and the population of those orbitals.
- ii) *Magnetic susceptibility measurements*- Spin polarization can be calculated using programs which determine electron density differences, where spin density data is available from the calculation.
- iii) *He I/II photoelectron spectroscopy*- Energy differences between the electronic states of the cation can be related to the energy gaps between the peaks in the photoelectron spectrum.
- iv) *Electronic excitation spectra*- This involves calculating the energies of different electronic states of the molecule relative to the ground state. Ideally the allowed transitions calculated would be consistent with those observed in the UV-Vis spectrum.

i), ii) and iv) should in theory be obtainable from calculations performed exclusively on the neutral CeCOT₂ molecule. However, iii) would also require calculations on the cation and will give information on the cation states rather than elucidating the bonding in the neutral significantly. This work aims to find agreement with i) and iv).

2.1.2 Previous Calculations

The earliest calculations have not attempted to reproduce experimental data but rather to determine the electronic structure of the molecule and note the f-orbital occupancy and thus the Ce oxidation state. A range of methods has been employed, as noted above, and indicated Ce(IV).

Dolg and Fulde subsequently carried out computational studies in the 1990s^{8, 9, 12} employing the Multi-Configurational SCF (MCSCF), Multi-Reference Configuration Interaction (MRCI) and Average Coupled-Pair Functional (ACPF) approaches. The results of these calculations suggested a ground state dominated by the 3+ oxidation state of cerium. These calculations will be discussed more fully in section **2.5.1**.

Despite both some experimental and computational data indicating Ce in the 3+ oxidation state in cerocene, Streitweiser¹³ has suggested that ‘it is chemically reasonable and consistent to regard the central metal in this case as formally +4’. Whilst the computational work of Streitweiser et al.⁶ also indicated a 4+ oxidation state the emphasis in Streitweiser’s statement is that, regardless of other analysis the basis on which to determine oxidation state is the chemistry and electrochemistry of the molecule which, after all, is why it is important to know the oxidation state of the metal.

2.2 Aims

The aim of this study is to use multiconfigurational methods to determine the electronic structure of the cerocene molecule and to add to the data currently available regarding the oxidation state of cerium within the molecule. Data which can be compared with experimental observables will be particularly focused on.

Some of the most recent computational work¹² on cerocene is purported to show agreement with experimental points i) and ii) on the previous page¹¹. To a certain extent, therefore, it is the aim of this work to corroborate the results of previous studies

using the latest techniques available and to extend the possibilities for comparison with the experimental data.

In addition, in order to better critique the comparison of experimental and computational results, XANES experiments were carried out on a range of formally Ce(III) and Ce(IV) compounds, synthesised by Dr Andrea Sella, in an attempt to benchmark Ce(III) and Ce(IV) standard positions of the Ce L_{III} edge.

2.2.1 Broader context of calculations

The calculations and experimental data on cerocene presented here form part of a broader work on actinocenes, to which they serve as a contrast. The calculations on actinocenes (thoracene and protactinocene) were carried out by Dr Andrew Kerridge. Some of the main differences between the results obtained for cerocene and those for the actinocenes are presented in section 2.5.1.

2.3 Computational and Experimental details

2.3.1 Experimental Details- XANES

Room temperature Ce L_{III} edge measurements were made at station 7.1 of the Daresbury Synchrotron Radiation Source, which operates at 2 GeV with a typical current between 120 and 200 mA. Station 7.1 is equipped with a double crystal Si(111) monochromator, and ion chambers for measuring incident and transmitted beam intensity. All spectra were calibrated by repeated measurements of the Ce L_{III} edge of CeO₂, the Ce(IV) standard. The data were processed using a suite of programs available at the Daresbury Laboratory, namely EXCALIB and EXBROOK and EXCURV98. The positions of the Ce L_{III} edges were determined by taking the inflection point of the "white line" of the absorption.

2.3.2 Computational Details

Geometry optimisations were performed using the Gaussian03⁵¹ suite of programs and the B3LYP hybrid density functional. The basis sets used were cc-PVDZ⁶⁵ for C and H. The relativistic effective core potential (RECP) of the Stuttgart-Dresden group was used for Ce⁶⁶, together with the valence basis set of Cao and Dolg in the segmented contraction with the g-functions removed. RHF/MP2 and TPSS geometry optimisations were also performed within this suite of programs.

RHF, B3LYP, CASCI and CASPT2 partial optimisations were carried out within the Molcas 6.4⁵² program. These partial optimisations involved single point calculations performed at a range of Ce-ring distances with the C₈H₈ ring structure fixed at that obtained from the calculations of Dolg et al.⁹. For each method employed these partial optimisations form a potential energy curve, the minimum of which approximates to the lowest energy geometry. ANO basis sets were used on all the atoms. For Ce this was of VQZ quality with contraction scheme (25s22p15d11f4g2h)/[9s8p5d4f]⁶⁷. For C and H the basis sets were of DZP quality with contraction schemes (14s9p4d3f2g)/[3s2p1d]⁶⁸ and (8s2p3d1f)/[2s1p]³⁸ respectively. This combination of basis sets will henceforth be known as basis A. In order to ensure that this basis was adequate larger basis set calculations were also subsequently performed. Basis B comprises Ce (25s22p15d11f4g)/[9s8p5d4f3g], of QZP quality and retains the DZP basis sets for C and H. Basis C comprises the QZP basis for Ce and TZP quality basis sets for C and H, (14s9p4d3f2g)/[4s3p2d1f] and (8s2p3d1f)/[3s2p1d], respectively. Relativistic effects were included via the Douglas-Kroll formalism⁴⁴⁻⁴⁶.

Spin orbit coupling was included in order to determine the effect on the electronic excitations by means of the RASSI⁵⁴ module in the Molcas program.

State-averaged calculations were performed for the ¹A_g state. The number of states used in the average was varied from two to ten, in all cases with equal weights.

Much of the computational analysis presented in this chapter involves natural orbitals (NOs) and their occupations (NOOs). These are specific to each state, *i.e.* they are

computed from the reduced density matrix of each state and not from the state averaged matrix (the latter is used to produce the pseudo-NOs which are output by default in MOLCAS).

The f electron occupancies, n_f , have been calculated as the product of the NOOs and f coefficient of the natural orbital squared, summed over all of the active space orbitals. This procedure implicitly assumes orthogonality of the metal and ligand basis sets. In actual fact, there is significant overlap between them, and this overlap can be estimated from the NO normalisation constants. This in turn is used to estimate a corresponding error in the quoted occupancies.

CASSCF, B3LYP and RHF calculations were also performed at the unpublished, but accepted, experimentally determined Ce-ring distance, for consistency with previous computational work⁶⁹.

2.3.2.1 Symmetry considerations and active spaces

Molcas allows the symmetry of a molecule to be defined as the highest Abelian point group to which it belongs for which all the symmetry operations can be generated by a combination of in-the-plane reflections and 180° rotations. Thus, although the cerocene molecule is D_{8h} it can only be described in terms of the irreducible representations of the D_{2h} point group. A subduction table showing the descent of symmetry from D_{8h} to D_{2h} is given below in table 2.1⁷⁰.

D_{8h}	D_{4h} C_{2v}, σ_v	D_{4h} C_{2d}, σ_d	D_{2h} C_{2v}	D_{2h} C_{2d}
A_{1g}	A_{1g}	A_{1g}	A_g	A_g
A_{2g}	A_{2g}	A_{2g}	B_{1g}	B_{1g}
B_{1g}	A_{1g}	A_{2g}	A_g/B_{1g}	A_g/B_{1g}
B_{2g}	A_{2g}	A_{1g}	B_{1g}/A_g	B_{1g}/A_g
E_{1g}	E_g	E_g	$B_{2g} \oplus B_{3g}$	$B_{2g} \oplus B_{3g}$
E_{2g}	$B_{1g} \oplus B_{2g}$	$B_{1g} \oplus B_{2g}$	$A_g \oplus B_{1g}/B_{1g} \oplus A_g$	$A_g \oplus B_{1g}/B_{1g} \oplus A_g$
E_{3g}	E_g	E_g	$B_{2g} \oplus B_{3g}$	$B_{2g} \oplus B_{3g}$
A_{1u}	A_{1u}	A_{1u}	A_u	A_u
A_{2u}	A_{2u}	A_{2u}	B_{1u}	B_{1u}
B_{1u}	A_{1u}	A_{2u}	A_u/B_{1u}	A_u/B_{1u}
B_{2u}	A_{2u}	A_{1u}	B_{1u}/A_u	B_{1u}/A_u
E_{1u}	E_u	E_u	$B_{2u} \oplus B_{3u}$	$B_{2u} \oplus B_{3u}$
E_{2u}	$B_{1u} \oplus B_{2u}$	$B_{1u} \oplus B_{2u}$	$A_u \oplus B_{1u}/B_{1u} \oplus A_u$	$A_u \oplus B_{1u}/B_{1u} \oplus A_u$
E_{3u}	E_u	E_u	$B_{2u} \oplus B_{3u}$	$B_{2u} \oplus B_{3u}$

Table. 2.1- Descent of Symmetry from D_{8h} to D_{2h}

The active space chosen for the CASSCF calculations comprised 8 electrons in 14 orbitals, namely the highest energy e_{2g} and e_{2u} occupied orbitals ($a_g \oplus b_{1g}$ and $a_u \oplus b_{1u}$ in D_{2h}) from the RHF calculation as well as unoccupied e_{1u} , e_{2u} , e_{3u} , e_{1g} and e_{2g} orbitals. These correspond to the four highest energy occupied ring orbitals and six of the seven f orbitals of the Ce (the two f_π span e_{1u} ($b_{2u} \oplus b_{3u}$), the two f_δ span e_{2u} ($a_u \oplus b_{1u}$) and the two f_ϕ span e_{3u} ($b_{2u} \oplus b_{3u}$)) as well as four of the five 5d orbitals of the Ce (d_π spans e_{1g} ($b_{2g} \oplus b_{3g}$), d_δ spans e_{2g} ($a_g \oplus b_{1g}$)). The f_σ and d_σ orbitals are not included explicitly as in D_{2h} these span the same irreps as one of the f_δ and d_π (b_{1u} and a_g , respectively). There is thus sufficient flexibility in the active space to utilise these orbitals if necessary. However, inclusion of additional unoccupied b_{1u} and a_g orbitals in the active space removes the degeneracy of the f and d orbitals, which are degenerate (e_{2g} and e_{2u}) in the correct D_{8h} symmetry and therefore it was considered that the most well-balanced active space would exclude these in order to prevent symmetry breaking.

A qualitative molecular orbital diagram for cerocene, with the active space orbitals highlighted in red, is presented below, fig. 2.1.

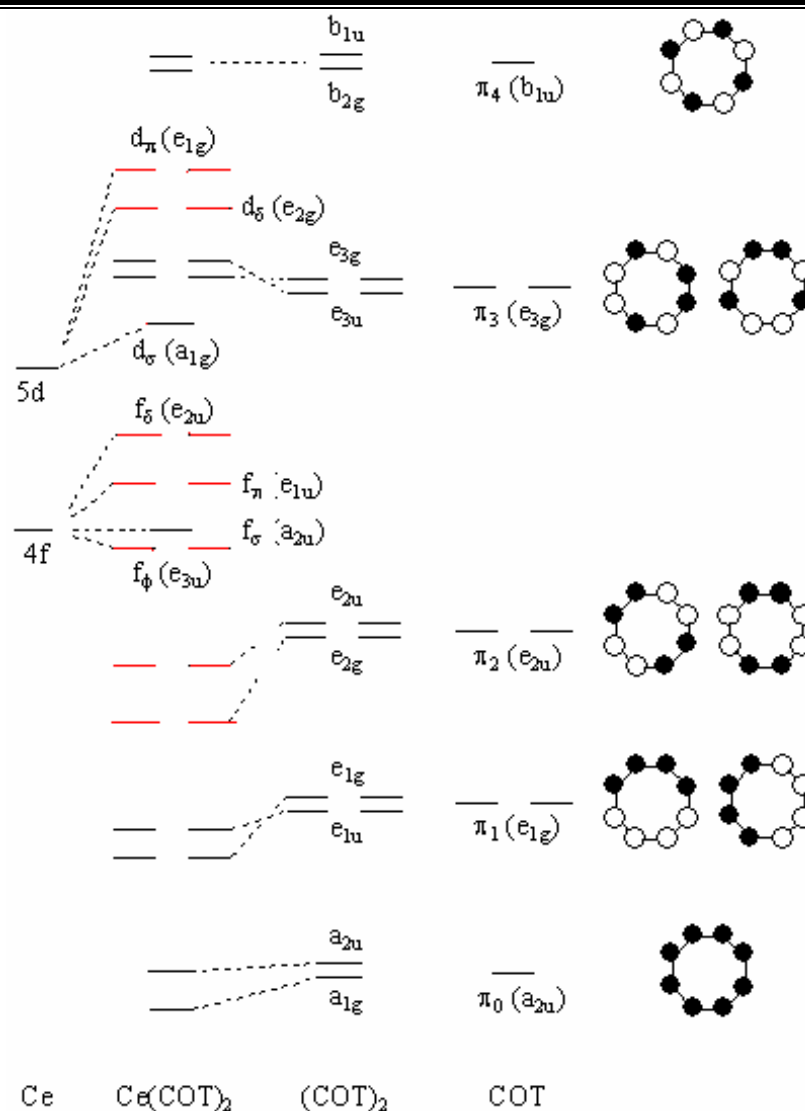


Figure 2.1- Qualitative molecular orbital diagram for cerocene. Orbitals highlighted in red are contained within the smallest active space.

This active space was chosen based on several criteria:

i) DFT calculations and RHF calculations using the improved-virtual-orbitals (IVO) method in Molcas⁷¹, as these two methods generate more chemically sensible virtual orbitals than the RHF method. It was found that the four highest occupied orbitals formed a group separated from the next highest in energy by a large energy gap of 2.7 eV.

ii) Chemically sensible symmetry choice. The chemically active orbitals are expected to be the e_{2u} and e_{2g} orbitals and the Ce f and d orbitals, therefore orbitals of the corresponding symmetry were chosen.

iii) Ideally as many orbitals as possible would be included within the active space. Therefore as many orbitals were included as chemically sensible within the computational limits. A 12 electrons in 16 orbitals active space was chosen initially, however, this is at the upper limit of computational possibility for the basis sets chosen and the point group of the molecule with the computational equipment available. Calculations using this active space suggested that the 2 lowest energy orbitals (of e_{1g} symmetry) were not involved to any significant extent (i.e. the natural occupancies of these natural orbitals did not vary much from integer values), thus for much of the analysis, the (8, 14) active space indicated in fig. 2.1 has been employed, although the (12, 16) active space was used for partial geometry optimisations.

iv) For genuine comparison of results it is essential to use the same active space as previous researchers. Previous theoretical studies¹² have used an 8 electron 11 orbital active space. Thus it is sensible to include as a minimum these orbitals.

v) There have been some suggestions from the developers of the Molcas program that for lanthanide systems the active space should be chosen based on a RASSCF calculation. However, results obtained using the RASSCF method are susceptible to variations in the number of excitations from/to RAS1/3 and size of RAS2 and therefore in this case the active space selection has been based on criteria i)-iv)

2.3.2.2 Note

The computational results detailed below were obtained from calculations carried out in conjunction with Dr Andy Kerridge.

The experimental results were obtained from experiments carried out on samples synthesised by Dr Andrea Sella.

2.4 Results

2.4.1 XANES results

Ce L_{III} edge data suggest that the spread of edge positions amongst a selection of generally accepted Ce(III) and Ce(IV) compounds is greater than the gap between the two groups of compounds, the data effectively forming a continuum. Although the Ce(III) compound edge positions are at lower energies than those of Ce(IV) compounds, it is questionable whether it is possible to unequivocally identify each compound as Ce(III) or Ce(IV). These data are detailed below in figure 2.2.

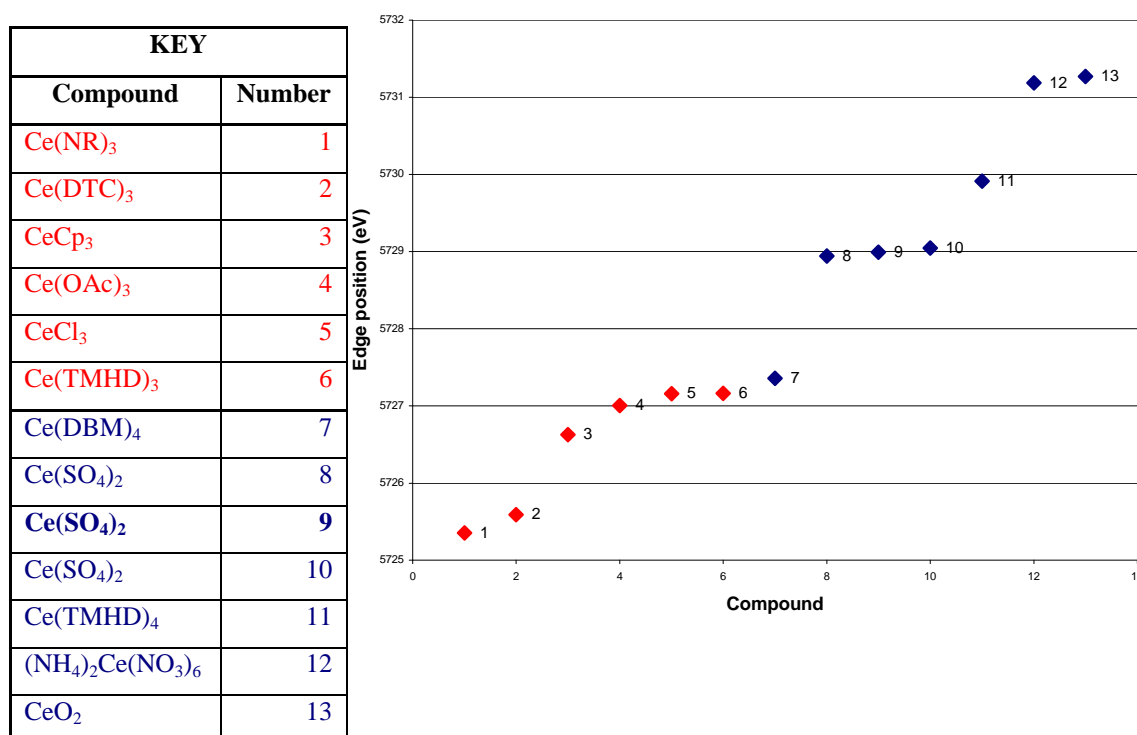


Fig. 2.2- XANES L_{III} edge white line positions for a range of formally Ce(III) (red) and Ce(IV) (blue) compounds. Compound 9 is the average of 8 and 10. TMHD is 2,2,6,6-tetramethyl-3,5-heptanedione. DBM is 1,3-Diphenyl-1,3-propanedione. DTC is dithiocarbamate. R is N(SiMe₃)₂

The conclusions drawn from this work are that, unlike the K edge used in earlier work¹⁰, the Ce L_{III} edge is a poor means of differentiating between Ce(III) and Ce(IV) compounds. This will be discussed subsequently in the comparison with other work (2.5.1).

2.4.2 Full geometry optimisations using Gaussian03

Table 2.2 below shows the Ce-COT distances (r_{RM}), COT ligand C-C separations (r_{C-C}) and C-C-H angles ($\angle CCH$) (highlighted in figure 2.3) obtained for cerocene generated from full geometry optimisations using several different computational methods, as well as the experimentally determined value for the Ce-COT distance⁶⁹. All calculations were carried out on the 1A_g ground state. No frequency calculations were carried out. The COT²⁻ rings are planar as they are aromatic. However, if electron-density were to move from the COT rings to the Ce centre the π -electron count would be reduced from 2 and the corresponding Hückel number of 10 would also be reduced with a potential loss in aromaticity. However, some studies have indicated that in some cases the planarity of the COT rings may be due to enhanced complexing ability in this geometry rather than aromaticity⁷².

	r_{RM} (Å)	r_{C-C} (Å)	$\angle CCH$ (°)
Exp.	1.969	-	-
RHF	1.988 (+0.019)	1.406	174.3
MP2	1.883 (-0.086)	1.425	173.5
B3LYP	2.002 (+0.033)	1.415	175.3
TPSS	1.978 (+0.009)	1.421	174.9

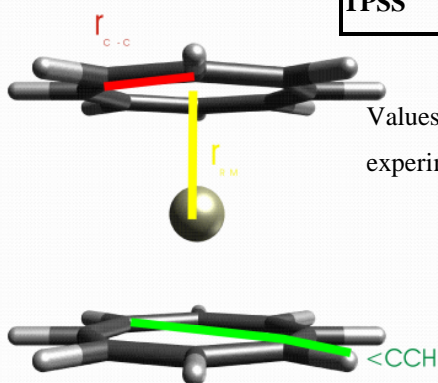


Figure 2.3- Relevant distances and angles in cerocene.

Table 2.2- Full geometry optimisation results using Gaussian03.

Values in brackets are the difference between the calculated result and the experimentally determined value.

It can be seen from these data that all of the methods employed result in comparable C-C distances and deviations from ring planarity. However, the ring-metal separation is more sensitive to method. The closest agreement with the experimentally determined value is obtained with the TPSS exchange-correlation functional. The poorest agreement occurs when using MP2, which underestimates the ring-metal separation, whilst RHF overestimates it. This is a good indication that the HF reference

wavefunction is a poor starting wavefunction, i.e. there is likely to be significant static correlation. MP2 includes dynamic, rather than static correlation and is premised upon the HF wavefunction being a reasonable first approximation. In the case of a multiconfigurational system this is not the case and thus MP2 is likely to perform poorly.

2.4.3 Partial geometry optimisations using Molcas

The geometry of the COT rings was kept constant at the geometry obtained from the calculations of Dolg et al.⁹ and the metal-ring centroid distance was varied at 0.02 Ångstrom intervals for the RHF and B3LYP methods and 0.001 intervals for the CASSCF and CASPT2 method.

Method	r_{RM} (Å)	Error in r_{RM} (Å)
RHF	1.98	+0.01 (± 0.02)
B3LYP	2.00	+0.03 (± 0.02)
CASSCF	2.09	+0.12
CASPT2	1.964	-0.005 (± 0.001)

Table 2.3- Geometry data from partial optimisations using Molcas. Error in r_{RM} is the deviation from experimental result. Numbers in brackets are the errors due to discrete nature of optimisations.

The results for RHF and B3LYP, table 2.3, show excellent agreement with those obtained using Gaussian03, thus validating the partial optimisation method, and also indicating that the change in basis set from Gaussian03 (RECP) to Molcas (all electron ANO) does not introduce any significant differences. The CASPT2 result gives excellent agreement with the experimental data. The CASSCF result was generated from an extrapolation of the curve generated at shorter Ce-COT distances, and grossly overestimates the Ce- ring distance.

The effect of varying the metal-ring centroid distance on the CASPT2 energy is given below, fig. 2.4.

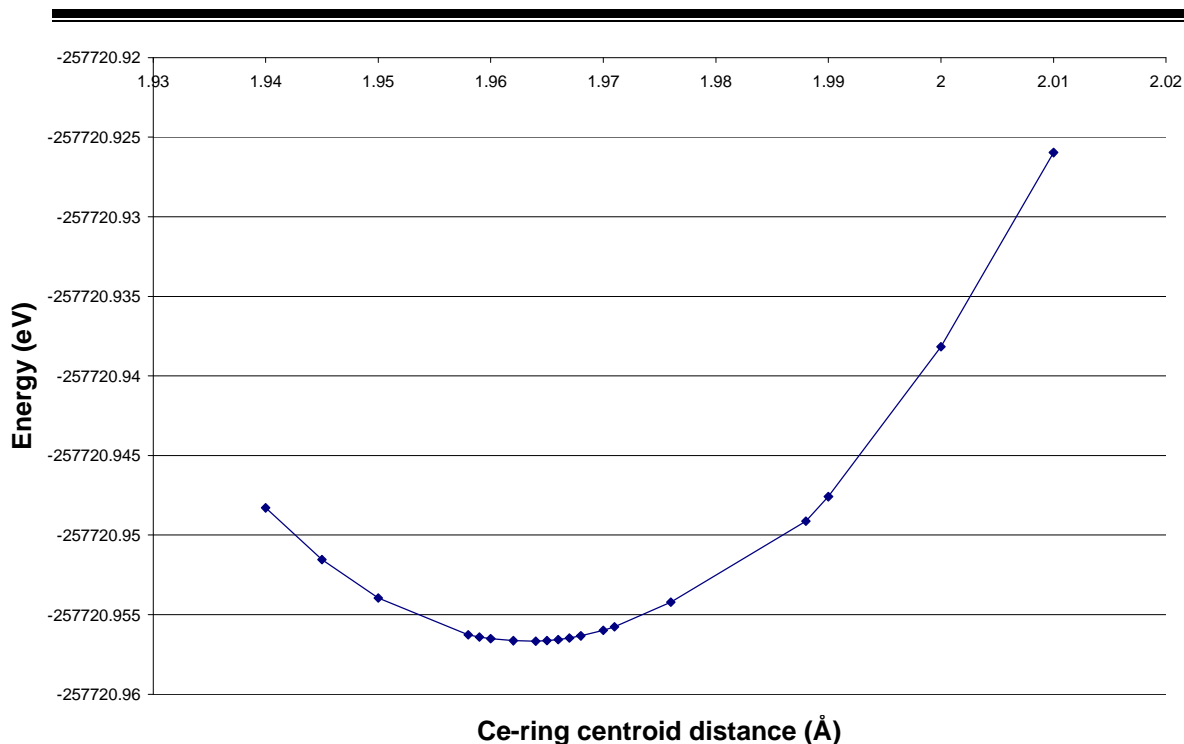


Figure 2.4- CASPT2 partial geometry optimisation energies.

This shows an extremely flat potential relative to the metal-centroid distance. However, reassuringly, there is very little change to the character of the CASSCF wavefunction across this potential.

2.4.3.1 Orbital Analysis

Whilst previous computational work¹² has analysed the wavefunction of the cerocene molecule in terms of configurations and their relative weights, this work adopts another approach. This is because the weights of configurations in a multiconfigurational calculation have been found to be unstable with respect to the number of states included in a state average calculation⁷³, configurational analysis is therefore not a consistent tool for state analysis. A better approach is to use the natural orbitals and their occupancies, which are stable with respect to state average size, as shown in fig. 2.5. Although analysis in terms of the natural orbital occupancies is a more meaningful approach to take than in terms of configurations it does lead to some conceptual difficulties associated with trying to visualise non-integer occupations of orbitals.

It could be said that orbital analysis has an inherent problem in that there is no unique 'correct' way of splitting the electron density up into orbitals and thus, whilst images of orbitals can be both striking and convincing, a unitary transformation of these orbitals, which would make no difference to the energy of the system, might yield a very different, and less convincing picture. This is quite true. However, natural orbitals are not an entirely arbitrary choice. The natural orbitals are formed from the diagonalisation of the 1-particle reduced density matrix⁷³⁻⁷⁵. Thus, there is one unique set of natural orbitals for any given density. Not only does this make the natural orbitals a reasonable choice for a representation of the density but it also means that their choice does not weight the analysis in any way, for example, they are not generated such that they maximise localisation (as in the case of Boys' localised orbitals⁷⁶) or any other imposed property.

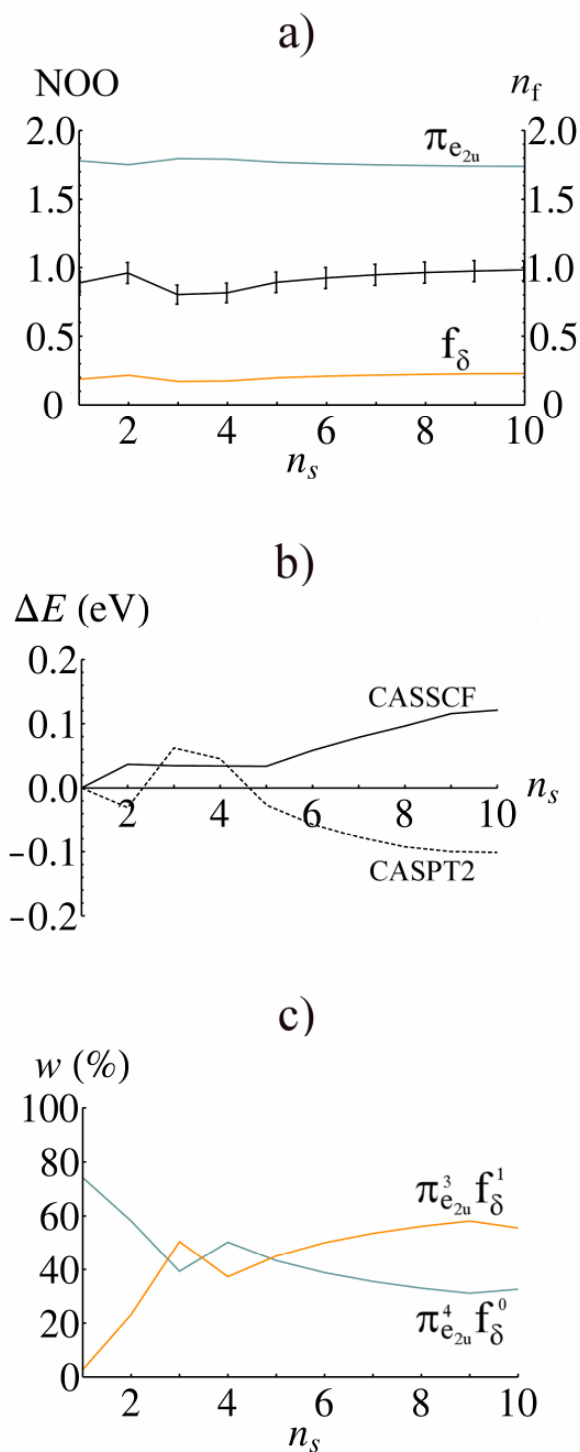


Figure 2.5. Variation of properties of the CeCOT_2 1A_g ground state as the size of a state-averaged calculation (n_s) is increased. a) Variation of the ground state natural orbital occupations (NOO) for the key a_u and b_{1u} (e_{2u}) orbitals, and corresponding n_f value. b) Variation of CASSCF and CASPT2 energies from those of the single state calculation. CASPT2 total energy for the single state is - 200895.2465 eV. c) Variation of the weights of the $\pi^4 f^0$ and $\pi^3 f^1$ configurations, these labels indicate the dominant characteristics of the occupied orbitals and are not ionic configurations⁵⁵.

2.4.3.2 Calculation of n_f values using MOLCAS

Single point calculations were carried out for the 1A_g ground state at the experimental ring-metal distance with the Dolg et al.⁹ optimized ring structure using RHF, B3LYP and CASPT2(8,14) methods. The resulting natural orbitals were analysed and the total f and d orbital occupancy calculated by multiplying natural orbital occupations by the square of the f/d coefficient of that orbital. This population analysis assumes orthogonality of the metal and ligand basis functions. The error is determined from the deviation of the sum of the squares of the coefficients contributing to the orbital from unity. The total n_z , where z is the atomic contribution, values are obtained from the sum of the n_z values of the contributing orbitals.

2.4.3.2.1 RHF Results

The total f and d occupancies of the highest occupied orbitals from the RHF calculation are given below, with their accompanying errors.

$$n_d = 0.761 \pm 0.0119 \quad n_f = 0.322 \pm 0.0002$$

2.4.3.2.2 B3LYP Results

The total f and d occupancies of the highest occupied orbitals from the B3LYP calculation are given below, with their accompanying errors.

$$n_d = 0.642 \pm 0.0093 \quad n_f = 0.864 \pm 0.0006$$

There is a marked increase in the f-occupancy when moving from the RHF to B3LYP case and a slight reduction in d-occupancy, indicating that inclusion of correlation results in an increased f-electron density on cerium. The B3LYP result gives an f occupancy which agrees well with those calculated by Dolg et al. ($n_f \approx 0.8$), but with only doubly occupied orbitals, not the $\pi_{e_{2u}}^3 f^1$ configuration found in those studies^{8, 9, 12}.

In fact, attempts to converge an open shell singlet configuration failed. This will be discussed more fully in section 2.5.1.

2.4.3.2.3 CASSCF (8,14) Results

There are 4 natural orbitals in the active space which have significantly non-integer occupation numbers (i.e. the ground state of cerocene is significantly multiconfigurational). These natural orbitals also contribute the most to the calculated n_f of 0.927 ± 0.001 and are shown, along with their natural occupancies, below, fig. 2.6. n_d is 0.631 ± 0.011 .

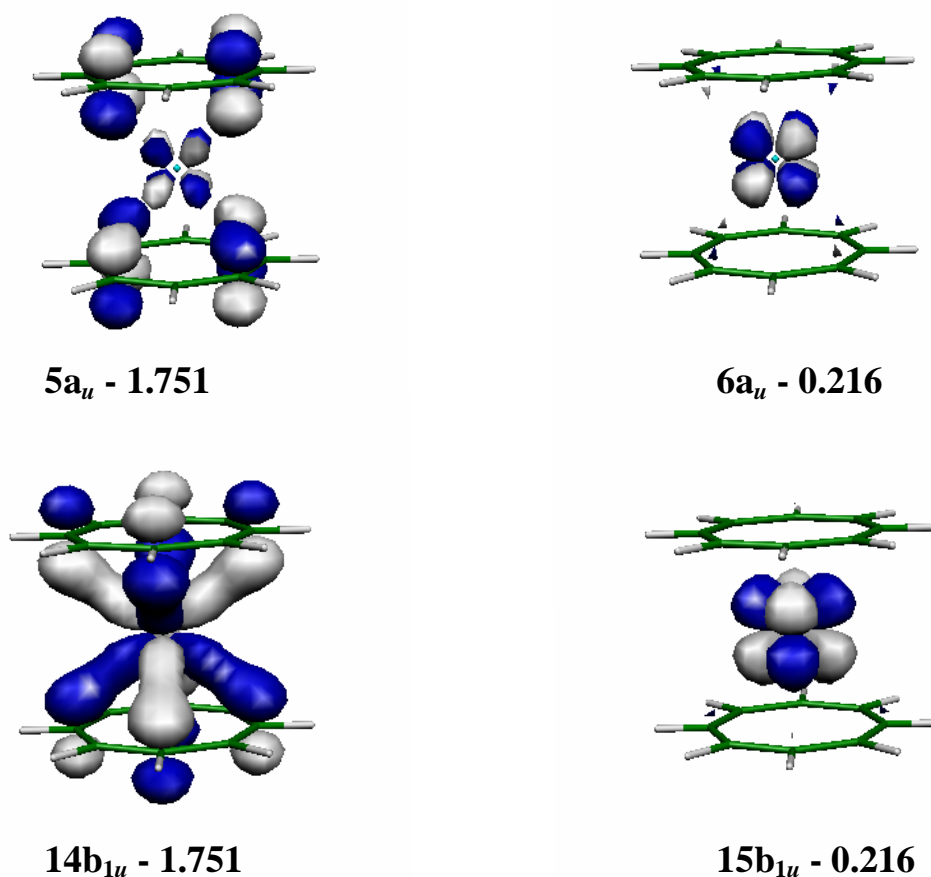


Figure 2.6- a_u & b_{1u} (e_{2u}) ground state natural orbitals along with natural occupancies of each orbital.

All four of these natural orbitals show both COT ring and Ce f_δ character. This could indicate a degree of metal-ligand covalency.

This is also supported by consideration of the effective bond order (EBO)⁷⁷. EBO analysis assumes that bonding orbitals and correlating, antibonding orbitals can be clearly identified. If the small (16.4%) f-component of the 5a_u and 14b_{1u} orbitals and their bonding phase is taken as indication that these are bonding orbitals with 6a_u and 15b_{1u} correlating them, an EBO can be determined.

EBO is calculated in the following way:

$$EBO = \frac{(n_b - n_a)}{2}$$

Equation 2.1- Calculation of effective bond order, n_b is the occupation of bonding orbital(s), n_a is the occupation of antibonding orbitals(s).

The EBO in this case is 1.535, indicating that these delta bonds have a bond order somewhere between that of a single and double bond. It is, however, important to note that these bonds are polarised. Further analysis of the density is also given below, (2.4.3.4).

Recalculation with basis B and C showed little deviation from these results showing that the inclusion of g-functions is not significant and that the basis set chosen is well-balanced.

2.4.3.3 Energies of excited states

2.4.3.3.1 Spin-orbit coupling free (SOF) energies

The energies of the CASSCF(8,14) 32 spin free states (the two lowest energy singlet and triplet states of each irrep) of cerocene, are shown in table 2.4, and fig. 2.7 below. In all cases the CASSCF wavefunctions used were the result of an equally weighted two state average. Oscillator strengths were calculated using RASSI.

State	Energy (eV) state1	Oscillator Strength state 1	Energy (eV) state 2	Oscillator Strength state 2
¹ A _g	0.00		1.55	
¹ B _{1g}	1.10		1.48	
¹ B _{2g}	1.14		1.15	
¹ B _{3g}	1.14		1.15	
¹ A _u	2.39		2.78	
¹ B _{1u}	2.47	6.60x10 ⁻⁶	2.93	0.224
¹ B _{2u}	2.47	9.47x10 ⁻⁵	2.49	1.72x10 ⁻⁴
¹ B _{3u}	2.47	1.28x10 ⁻⁴	2.49	2.15x10 ⁻⁴
³ A _g	1.10		1.47	
³ B _{1g}	1.10		1.50	
³ B _{2g}	1.16		1.16	
³ B _{3g}	1.16		1.16	
³ A _u	2.38		2.80	
³ B _{1u}	2.38		2.74	
³ B _{2u}	2.46		2.48	
³ B _{3u}	2.46		2.48	

Table 2.4- Calculated energies and oscillator strengths of electronic states of cerocene at the CASPT2 level. States to which transitions are allowed from the ground state are highlighted in red. Note, despite the apparent degeneracy of these states, the oscillator strength of the ¹B_{1u} state is significantly different from the other two, indicating that this is not the case. The ¹B_{2u} and ¹B_{3u} states would both be expected to span ¹E_{1u} or ¹E_{3u} in D_{8h} symmetry. Oscillator strengths not noted are less than 1x10⁻⁸. State 1 indicates ground state of specified symmetry and State 2 1st excited state.

The only transition with a significant oscillator strength ($f=0.224$) is the second ¹A_g→¹B_{1u}; π→f_δ transition (2.93 eV).

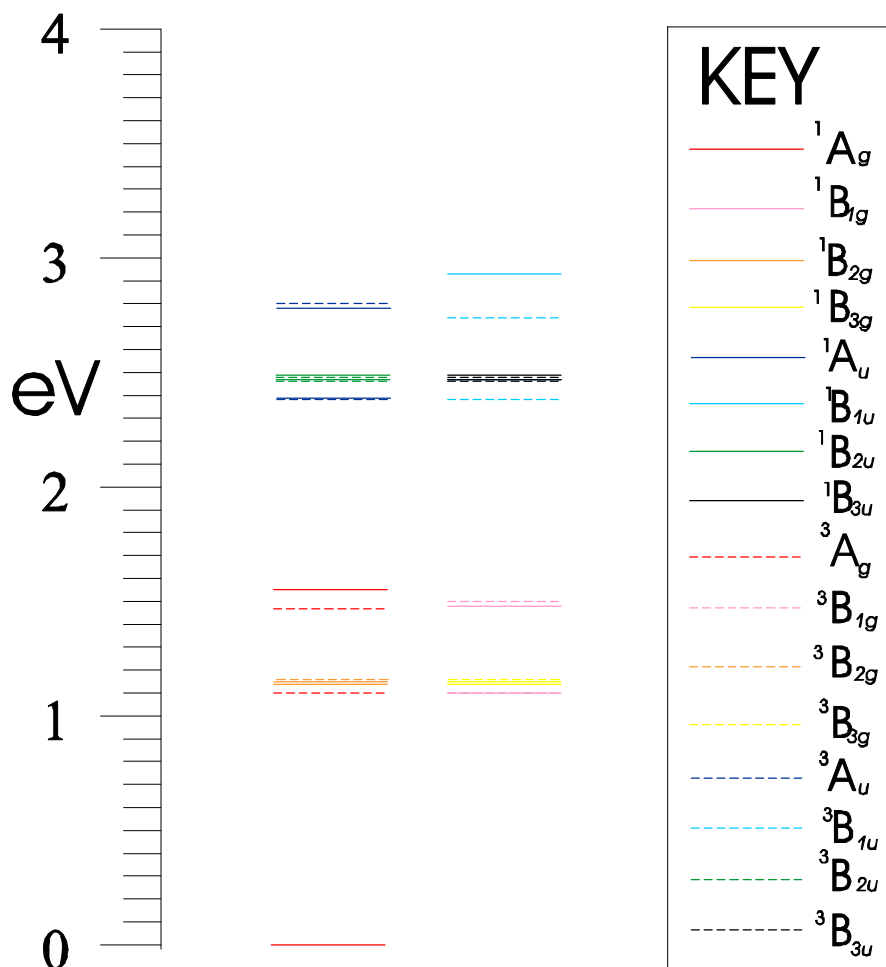


Figure 2.7- CASPT2 energy level diagram at the SOF level. A_g , A_u , B_{2g} and B_{2u} on left hand side, B_{1g} , B_{1u} , B_{2g} and B_{2u} on the right hand side to show (near) degeneracies of states which would be E_{1g} , E_{2g} , E_{3g} , E_{1u} , E_{2u} or E_{3u} .

2.4.3.3.2 Spin-orbit coupled (SOC) energies

Spin orbit coupling of the SOF states was performed using RASSI. The spin orbit coupled ground state is composed of 99.3% of the spin-free ground state. There is only one strongly optically allowed transition ($f = 0.207$) between the ground state and the 94.9% ${}^1B_{1u}(2)$ excited state (2.96 eV) and another weakly optically allowed transition, but with a much smaller oscillator strength ($f = 0.016$) from the ground state to an excited state 2.51 eV above this (this state is 50% ${}^3B_{3u}$, 35% ${}^3B_{2u}$ and 14% ${}^3B_{1u}$).

2.4.3.3.3 Comparison with experimental data

The UV-Vis spectrum of cerocene shows an intense band at 2.63 eV with a broad shoulder which has a λ_{\max} of 2.18 eV on deconvolution⁶. These electronic absorption bands must correspond to electronic state changes with a change in parity and no change in spin, i.e. from the 1A_g ground state to a singlet state of *ungerade* parity. The data in table 2.4 would suggest these transitions to be $^1A_g \rightarrow ^1B_{1u}$; $\pi \rightarrow f_\sigma$ and $^1A_g \rightarrow ^1B_{2u}/^1B_{3u}$; $\pi \rightarrow f_\pi$, respectively, although no significant oscillator strength was found for the latter. However, at the SO-coupled level such a transition was identified. The CASPT2 method is typically expected to yield results agreeing with experiment to within ~0.3 eV, supporting these results⁷⁸ and therefore the agreement here between experiment and the SO-coupled results in particular is excellent, especially when one considers that the experimental data have unspecified but presumably fairly significant errors due to the broad nature of the bands observed. The calculated results are 2.51 eV and 2.96 eV compared with the experimental peaks at 2.18 and 2.63 eV. Perhaps more importantly, however, the transitions calculated involve a transfer of electron density from the ligand system to the metal centre, as suggested by Streitwieser et al.⁶ in the UV-Vis experimental paper.

2.4.3.4 Density difference plots

Densities were obtained from MOLCAS RHF, CASSCF and B3LYP calculations and density differences between RHF and CASSCF, RHF and B3LYP, and B3LYP and CASSCF obtained. The differences are represented using an isosurface of 0.00075 a.u. Violet isosurfaces correspond to a positive charge density, turquoise to a negative density. The CASSCF density described is that formed from all the active space orbitals from the CASPT2(8,14) ground state of a 2 state-average calculation. The RHF and B3LYP densities are formed from the four highest energy doubly occupied orbitals.

Fig. 2.8 shows the CASSCF(8,14) result with the RHF result for the relevant orbitals subtracted.

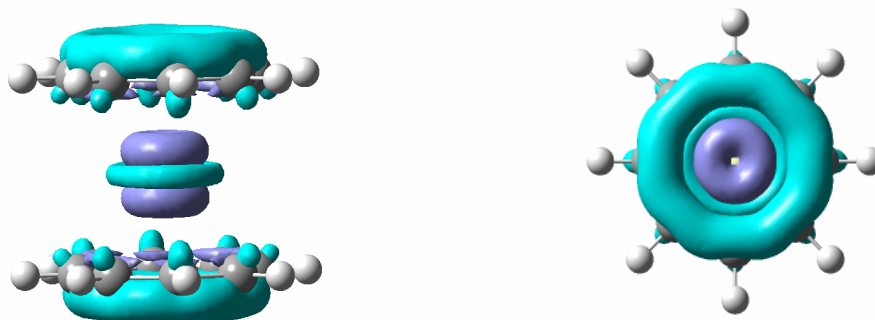


Figure 2.8- Density difference between CASSCF and RHF(active space and four highest energy occupied orbitals, respectively) side and top views.

Figure 2.8 shows that the inclusion of correlation via the CASSCF method causes electron density to move from the ligand ring orbitals to the metal. It is just possible to see that there is also a small amount of electron density transferred to the ligand ring orbitals on the Ce side of the rings. This indicates a degree of covalent interaction between the Ce and the COT rings present in the CASSCF result which is absent in the RHF result due to the lack of correlation.

Fig. 2.9 shows the B3LYP result with the RHF result subtracted, active space orbitals only.

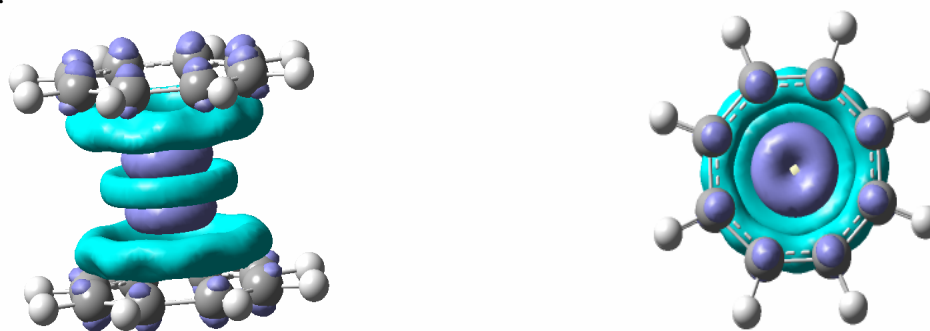


Figure 2.9- Density difference between B3LYP and RHF (four highest energy occupied orbitals) side and top views.

Density functional methods include some correlation, however, B3LYP is still a single configuration method and thus cannot occupy antibonding orbitals, as CASSCF can. Therefore, whilst the B3LYP method does move some electron density to the Ce, the covalency seen in the CASSCF result is absent, instead electron density is removed

from the ligand ring orbitals closest to the Ce. This reduces the charge on the Ce without increasing any covalency between the Ce and the COT rings, in fact, the electron density between the rings and Ce is reduced relative to the HF result.

Fig. 2.10 shows the CASSCF(8,14) result with the B3LYP result for the relevant orbitals subtracted.



Figure 2.10- Density difference between CASSCF and B3LYP (active space orbitals and four highest energy occupied orbitals) side and top views.

Fig. 2.10 shows that the B3LYP result has less electron density between the COT rings and the metal than the CASSCF result, the CASSCF result therefore shows a system with more covalent character.

2.5 Discussion

The calculations detailed above were carried out in order to understand the cerocene molecule better. Before the results can be used to interpret the electronic structure of cerocene it is important to determine whether they agree within reasonable limits with experimental evidence (XANES and UV/Vis) and with previous calculations.

2.5.1 Comparison of results with other theoretical work

As described in section 2.2.1 these calculations on cerocene form part of a broader study comparing these results with those for the actinocenes thoracene and protactinocene. The main difference between cerocene and the actinocenes is the pronounced

multiconfigurational ground state in cerocene. No such ground state is found in the actinocene systems and multiconfigurational character only becomes apparent in the higher excited electronic states. An increase in multiconfigurational character for higher excited states is not exceptional as these states are closer to the dissociation level and thus would be expected to be less well described by a single configuration. However, the considerable difference in the ground state electronic structure of cerocene and its actinocene analogue, thoracene, are more unusual.

The most extensive theoretical work prior to this study is that carried out by Dolg et al.⁹. As mentioned previously, this work of 1995 employed three computational techniques: State averaged CASSCF; MRCI; and ACPF, the former to include static correlation and the latter two to include dynamic. The highest 8 ligand π orbitals (e_{2u} , e_{2g} , e_{1u} and e_{1g}) and the Ce f orbitals were treated as active in the MRCI and ACPF calculations. It is not absolutely clear from this work what active space was used for the CASSCF calculation. However if we assume it is the 16 electron-15 orbital space treated as active in the MRCI and ACPF calculations it would appear to be superior to the active space used in the current work. The apparent superiority may not, however, be as significant as it first appears (1 additional orbital and 8 electrons correlated). SCF calculations show the e_{1g} and e_{1u} orbitals to lie 3.9 and 4.6 eV respectively lower in energy than the e_{2g} orbitals and are therefore unlikely to contribute to near degenerate states, i.e. are not predicted to play an important role in the static correlation of the system (see section 4 on CASSCF active space choice). This was verified by larger active space calculations which did include these orbitals. Furthermore although the MRCI and ACPF calculations would certainly improve the results of the CASSCF calculation they do not seem to include much of the system's dynamic correlation.

The lack of dynamic correlation included in the previous calculations can be seen from the optimised geometry obtained using these methods which has a Ce-ring distance 0.1 Å longer than the experimental value, comparable with the CASSCF results presented here, and poorer than the CASPT2 results (see section 2.4.3.1). Both this work and Dolg et al.'s yield similar n_f values but this appears to arise from a f^1 state in the previous work as a result of the analysis in that work being carried out on the configurations rather than natural orbitals and their occupancies. The current work does

not assume ionic bonding and the analysis is performed using the natural orbitals and their occupations therefore enabling the identification of some covalent character.

The works of Dolg, Fulde et al.^{8, 9, 12} were analysed by Booth et al.¹¹ with particular reference to the speculation of Neumann and Fulde that there might be a molecular Kondo state⁵⁸. This analysis was carried out with reference to experimental magnetic and XANES data.

The difference in the method of analysis of the CASSCF wavefunction between this work and that of Dolg et al. is important, as discussed in section 2.4.3.4 the configurational analysis approach to analysing the multiconfigurational result is highly variable to state average size. The interpretations of Booth et al. rely heavily on the configurational analysis. Thus, the XANES data is said to match the calculations as the fit uses ~80% $4f^1$ curve and ~20% $4f^0$ curve, and is therefore consistent with the configurational breakdown of the CASSCF result. Furthermore, the speculation regarding a possible Kondo state arises due to the leading $4f^1$ configuration of the CASSCF wavefunction. The apparent strength in the agreement between the experimental and calculated results are highly dubious when the unreliability of the configurational analysis approach is considered. Furthermore, a Kondo state requires a localised 4f electron, neither the CASPT2 calculation nor the B3LYP calculation indicate this, whilst both have similar values of n_f , which are also very close to that obtained from the calculations of Dolg et al.⁹.

The key differences between the calculations from the current study and previous theoretical work are:

a) Oxidation state

Previous work finds the Ce to be in the 3+ oxidation state in cerocene, even when the bonding is assumed to be largely ionic, while this study shows that, whilst there is significant 4f density, this is delocalised rather than a localised 4f electron. This indicates a formally Ce(IV) state but with significant ligand to metal charge transfer stabilising this high oxidation state.

b) Kondo effect

The previous work supports the concept of cerocene as an example of a molecular Kondo state while the current work makes for a less convincing argument as the ionic state identified in the previous work is not supported. A molecular Kondo system would require a localised f-electron on the Ce, no such electron is found in this study.

2.5.2 XANES

The n_f value calculated for cerocene in the current work using the CASSCF method is 0.927 ± 0.001 . The experimentally determined value from XANES Ce L_{III} edge studies was 0.89 ± 0.03 ¹¹ while that obtained in Dolg et al.'s previous calculations was 0.80 ¹². Thus the current study shows a closer match to experiment than the previous computational work.

Despite the close agreement of the present calculations with the experimental work, there is some reason to be cautious in accepting the experimental value of n_f . This is largely due to the choice of edge, as the L_{III} edge may not be a suitable choice when attempting to determine Ce oxidation state, as shown in section 2.4.1. These data suggest that it is not appropriate to use the L_{III} edge of Ce to determine the Ce oxidation state, as is done in the previous work¹¹. This approach seems particularly contentious as the Ce(IV) standard used was then later shown to have very similar magnetic behaviour to cerocene⁷⁹. The Ce(IV) standard employed was bis-tetramethyldibenzotetraaza[14]annulenyl cerium (Ce(tmtaa)₂) which, according to the authors of reference⁷⁹ is strongly mixed valent (and therefore surely not an appropriate choice of Ce(IV) standard), and shows the same van Vleck Temperature Independent Paramagnetism which they suggest confirms the molecular Kondo singlet nature of cerocene (see section 2.5.4 for further discussion on this point).

It is rather unclear how both of these experimental observations can be acknowledged and Ce(tmtaa)₂ still asserted to be a good Ce(IV) standard. It could be argued that the magnetic data for Ce(tmtaa)₂ were unknown when it was used as the Ce(IV) standard in the cerocene study; however after the publication of these data it was again used as a Ce(IV) standard in XANES fitting to determine the n_f value of

bis(permethylpentalene)cerium, predicted to be analogous to cerocene⁷. There seems to be little justification for this approach. The Ce(III) and Ce(IV) edge positions are much more distinct when using the K-edge¹⁰ and it is suggested that it would be more appropriate to use this edge to determine n_f values. However, the L_{III} edge continues to be used for similar analysis, again comparing the results of edge analysis with CASSCF results analysed in terms of configurations and their weights⁸⁰.

2.5.3 UV-Vis

As the results detailed in table 2.4 shows, there is excellent agreement between the calculated excited states and the experimental UV-Vis spectrum, especially at the SOC-level, within the typical 0.3 eV errors of the CASPT2 method. This is particularly satisfying as no other theoretical studies have attempted to predict the electronic transition energies of cerocene.

2.5.4 Magnetic measurements

Spin polarisation data have not been analysed in the current work. However, it is worth commenting on the current interpretations of the experimental magnetic data for cerocene. The cerocene molecule appears diamagnetic. However, as noted earlier, when diamagnetic corrections are made for the COT rings using Pascal's values the results show temperature independent paramagnetism (TIP)¹¹. The magnitude of the TIP is approximately the same as the magnitude of the diamagnetic correction made and is consistent with van Vleck temperature independent paramagnetism.^{vii} The magnitude of the COT ring diamagnetic correction is -1.67×10^{-4} emu/mol and the resulting TIP is 1.4×10^{-4} emu/mol.

^{vii} The corrections made for cerocene neglect the diamagnetism of cerium, however this is a small error. It is interesting to note that other researchers have attempted to remove the error involved in using Pascal's constants by equating the diamagnetic correction with that of a related entirely diamagnetic molecule.⁸¹ G.Balazs; F.G.N.Cloke; J.C.Green; R.M.Harkar; A.Harrison; P.B.Hitchcock; C.N.Jardine; R.Walton, *Organometallics* **2007**, 26, 3111-3119. The magnitude of the TIP identified is rather small in comparison with that obtained in other studies⁸². S.A. Kozimor, B. M. B., J.D. Rinehart, J.R. Long, *Journal of American Chemical Society* **2007**, 129.

Van Vleck TIP occurs when a non-magnetic ground state (i.e. a singlet state) and a magnetic excited state mix. The effect is independent of temperature because the energy difference between the ground and excited state is much larger than $k_B T$ and therefore thermal population of the excited state is negligible. It is important to note that this mixing can occur only when S and L cease to be good quantum numbers, i.e. when spin-orbit coupling is significant, as it is for the heavier elements.

In their 2005 paper¹¹ Booth et al. suggest that the apparent van Vleck TIP exhibited by cerocene is a predictable consequence of a self-contained Kondo effect in the cerocene molecule. In fact, this is not obviously the case, for the following reasons:

- a) The observed effect could be produced by van Vleck TIP, as described above, which does not require the system to be Kondo-like.
- b) In the case of a Kondo system, if the Landé g -values of the COT rings and Ce differ the localized spin polarisation on the cerium will not counter that on the rings (Booth et al. suggest a g -value of $6/7$ for Ce and 2 for the rings) which would lead to behaviour similar to van Vleck TIP below the Kondo temperature.
- c) It would also be possible for an open-shell singlet ground state to mix with a magnetic triplet state such that the observed TIP would be due to both a Kondo singlet with differing Landé g -values for the two unpaired electrons and van Vleck TIP.
- d) If a system was a Kondo singlet but the unpaired electrons had equal Landé g -values there would be no net paramagnetism below the Kondo temperature, though it is unlikely that this situation would arise as there would be expected to be some difference in Landé g -values.

Thus, van Vleck TIP is neither exclusively displayed by molecular Kondo systems nor are all such systems expected to exhibit it. However, most Kondo systems are likely to display TIP as a result of differences in Landé g -values, which could be mistaken for van Vleck TIP (in fact Booth et al. conflate these two quite different causes).

The question now is whether or not we can tell whether a system is exhibiting van Vleck TIP or Kondo-based TIP. This does not appear, from the current literature, to be a trivial matter. Booth et al. suggest that the small TIP they observe for cerocene is indicative of a Kondo system¹¹. However, strikingly similar results obtained for Ce(tm₂aa)₂ apparently do not support the same conclusion⁷⁹. Cloke et al. choose to avoid the subject of Kondo altogether when faced with similar data for Ce(η^8 -pentalene)₂⁸¹.

It appears that which interpretation one chooses is largely directed by the results of computational studies. This makes the results of the current work particularly significant as the interpretation of cerocene as a Kondo system is strongly influenced by the computational work of Dolg and Fulde^{8, 9, 12}, work which the current study does not fully corroborate.

In particular, no localised f-electron is found, which is a necessary requirement for a Kondo system. Whilst both B3LYP and CASPT2 calculations find an n_f value of close to 1, this is obtained with singlet configurations only, and, in the case of the B3LYP calculation, a closed shell structure. Furthermore, SOC calculations also show that there is almost no ground state mixing with excited triplet states, therefore Van Vleck TIP is also not predicted.

2.5.5 Chemical implications

It appears that the bonding in cerocene is somewhat more covalent than previous studies have suggested, as shown in the density differences, **2.4.3.4**. Previous studies have suggested largely ionic bonding between the rings and metal while this work suggests that there are significant Ce 4f and 5d orbital contributions to some of the occupied molecular orbitals. It is this increased covalency that results in the Ce n_f being close to 1. This covalency involves both the d and f orbitals, suggesting that this is a molecule in which the lanthanide f-orbitals are important in bonding and are not, as is often stated, too contracted to be involved in chemical bonding. However, the interaction is small and is likely to be as a consequence of the formal charge difference between the metal and the ligands⁶.

The most important chemical implication of this study and those which it succeeds relates to the concept of oxidation state. A considerable amount of the work carried out on cerocene, both theoretical and experimental and including the current study, has been aimed at determining the oxidation state of Ce within the molecule. It appears, however that part of the reason for the continued disagreement on this matter may be due to the fact that the question posed is not an appropriate one! Although in some cases considering oxidation state can be useful to aid chemical understanding, cerocene may not be an example of such a situation. In covalently bonded molecules the formal oxidation state of the metal bears little relation to the charge localised on it⁸³. It is important to consider both what we mean by oxidation state and why knowledge of it would be useful before setting ourselves the task of determining it. The main reason for knowing what the oxidation state of a metal in a compound is is in order to determine whether reduction/oxidation is likely to be possible rather than to know something about the charge density on the metal. In this case it appears that, whilst there is significant f density on the Ce, there is not a localised f electron and thus oxidation of the cerium is not predicted whilst reduction to a more recognisably Ce(III) f^1 state would be possible.

2.5.6 Theoretical implications

This study has reinforced the necessity for the inclusion of correlation using well-defined, multiconfigurational methods. It is particularly important to include static correlation appropriately for an accurate understanding of electronic states and to include as much dynamic correlation as possible in order to obtain reliable geometries.

2.5.7 Further work

The surest test of calculations and the only way to determine a theory's usefulness is by comparison with experiment. If a theory is able to model known experimental behaviour and to elucidate the causes of this behaviour it can be said to be useful. If it cannot satisfactorily model the main features of experiment or give additional rationale which enables greater understanding of the system(s) under investigation it serves little

purpose. At times it is easy to forget the Empiricist's doctrine '*Nihil est in intellectu quod non prius fuerit in sensu*' and it is particularly easy to do so when interesting theoretical problems arise and tease us away from the problems of the laboratory, but it is important to remain aware of the theoretician's role which is not to tell experimentalists how nature ought to be behaving but rather rationalise those of her quirks which they unearth. It is with this in mind that the majority of the work which might be able to further elucidate the problem in question is proposed to be experimental.

It would certainly be helpful to perform a XANES Ce K-edge fitting comparable to the L_{III} edge fitting performed by Booth et al.¹¹ which should give a more reliable value of n_f . VEPES could also be carried out and would provide another means of identifying the presence, or absence, of an f-orbital based electron in cerocene. This technique allows identification of cation states arising from ionisations of an f-electron, and has proved invaluable in the determination of the electronic structure of $CeCp_3$, as shown in chapter 3.

2.6 Conclusions

The cerocene molecule has been studied using the CASPT2 method. The results obtained have been compared with experiment and found to provide excellent agreement with available data; structural, UV/Vis and XANES. The molecule has been found to bond more covalently than had previously been asserted, this bonding involving both the Ce d and f orbitals. The suggestion that cerocene is an example of a molecular Kondo system is not supported by this work and it is proposed that more investigations be undertaken in order to more fully corroborate this suggestion.

Most significantly, in terms of oxidation state ambiguity, Ce in cerocene is found to be best described as Ce(IV) but that this high oxidation state is stabilised by covalent bonding from the ligands, reducing the oxidation state to closer to that of a formally Ce(III) system. A genuinely Ce(III) system would be predicted to have a localised 4f

electron, which is not found here. Thus, the claim made by Streitweiser that cerocene is best described as a Ce(IV) system is supported.

Much of this work has been published in Journal of Physical Chemistry A⁵⁵.

3. Cerium tris-cyclopentadiene

3.1 Experimental Approach

Given the controversy surrounding the electronic structure of cerocene it is interesting to consider other formally Ce(IV) molecules. This has resulted in a collaboration with experimentalists, synthesising and analysing the bonding in $\text{Ln}(\eta^5\text{-C}_5\text{H}_5)_3$ (LnCp_3) as part of an ongoing project. One might think that these systems could offer little insight as they are formally Ce(III) rather than Ce(IV). However, the experimental project makes use of photoelectron spectroscopy. Photoelectron spectroscopy probes the electronic states of the cation of the compound under investigation. Which is useful as in this case it is the formally Ce(IV) states of the cation which are, themselves, of interest.

3.1.1 Photoelectron spectroscopy

Photoelectron spectroscopy (PES) is one of the most direct experimental techniques for obtaining information on molecular electronic structure. This is particularly so for gas-phase measurements, which do not suffer from the disadvantage of broad bands and calibration problems that can plague solid state studies. An especially powerful approach to gas-phase PES is to employ synchrotron radiation, where the ability to tune the incident photon energy frequently facilitates unambiguous determination of ion state parentage, yielding valuable information on, for example, metal–ligand covalency^{84, 85}.

Access to synchrotron radiation is particularly valuable in the study of trivalent lanthanide compounds. In Ln(III) systems the 4f ionizations typically lie under the first ligand band and therefore the 4f bands can be identified only when incident photon energies which maximize the 4f cross section and minimize the ligand cross section are used. This is achieved by using photon energies in the region of the delayed maximum in 4f cross sections, or by exciting 4d→4f giant resonances.

3.1.1.1 Delayed Maxima and Giant Resonances

Both the delayed maxima of f-ionisations and the giant resonances, which together enable the f-ionisations to be identified, occur when the incident photon energy is significantly greater than the ionisation energy of the valence electron. Simplistically, photon energies above the threshold for the ionisation of interest are not considered to yield additional information, following Einstein's expression of the photoelectric effect, equation 3.1.

$$h\nu = I_k + E_k$$

Equation 3.1-⁸⁶The photoelectric effect, where ν is the frequency of the incident photon, I_k is the ionisation energy of the electron removed and E_k is the kinetic energy of this photoelectron when unbound.

However, in this case, increasing the incident photon energy significantly above this threshold yields valuable data. It is therefore worth considering the origin of the two effects which occur at these higher photon energies. First the delayed maxima for f ionisations, the less significant of the two effects.

Delayed maxima occur for d and f ionisations. This is due to the high angular nodality of such orbitals. Whilst for s and p ionisations the maximum intensity of the ionisation occurs when the incident photons have an energy equal to the ionisation energy and reduces for higher energy photons, for d and f ionisations the maximum of intensity for the ionisation occurs when the incident photons have an energy slightly above the ionisation energy and then subsequently reduces for higher energy photons.

Giant resonance occurs when the incident photon energy is close to that of the $4d \rightarrow 4f$ transition. At this energy a 4d electron may be excited to the 4f level. This process has a large cross section due to the spatial overlap of the 4d and 4f orbitals. For a $4f^n$ system there are now $n+1$ electrons in the 4f level. Any one of these may now drop back down to the 4d level and in the process release a photon with sufficient energy to ionise another of the 4f electrons. Again, this process has a large cross section. The result of these excitations and de-excitations is to vastly increase the apparent 4f ionisation cross section. At the same time the ligand ionisations are much reduced as, at high incident photon energies, their largely p-ionisations are very far from the maxima of their cross-

sections. The overall effect is therefore that the 4f-ionisations dwarf those of the ligands.

The effect of giant resonance is more pronounced than the effect of the f-ionisation delayed maximum. Together, the increase in the cross-section for the f-ionisation at higher incident photon energies is so unambiguous as to be a clear method for identification. The consequence of these effects is that enhancement of any f-ionisations around the energy of the Ce 4d_{3/2} and 4d_{5/2} ionisations (112 and 109 eV, respectively) is expected⁸⁷.

3.1.1.2 Experimental Results

Synchrotron radiation was used to study the photoelectron spectrum of CeCp₃. As an f¹ system, this was expected to yield a simple photoelectron (PE) spectrum with just one f ionisation which could be used as a benchmark for the interpretation of more complicated spectra arising from fⁿ systems ($n > 1$). Rather surprisingly, the PES data showed unequivocally that ionisation of the single 4f electron yields not one but *two* ion states which have an enhanced cross section in the 4d-4f resonance region, separated by a large energy gap (3.2 eV, see bands A and D on Figure 3.1)¹⁴. Such a large energy gap rules out the possibility of thermal population of two different states of the neutral molecule leading to two different ionisation energies, or of spin-orbit coupling being responsible.

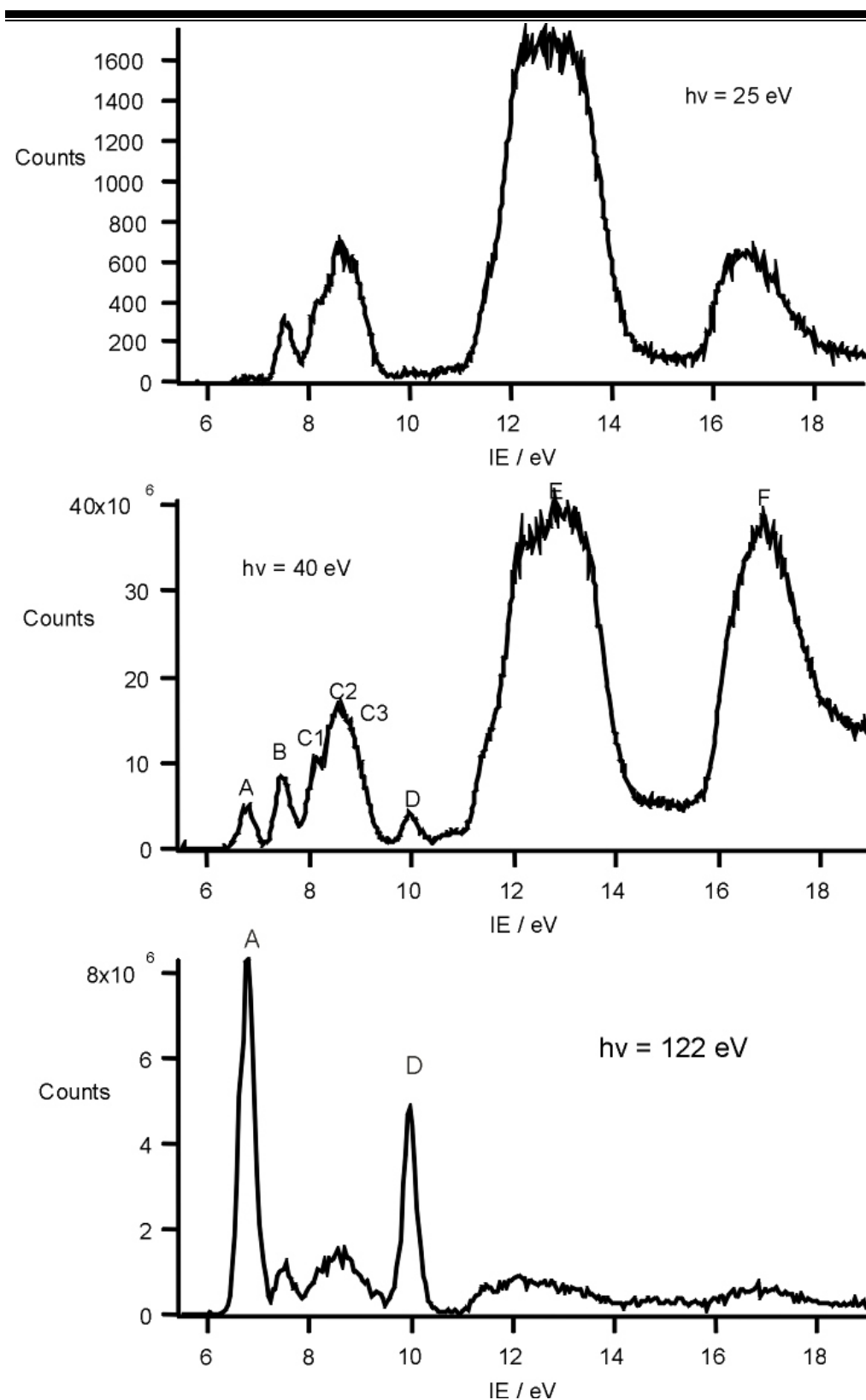


Figure 3.1- PE spectra of CeCp₃ measured with incident photon energies of 25, 40 and 122 eV. The peaks due to f ionisation increase in relative intensity as the incident photon energy increases and thus are clearly identifiable as bands A and D.⁸⁸

3.2 Computational Approach

3.2.1 Computational Details

The geometry of CeCp₃ was optimised, under the constraint of C_{3v} symmetry, using the B3LYP form of hybrid density functional theory, in the Gaussian03 suite of programmes. The relativistic effective core potential (RECP) of the Stuttgart-Dresden group was used for Ce⁶⁶, together with the valence basis set of Cao and Dolg in the segmented contraction with the g-functions removed as these are unlikely to make very much difference to the geometries but greatly increase the calculation time and the cc-pVDZ basis for C and H. The unique Ce–C distances obtained were 2.845 Å, 2.851 Å (x2) and 2.828 Å (x2), which compare very favourably with experimentally determined mean Ce–C values for Ce(C₅H₄(CMe₃))₃ (2.86 Å) and Ce(C₅H₃(SiMe₃)₂)₃ (2.83 Å)⁸⁹. The optimised geometry was subsequently used in CASSCF/CASPT2 calculations employing MOLCAS-6.4, although restrictions within this code meant that the calculations were run in the C_s point group. The same geometry was used for both CeCp₃ and CeCp₃⁺, as the maxima of intensity in the photoelectron spectrum are experimentally defined as the vertical transitions⁸⁵.

In the MOLCAS calculations, all electron, relativistic ANO-RCC basis sets were used for all atoms. Two basis set combinations were employed. Basis A was of QZ quality for Ce and DZP for C and H: Ce [25s22p15d11f/9s8p5d4f]; C [14s9p4d/3s2p1d]; H [8s4p/2s1p]. In order to verify that any potential imbalance in basis A does not significantly affect the results, basis B was also employed, of TZP quality on all atoms: Ce [25s22p15d11f/8s7p4d3f1g]; C [14s9p4d/4s3p1d]; H [8s4p3d/3s2p1d].

Fig. 3.2 presents a qualitative valence MO energy level diagram for CeCp₃, showing the interaction of the highest occupied Cp π_{2,3}-based levels with the metal's 4f and 5d_{z²} orbitals. In the CASSCF/CASPT2 calculations, an active space was chosen based on all 14 of the MOs shown in Figure 3.2 (subject to the reduction from C_{3v} to C_s; a₁ → a', a₂ → a'', e → a' + a''). This active space, designated active space I, is (13,14) for CeCp₃ and (12,14) for CeCp₃⁺ (*i.e.* 13 electrons in 14 MOs for the neutral molecule and 12

electrons in 14 MOs for the cation). A second, smaller active space (II) was also employed, (5,8) for CeCp₃ and (4,8) for CeCp₃⁺. These latter active spaces feature four orbitals of a' symmetry (48–51a') and four of a'' (33–36a''). State-averaged calculations have been performed for the ¹A' and ¹A'' states of CeCp₃⁺ with active space II. The number of states used in the average was varied from two to ten, in all cases with equal weights.

In the CASSCF/CASPT2 calculations, active space I was based on all 14 of the orbitals shown (subject to reduction in symmetry from C_{3v} to C_s; a₁ → a', a₂ → a'', e → a' + a''), while active space II has four orbitals of a' symmetry and four of a''. This smaller active space corresponds to the occupied e (a' ⊕ a'') orbitals as well as 6 of the 7 Ce 4f orbitals, all 7 orbitals are not included as there are orbitals of each symmetry included such that if any of the orbitals should be significantly occupied this can be accommodated. However, if all 7 are included the orbitals which have e symmetry in C_{3v} but a' ⊕ a'' in C_s are unbalanced.

An imaginary level shift^{18, 19} of 0.1 was applied in some state-averaged CASPT2 calculations to ensure a balanced treatment of dynamic correlation for all states. All CASPT2 reference weights obtained were 0.50 ± 0.03 (in the absence of the imaginary level shift, the reference weights ranged from 0.42–0.52).

Relativity was included using the the Douglas-Kroll-Hess formalism⁴⁴⁻⁴⁶.

Subsequent DFT calculations were performed in ADF2008, using the same geometries as those used for the multiconfigurational calculations. The ground state of the neutral was calculated using DFT with the SAOP functional. The ground and first 100 excited states of the cation were calculated using TD-DFT with the SAOP functional. The basis sets were ZORA TZP, as implemented in ADF, for all atoms, and relativity was included using the ZORA formalism.

As in chapter 2, much of the computational analysis presented in this chapter involves natural orbitals (NOs) and their occupations (NOOs). These are specific to each state, *i.e.* they are computed from the reduced density matrix of each state and not from the

state averaged matrix (the latter is used to produce the pseudo-NOs which are output by default in MOLCAS).

The f electron occupancies, n_f , have been calculated as the product of the NOOs and f coefficient of the natural orbital squared, summed over all of the active space orbitals. This procedure has been extended to all of the metal orbital occupancies, the sum of which is reported as n_m . This procedure implicitly assumes orthogonality of the metal and ligand basis sets. In actual fact, there is significant overlap between them, and this overlap can be estimated from the NO normalisation constants. This in turn is used to estimate a corresponding error in the quoted occupancies.

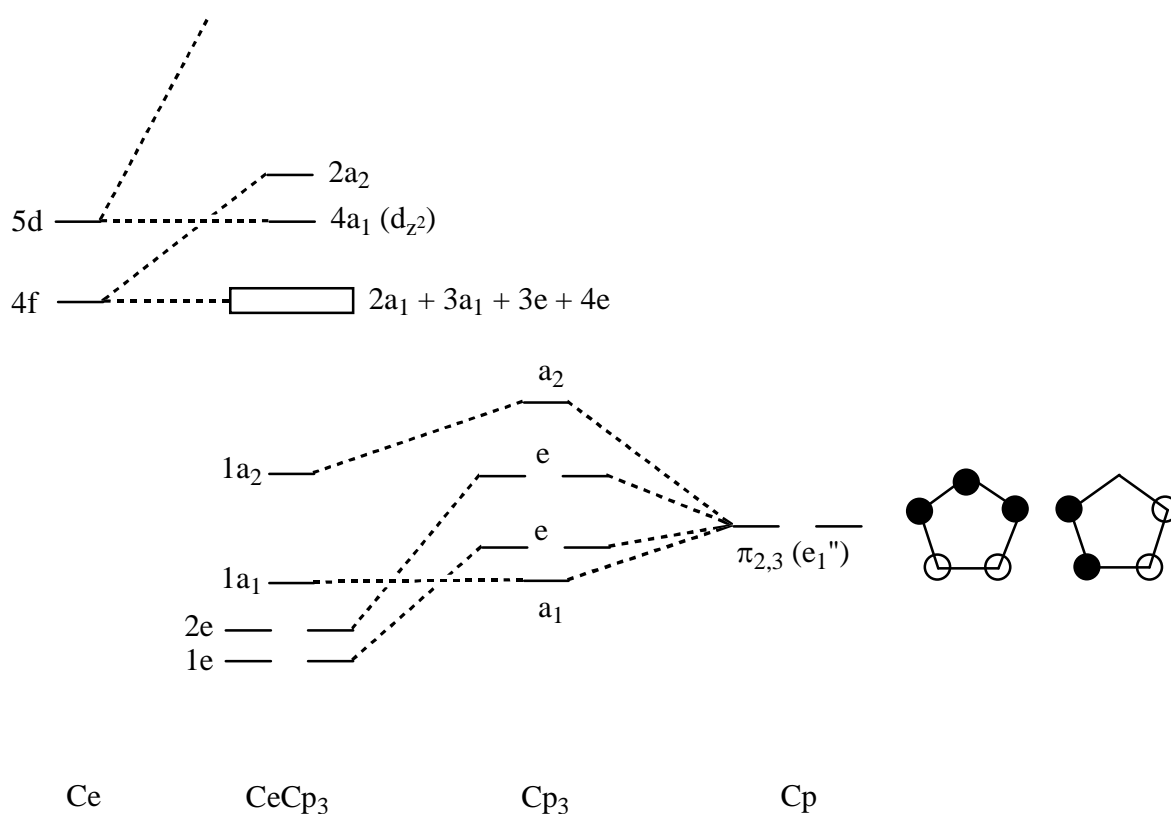


Figure 3.2- Qualitative valence molecular orbital energy level diagram for CeCp_3 , showing the interaction of the highest occupied Cp π_1 -based levels with the metal's 4f and $5d_{z^2}$ orbitals.

3.2.2 Results

In order to understand the experimental photoelectron spectrum of CeCp_3 computationally we must first understand the characteristics of the states we are looking for. Band A is easy to identify as it corresponds to the 1st ionisation energy of CeCp_3 . This is calculated from the energy difference between the ground state of CeCp_3 and the ground state of CeCp_3^+ , calculated at the CeCp_3 optimised geometry. Bands B and C correspond to ligand ionisations, as there are many such ionisations these are very broad on the experimental spectrum and difficult to identify computationally. Given that band D must share characteristics with band A in terms of f-ionisation, in order to behave in a similar way in the resonance region of the photoelectron spectrum, it is reasonable to search for the excited states of the cation to which this band corresponds in terms of its shared characteristics with the ground state of CeCp_3^+ . This shared characteristic is that both states must correspond to the ionisation of an f-electron. Thus, we would expect the f-occupancy of these two states to be similar.

The method chosen to analyse this similarity and thus to identify the excited state responsible for band D was inspection of the natural orbitals, their natural occupancies and the calculation of n_f , a measure of f-density, as described above, **3.2.1** and in **2.4.3.2**.

It was essential to use a small active space (active space II) in order to identify the state(s) responsible for band D as the energy gap between bands A and D is so large that there would be a vast number of states between the ground state of the cation and the excited state of interest which would need to be analysed (as is apparent from the broad nature of bands B and C in the photoelectron spectrum). A small active space, comprising only the highest energy occupied orbitals at the HF level and those f-orbitals spanning the same irreducible representation in C_{3v} symmetry, allows states involving these orbitals to be probed, without also calculating all the intermediate states.

3.2.2.1 Natural Orbital Analysis

3.2.2.1.1 Rationale for Natural Orbital Analysis

Natural orbital analysis was chosen as the preferred method for state comparison, rather than configurational analysis, as this method is more stable to variation in the number of states in a state averaged calculation and consequently the analysis is more reliable. This has been shown by several other groups, as well as in chapter 2^{55, 73, 77}. Further justification is given in tables 3.1 and fig. 3.3, below.

Number of states in average	Configuration 1 ^a	Configuration 2 ^b	Configuration 3 ^c
1	75.1	21.3	0.0
2	51.3	31.0	12.0
3	35.6	54.2	5.6
4	24.9	67.0	2.2
5	24.5	66.6	0.9
6	23.0	68.0	0.6
7	24.4	71.4	2.5
8	21.2	71.8	1.9
10	20.1	65.5	1.5

Table 3.1- Contribution (%) of the three leading CASSCF configurations to the ¹A' ground state of CeCp₃⁺ as a function of the number of states included in the state average. Active space II, basis A.
^a 2000 2000 ^b 2000 u0d0 ^c 2000 0020. The first four symbols in each configuration are the occupation of the a' orbitals, and the second four the a'' occupation. u = up-spin electron, d = down-spin electron.

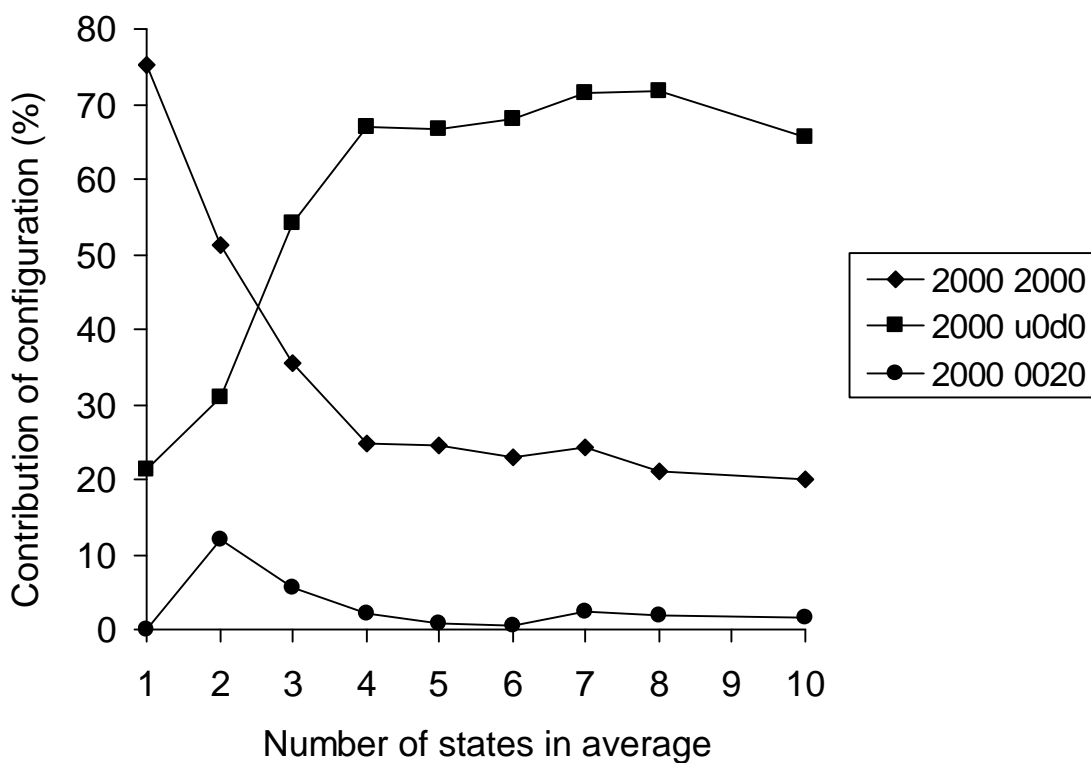


Figure 3.3- Contribution (%) of the three leading CASSCF configurations to the $^1A'$ ground state of $CeCp_3^+$ as a function of the number of states included in the state average. Active space II, basis A⁸⁸.

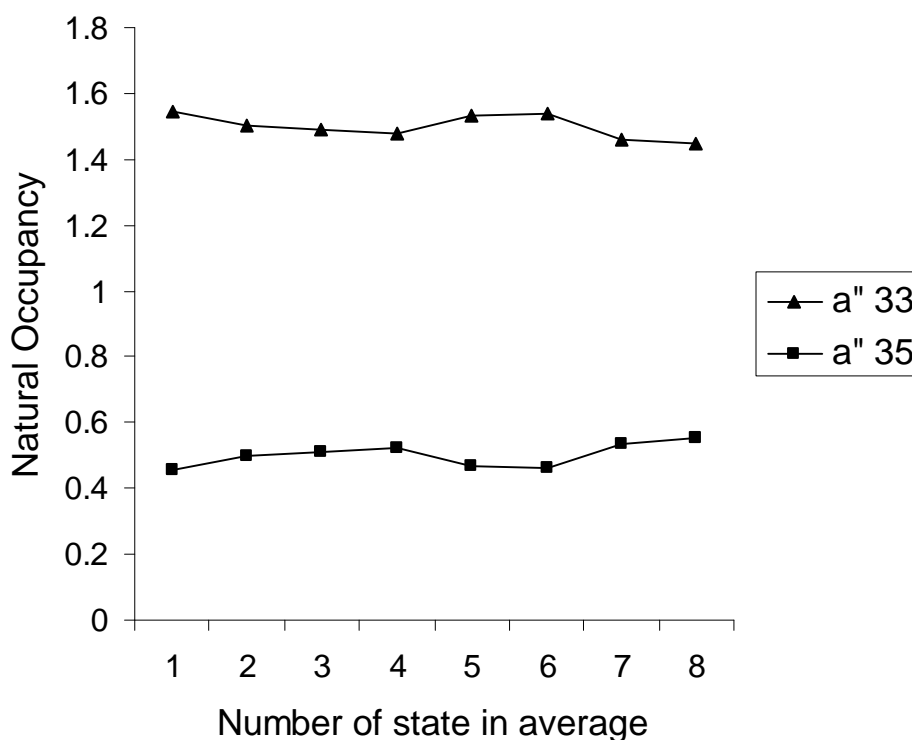


Figure 3.4- Natural occupancies for a'' orbitals 33 and 35 of the ground state of $CeCp_3^+$ as a function of the number of states included in the state average. Active space II, basis A.⁸⁸ Orbitals 33a'' and 35 a'' ($1a_2$ and $2a_2$ in fig. 3.2) are chosen as these orbitals are found to have occupancies significantly deviating from integer values.

From these data it can be seen that the configuration weights vary considerably with varying state average size. Configurational analysis is therefore not a consistent tool for state identification. Natural orbital occupation is much more stable with respect to changes in state average size, as was shown in 2.4.3.1 and below in fig. 3.4, and is therefore preferable for this study.

3.2.2.1.2 Performing the analysis

3.2.2.1.2.1 Symmetry Considerations

The CeCp₃ molecule is of C_{3v} symmetry. Its orbitals should therefore span the irreducible representations of this point group. However, the Molcas programme allows symmetry to be invoked only for Abelian point groups with the added constraint that all the symmetry operations must be generated by a combination of in-the-plane reflections and 180° rotations. Thus, the highest symmetry point group which can be used for CeCp₃ is C_s. Performing a CASSCF calculation in a reduced symmetry can be problematic. This is due to two factors. The first is that excitations in the active space which are forbidden in the true symmetry may be allowed in the reduced symmetry. This can be dealt with either by modifying the chosen active space or post hoc, as will be described in more detail in 3.2.2.1.2.3. The second symmetry-related problem is that orbitals which in the true symmetry form a degenerate pair may now span different irreps. This can lead to preferential occupation of one rather than the other.

In this study a problem was encountered for formally 4f¹ states of the cation (those formed from a ligand ionisation of the neutral species and responsible for bands B and C) of A' symmetry. Indirect coupling to ligand levels, forbidden in C_{3v}, is possible in C_s and leads to pairs of orbitals with almost identical occupancies, deviating by a very small amount (and symmetrically) from unity and each contributing ~50% of the f density. This forbidden mixing can be controlled in the pseudo-natural orbitals used in the CASSCF optimisation using CLEANUP and SUPSYM options in the Molcas code. However, this does not follow through in to the state specific NOs used in the analysis. Instead, the two orbitals with near integer occupancies were combined in the most

simple way: as orbital(1) + orbital(2) and orbital(1) – orbital(2). This yields a ligand orbital and a localised f-orbital, each with single occupancy, as would be expected for such a state. The original orbitals and the linear combinations for orbitals 33a" and 36a" are shown below, fig. 3.5

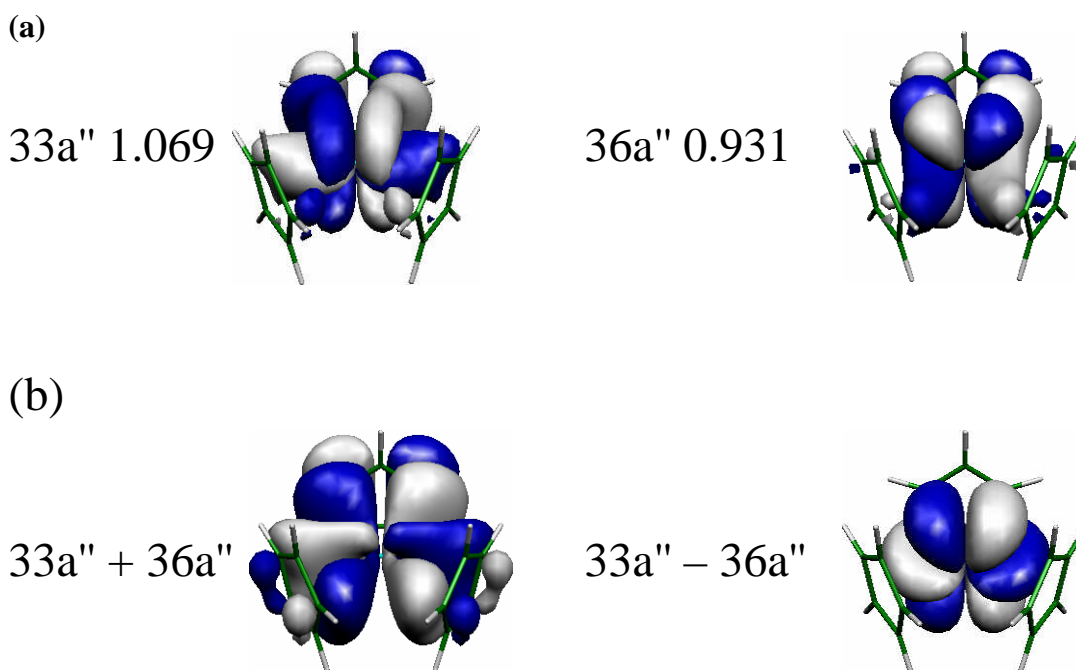


Figure 3.5- Natural orbitals and occupations for the A ¹A' (first excited) state of CeCp₃⁺. (a) Unaltered NOs and (b) linear combinations 33a" + 36a" and 33a" – 36a". Active space II, basis A, 10 state average.

3.2.2.1.2.2 Visualising the Orbitals

Perhaps the best way to get an initial idea of similarity between states is to look at the natural orbitals and see if the ground state orbitals look similar to any of the higher excited states.

Fig. 3.6 shows selected natural orbitals, and their occupancies, for the ground state of the neutral CeCp₃ molecule. This shows two doubly occupied orbitals (48a' and 33a") which are ligand based (and which form a degenerate e pair in C_{3v}) and one singly occupied 4f orbital (36a") localised on the Ce, as would be expected for a Ce(III) system.

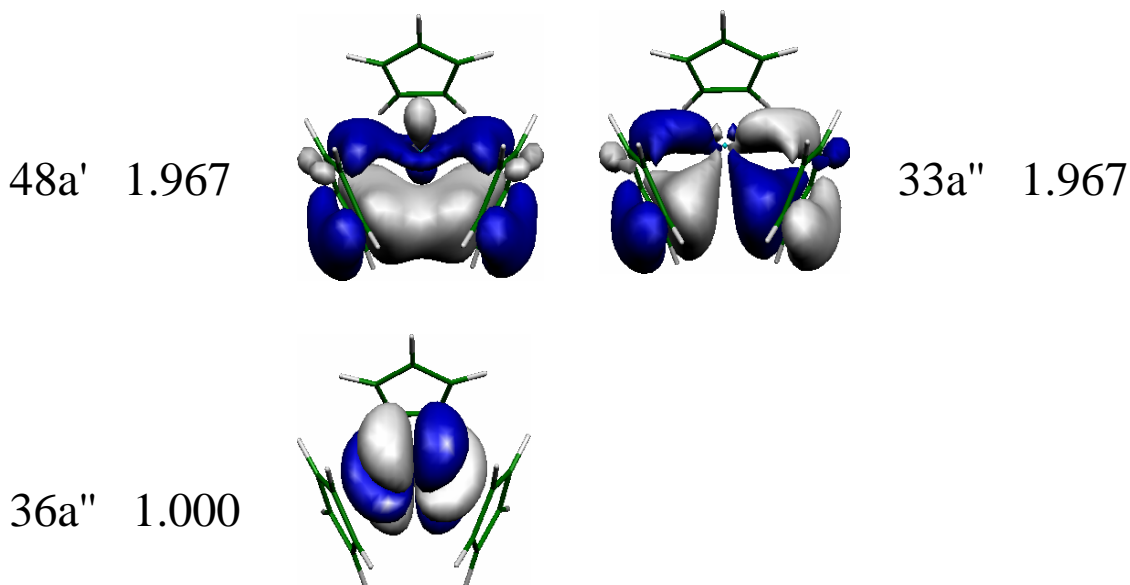


Figure 3.6- Selected natural orbitals and occupations for the X^2A'' (ground) state of $CeCp_3$. Active space II, basis A, single state.

Fig. 3.7 shows selected natural orbitals and their occupancies for the $CeCp_3^+$ ground state. These orbitals look somewhat different than might be expected. Simplistically, one would think of the ground state of the $CeCp_3$ cation looking like the ground state of the neutral molecule with the 4f localised electron removed. In fact, the natural orbitals show one doubly occupied ligand based orbital and then two orbitals each with some ligand and some 4f character, each with non-integer occupancies.

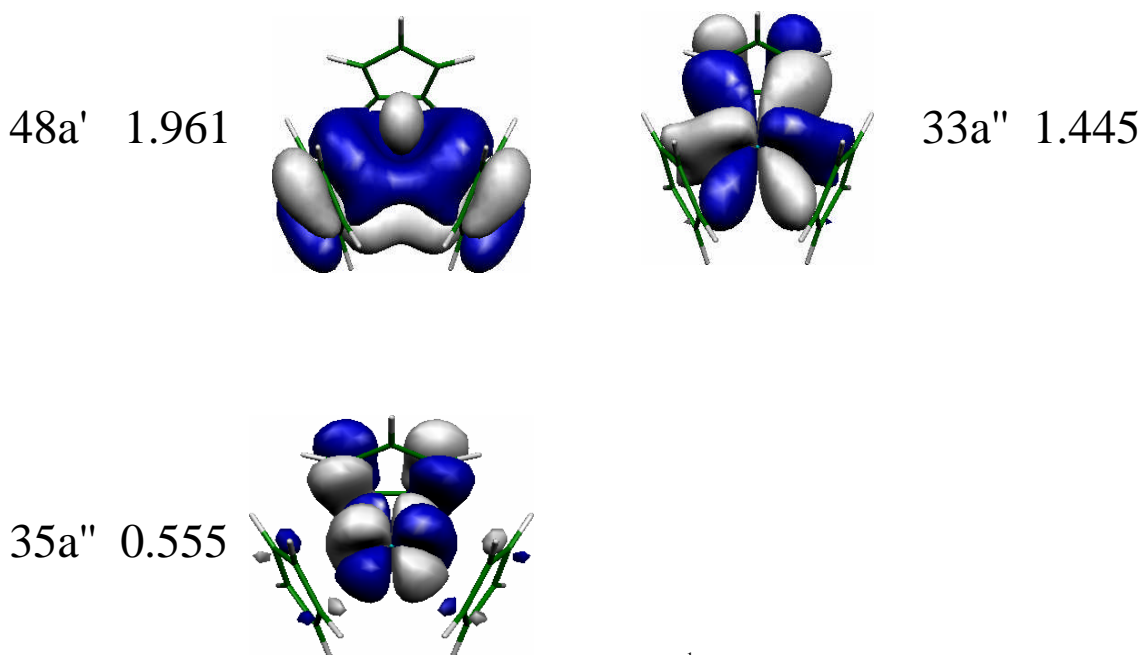


Figure 3.7- Selected natural orbitals and occupations for the X^1A' (ground) state of $CeCp_3^+$. Active space II, basis A, 10 state average.

Whilst this set of natural orbitals may not be expected when first considering the system, it is fairly easy to rationalise. Once the 4f electron has been ionised the central cerium ion, now with a 4+ charge, is surrounded by electron rich π -bonds on the ligands. It is not unreasonable to expect some of the electron density from these orbitals to transfer to the metal valence orbitals of the same symmetry, the $4f_{y(3x^2-y^2)}$, as is seen in orbitals 33a'' and 35a''. It is also noteworthy that these two orbitals have occupancies deviating significantly from integer values, indicating a large amount of static correlation in the system. This implies that this system can only be modelled properly using a multiconfigurational technique.

Given the nature of the ground state of the cation, responsible for band A in the photoelectron spectrum, we would expect the excited state responsible for band D in the photoelectron spectrum to exhibit similar behaviour whilst other, intermediate states would result from ligand ionisations with the localised, singly occupied 4f orbital observed for the neutral still present.

Fig. 3.8 shows an example of one of the excited states of the cation, which shows the expected orbital occupations of a ligand ionisation (i.e. one of the ionisations responsible for bands B or C). There is one doubly occupied ligand orbital (33a''), one single occupied ligand orbital (48a'), and one localised f-electron (34a''). This clearly corresponds to a ligand ionisation from the neutral system, fig. 3.6.

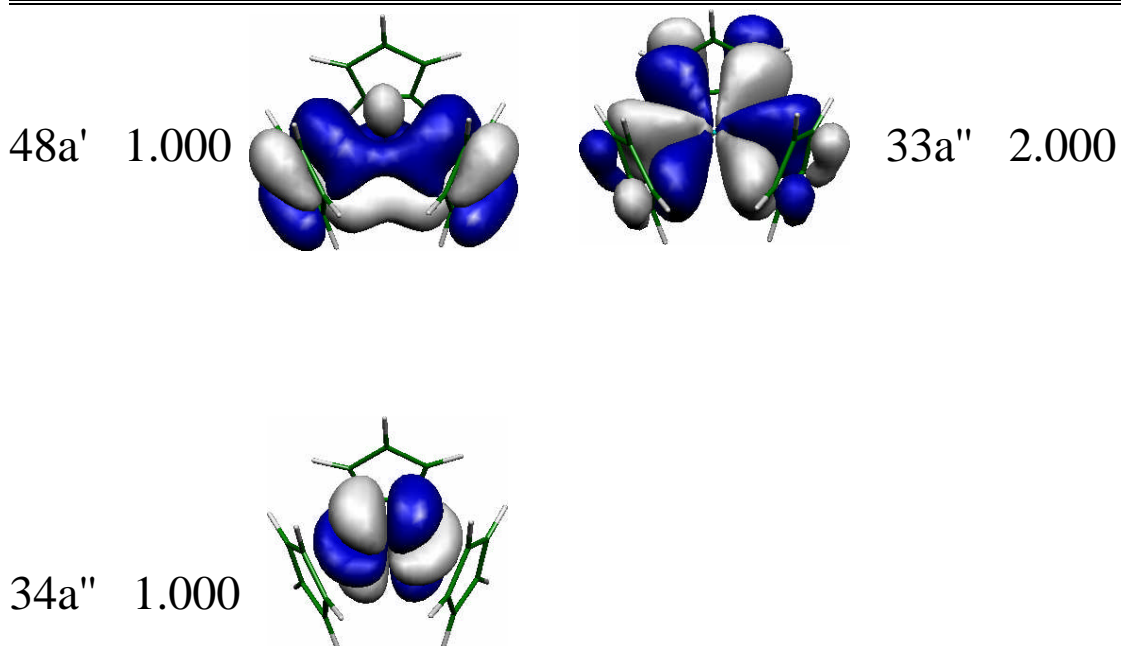


Figure 3.8- Selected natural orbitals and occupations for the B ¹A'' (second excited) state of CeCp₃⁺.

Active space II, basis A, 10 state average.

Figs. 3.9 and 3.10, on the other hand, show higher excited states mirroring some of the characteristics of the cation ground state. Specifically, non-integer occupations of two orbitals, both of which have some ligand and some $4f_{y(3x^2-y^2)}$ character.

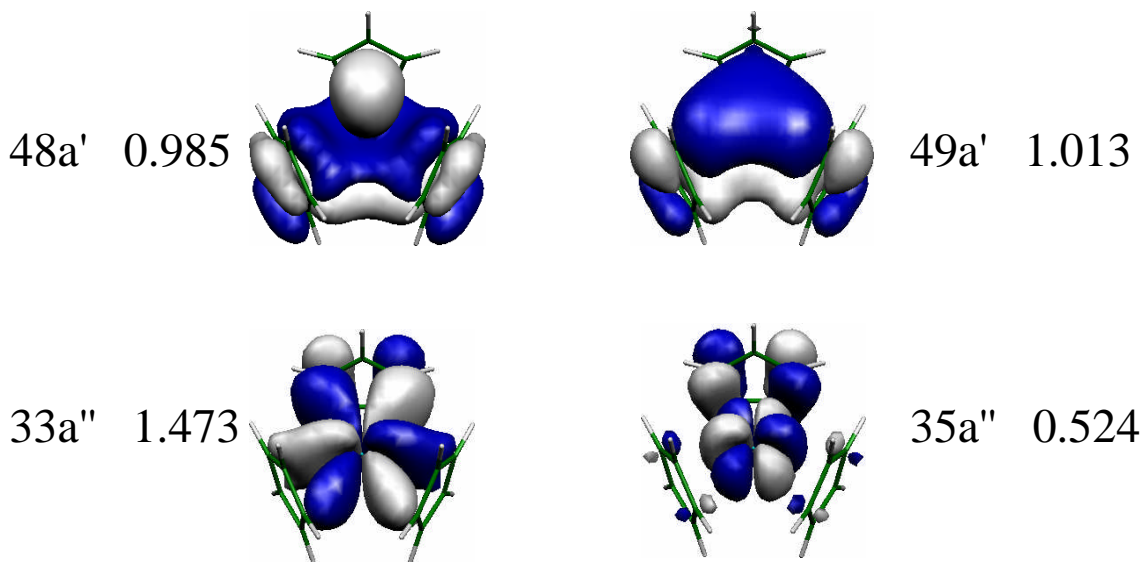


Figure 3.9- Selected natural orbitals and occupations for the E ¹A' (fifth excited) state of CeCp₃⁺. Active

space II, basis A, 10 state average.

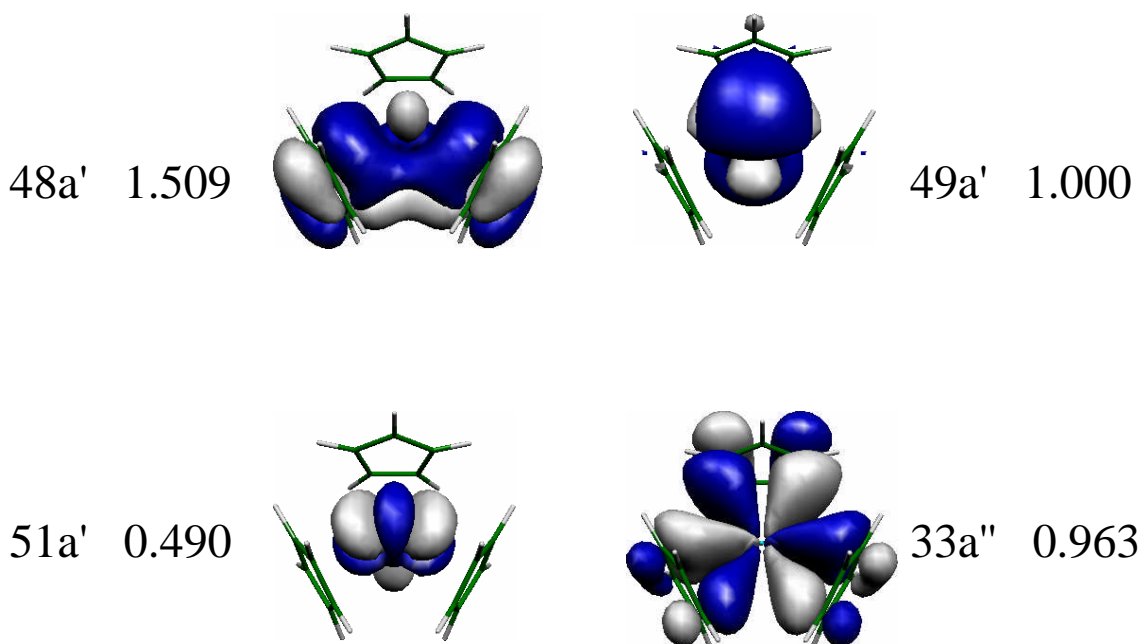


Figure 3.10- Selected natural orbitals and occupations for the E $^1A''$ (fifth excited) state of $CeCp_3^+$. Active space II, basis A, 10 state average.

3.2.2.1.2.3 Comparison with Experiment

Having identified the excited states which appear to have characteristics in common with the ground state, the energetics of these states must be considered. If the difference between the energy of the ground state of the neutral and the ground state of the cation is close to that for band A in the photoelectron spectrum, this lends support for the method chosen and the conclusion drawn. If the difference in energy between the ground state of the neutral and the identified excited states is close to that of band D, this would tend to suggest that these states are indeed responsible for the appearance of this band.

Table 3.3 shows all the states calculated, the natural occupancies of the active space orbitals, the energies (relative to the ground state of the neutral) and assignment of the corresponding bands in the photoelectron spectrum. The match for both bands A and D is extremely good, suggesting that the assignment based on natural orbital analysis is correct.

	Active space orbital								Energy	Band
	48a'	49a'	50a'	51a'	33a''	34a''	35a''	36a''		
CeCp ₃ \tilde{X}^2A''	1.967	0.001	0.027	0.005	1.966	0.029	0.005	1.000	0	
CeCp ₃ ⁺ \tilde{X}^1A'	1.961	0.000	0.000	0.038	1.445	0.000	0.555	0.000	7.07	A (6.77)
CeCp ₃ ⁺ \tilde{X}^1A''	2.000	0.000	1.000	0.000	1.000	0.000	0.000	0.000	7.30	B (7.45)
CeCp ₃ ⁺ \tilde{A}^1A''	2.000	0.000	0.000	1.000	1.000	0.000	0.000	0.000	7.35	B
CeCp ₃ ⁺ \tilde{A}^1A'	1.998	0.000	0.000	0.002	1.069	0.000	0.000	0.931	7.64	B
CeCp ₃ ⁺ \tilde{B}^1A'	1.999	0.000	0.000	0.000	1.023	0.977	0.000	0.000	7.67	B
CeCp ₃ ⁺ \tilde{C}^1A'	1.181	0.000	0.000	0.818	1.921	0.000	0.078	0.000	7.86	C1 (8.13)
CeCp ₃ ⁺ \tilde{B}^1A''	1.000	0.000	0.000	0.000	2.000	1.000	0.000	0.000	7.96	C1
CeCp ₃ ⁺ \tilde{D}^1A'	1.009	0.000	0.990	0.000	1.999	0.001	0.001	0.000	8.06	C1
CeCp ₃ ⁺ \tilde{C}^1A''	1.000	0.000	0.000	0.000	2.000	0.000	1.000	0.000	8.06	C1
CeCp ₃ ⁺ \tilde{D}^1A''	1.000	0.000	0.000	0.0000	2.000	0.000	0.000	1.000	8.25	C1
CeCp ₃ ⁺ \tilde{E}^1A''	1.509	1.000	0.001	0.490	0.963	0.000	0.000	0.037	10.00	D (9.97)
CeCp ₃ ⁺ \tilde{E}^1A'	0.985	1.013	0.000	0.002	1.473	0.000	0.526	0.001	10.17	D

Table 3.3- Natural orbital occupations of the ground and low-lying excited states of CeCp₃⁺, and the ground state of CeCp₃. CASPT2 energy (eV) relative to CeCp₃ \tilde{X}^2A'' state. Active space II, basis A. 'Band' is the photoelectron spectrum band, bracketed numbers are experimental band energy (eV), see fig. 3.1 for experimental band assignment.

3.2.2.1.2.4 Oxidation State

The two bands of the photoelectron spectrum corresponding to states with formally Ce(IV) centres have been identified. Given that the broader scope of this thesis is to better understand oxidation states of cerium organometallics it is worth considering the relation between formal oxidation state and 4f electron density of the cerium centre in these states.

The method chosen for analysis of 4f-electron density here is the same as that used in chapter 2. For a formally Ce(III) system, an n_f of ~ 1 would be expected and for a formally Ce(IV) system, an n_f of ~ 0 would be expected. Therefore, one would expect n_f 's of 1 for the CeCp₃ ground state and CeCp₃⁺ states corresponding to ligand ionisations. An n_f of ~ 0 would be expected for the ground state of CeCp₃⁺ and the other f-ionisation state (the fifth excited states of A' and A'' symmetry using active space II and basis A). However, table 3.4, below, shows that this is not the case. Instead n_f 's of ~ 1 are calculated for all states.

	State	n_f	NOs contributing to n_f (contribution)	n_m	Formal Ce oxidation state
CeCp ₃	\tilde{X}^2A''	1.02 ± 0.01	36a'' (0.998)	1.29 ± 0.08	III
CeCp ₃ ⁺	\tilde{X}^1A'	1.07 ± 0.09	33a'' (0.654), 35a'' (0.333)	1.23 ± 0.11	IV
CeCp ₃ ⁺	\tilde{B}^1A''	1.04 ± 0.01	34a'' (0.998)	1.13 ± 0.02	III
CeCp ₃ ⁺	\tilde{E}^1A''	1.01 ± 0.09	48a' (0.603), 51a' (0.336)	1.97 ± 0.18	IV
CeCp ₃ ⁺	\tilde{E}^1A'	1.02 ± 0.10	33a'' (0.701), 35a'' (0.305)	2.18 ± 0.10	IV

Table 3.4- Ce f electron occupancy n_f , and total metal electron occupancy n_m , in selected states of CeCp₃ and CeCp₃⁺. Active space II, basis A.

These n_f 's beg the question, what is the oxidation state of Ce in the ground state of CeCp₃⁺? Whilst all the states shown in table 3.4 have an n_f close to 1, they arise in very

different ways. Those which have formal Ce(III) oxidation state all have a natural orbital with a localised f-electron, those which have formal Ce(IV) oxidation state all have natural orbitals with delocalised f-density, mixed with ligand density and spanning two natural orbitals.

Thus there is a clear distinction between a formally Ce(III) state and a Ce(IV) state, with a Ce(III) state possessing an ionisable f-electron and a Ce(IV) state having a significant, but delocalised, f-density. As this f-density is not localised, these Ce(IV) states would not be expected to display the same chemical properties as the Ce(III) electron density. As oxidation state is merely a useful tool for predicting likely chemistry, and the chemistry of the formally Ce(III) states would be expected to be similar, whilst that of the Ce(IV) states would be different, the formal oxidation state labels for the states described in table 3.4 are the most useful ones. However, it is clearly the case that the Ce(IV) states identified here do in fact possess significant f-electron density. This should be borne in mind in further studies, both experiment and computational.

The next most important question is, what is the difference between the two states responsible for bands A and D in the photoelectron spectrum? A comparison of n_m 's shows that the main difference between the ground state of the CeCp₃ cation and the fifth excited state is the presence of an additional metal electron, which can be identified as a 5d electron, by inspection of the natural orbitals, fig. 3.9 and 3.10. Analysis of the atomic orbital contributions to orbital 49a' show that it is almost entirely Ce 5d. Inspection of this orbital corroborate this, showing a taurus and two radial nodes. Thus, the large energy gap between bands A and D can be interpreted as the energy difference between a state formed from an f-ionisation of the neutral CeCp₃ molecule and a state formed from this ionisation plus a ligand to metal excitation into a 5d orbital, which is a significantly higher energy process.

3.2.2.2 Summary of CASPT2 results for CeCp₃ and CeCp₃⁺

Many of the data presented above for the ground state of CeCp₃, and the ground and excited states of CeCp₃⁺, have been obtained from CASPT2 calculations performed using a fairly small active space and a basis set without Ce g-functions. This was

essential in order to be able to identify the excited state of interest, due to the large energy gap between this state and the ground state.

However, the first ionisation energy of CeCp_3 was also calculated with a larger active space in order to check that the reduction of active space still included all the energetically and chemically important orbitals. Subsequent calculations were also performed using larger basis sets, basis B, with Ce g-functions. The excited states of interest were also identified with this larger active space. A summary of these results, along with the experimental data, is given below, table 3.5.

It can be clearly seen from this table that using a smaller active space and basis set makes little difference to the accuracy of the results. Qualitatively, the results are the same in all cases, and quantitatively the data are very similar and the deviation from the experimental ionisation energies consistent and remarkably small.

3.2.2.3 TD-DFT approach

The CASSCF results indicate that the Ce(IV) states of the CeCp_3 cation must be represented by a multiconfigurational method. However, DFT is a much less resource intensive technique to use which, although not as theoretically robust as CASSCF often gives reasonable agreement with experiment. TD-DFT can be used to identify excited states. Therefore, TD-DFT calculations were performed on CeCp_3^+ and DFT on CeCp_3 . Given that the excited state of the cation resulting in band D in the photoelectron spectrum had been identified by CASSCF as arising from a ligand to 5d charge transfer, the TD-DFT excitations were inspected to identify the excitations due to this transfer and the excitation energies of these transitions noted. This has several advantages over the CASSCF calculations, namely that the calculations may be performed in the correct point group, there is no requirement to select the active space, with accompanying errors introduced, and the calculations are not computationally demanding.

Eight excited states of the cation relating to $\text{Cp} \rightarrow \text{Ce}$ 5d electron transfers were identified, with excitation energies ranging from 2.99 eV to 3.82 eV relative to the SAOP ground state, as shown in table 3.5. This energy gap between the ground state of

the cation and the Ce(IV) excited states compares fairly well with experiment. However, these states would have been very difficult to identify without the prior guidance of the CASSCF calculations. Thus, whilst the TD-DFT calculations support the results determined using the CASSCF method, this is not likely to be a practical method for rationalising photoelectron spectra over such a large energy range in subsequent calculations, especially if, as in this case, the system is multiconfigurational.

	Band A (ground $^1A'$ state)	Band D
Experiment	6.77	9.97
Active space I, basis A	6.62	
Active space II, basis A	7.02	
Active space II, basis A, 10-state average, imaginary level shift	7.07	10.00, 10.17
Active space II, basis B, 10-state average, imaginary level shift	6.67	9.64, 9.79
TDDFT SAOP	6.07	9.06, 9.15, 9.36, 9.51, 9.70, 9.78, 9.86, 9.89

Table 3.5- Experimental vertical ionisation energies (eV) of CeCp₃, and calculated (CASPT2) energy difference between the ground $^2A''$ state of CeCp₃ and the ground and fifth excited $^1A'$ states of CeCp₃⁺

3.2.3 Anion calculations

Having published these results⁸⁸ experimental workers studying substituted LnCp₃⁻ anion systems enquired of us as to whether a single configurational method was suitable for these systems, having used DFT to model them⁹⁰. Consequently additional calculations were performed on two anion systems, LaCp₃⁻ and CeCp₃⁻.

A reasonable initial hypothesis might be that LaCp_3^- would closely resemble CeCp_3 in its electronic structure. CeCp_3^- is particularly interesting as information on the two singly occupied orbitals might help to understand the excited states of CeCp_3^+ , as which orbitals are occupied in the anion might give information on the ordering of unoccupied orbitals in the cation, and hence the ordering of excited states.

3.2.3.1 Ground state analysis

Molcas 6.4 calculations were performed at the CASPT2 level with ANO basis sets $\text{La}(24,21,15,5/9,8,6,3)$; $\text{Ce}(25,22,15,11/9,8,5,4)$; $\text{C}(14,9,4/3,2,1)$; $\text{H}(8,4/2,1)$ and a (5,10) active space for the lanthanum complex and (6,10) for the cerium complex (to allow both 4f and 5d orbital occupation). The geometries used were those from the crystal structure⁹⁰ for the lanthanum complex and the optimised geometry used earlier in the chapter for the cerium complex.

3.2.3.1.1 LaCp_3^-

The ground state was identified to be $^2A'$ with the natural occupations shown below, table 3.6.

Orbital A'	48	49	50	51	52	53
Occupancy	1.973	0.999	0.020	0.001	0.003	0.004
Orbital A''	33	34	35	36		
Occupancy	1.973	0.004	0.003	0.020		

Table 3.6- Natural Occupancies of LaCp_3^- $^2A'$ ground state active space orbitals.

It can be seen from table 3.6 that the LaCp_3^- anion is not multiconfigurational, and hence DFT is predicted to model this system adequately. One orbital is singly occupied. Figure 3.11, below, shows this orbital, which has 53% d character and 33% s character. Thus, LaCp_3^- does not mimic CeCp_3 exactly as the unpaired electron is in a d/s orbital, not an f orbital.

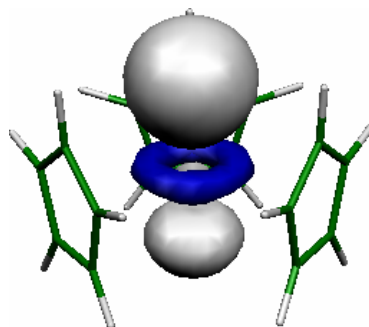


Figure 3.11- Natural orbital 49a' of LaCp₃^{-2A'} ground state

3.2.3.1.2 CeCp₃⁻

The ground state was identified to be ^{3A''} with the natural occupations shown below, table 3.7.

Orbital A'	48	49	50	51	52	53
Occupancy	1.9814	0.9970	0.0020	0.0058	0.0051	0.0108
Orbital A''	33	34	35	36		
Occupancy	1.9848	0.0143	0.0026	0.9962		

Table 3.7- Natural Occupancies of CeCp₃^{-3A''} ground state active space orbitals.

It can be seen from table 3.7 that the CeCp₃⁻ anion is not multiconfigurational, and hence DFT is predicted to model this system adequately. Two orbitals are singly occupied. Figure 3.12, below, show these orbitals.

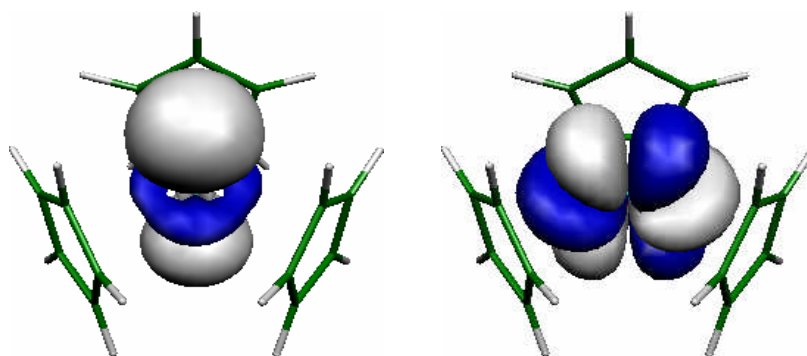


Figure 3.12- Natural orbitals 49a' and 36a'' of CeCp₃^{-A''} ground state

Orbital 49a' has 41% d character and 47% s character. Orbital 36a" has 99% f character. In addition to the single f orbital occupancy seen in the CeCp₃ case the 5d₂₂ orbital is also occupied. This suggests that the 5d₂₂ orbital is low-lying, an encouraging result in the light of the analysis of the CeCp₃ photoelectron spectrum.

3.2.4 Conclusions

The photoelectron spectrum of CeCp₃ has been rationalised with remarkably good agreement between the experimental ionisation energies and those calculated. The two states relating to f-ionisations have been identified. The large energy gap between these states (3.2 eV) results from a Cp→Ce 5d electron transfer in the higher energy state. Both these formally Ce(IV) states have significant 4f density, equivalent in terms of calculated n_f value to the 4f density in the Ce(III) excited states of the cation and of the neutral. However, in the case of the Ce(IV) states this electron density is delocalised and would not, therefore be expected to be accessible in the same way as the f-density in the Ce(III) systems. This result is strikingly similar to that obtained for cerocene in chapter 2. The Ce(IV) states of CeCp₃⁺ are highly multiconfigurational and these states can, therefore, be modelled effectively only using a multiconfigurational method. This suggests that other Ce(IV) organometallics with aromatic ligands might also require a multiconfigurational approach. Whilst TD-DFT can mimic the general trends of the CASSCF results, the calculations are less accurate and cannot properly represent the delocalised f-electron density observed for the formally Ce(IV) states. Much of this work has been published in Dalton Transactions⁸⁸.

LaCp₃⁻ is not multiconfigurational, as would be expected. However, unlike the isoelectronic CeCp₃ the singly occupied orbital is predominantly La 5d₂₂, rather than 4f. CeCp₃⁻ is also not multiconfigurational. The electronic configuration of this molecule, and especially the fact that the 5d₂₂ orbital is singly occupied corroborates the analysis of the CeCp₃ photoelectron spectrum. These results also suggest that, whilst single determinant methods are not adequate for the formally f⁰ CeCp₃⁺ system they are typically reasonable for f¹ and f¹d¹ systems, as shown by the very small deviations from integer values of the natural occupancies of the natural orbitals for CeCp₃ and CeCp₃⁻.

4. Bis-cyclopentadienyl complexes

4.1 Previous work

Having previously investigated two formally Ce(IV) systems to gain a better understanding of the oxidation state of Ce in these complexes using a multiconfigurational method it was decided to extend these investigations to other systems which might be of interest to experimentalists. Several formally Ce(IV) sandwich systems have been synthesised by Bian et al.⁹¹ and the oxidation state of Ce in them determined using XANES L_{III} edge analysis. One of these systems was identified as Ce f¹ whilst three others appeared to be closer to Ce f⁰. It was suggested that the reason for this difference was the nature of the ligands involved: the apparently Ce(III) system having very electron-rich naphthalocyaninato ligands. A computational study of this molecule might be possible, aided by the high symmetry of the ligand. However, the ligands are very large (132 atoms each) and therefore a high level study would unfortunately be computationally unfeasible.

More computationally tractable molecules for study are provided by a DFT study by Hay et al. of 2005¹⁵. Their study investigates the nature of the Ce-X bond in the series CeCp₂X where X=F⁺, O, NH, CH₂ and CH⁻ and proposes that these molecules may be synthesisable. All structures, except for that with the methylene ligand, have C_{2v} symmetry. This is highly advantageous for a Molcas multiconfigurational study as C_{2v} is an Abelian point group with only reflections and C₂ rotations and thus calculations on these molecules will not be subject to the problems with lowering symmetry encountered for both cerocene and cerium tris-cyclopentadiene. There are two additional points that make these systems interesting. The first is that the series of molecules gives an opportunity to ‘tune’ the valence of Ce depending on the electronegativity of the X ligand. This allows consideration of the underlying chemistry giving rise to the speculations of Bian et al.⁹¹ regarding the differences seen in the synthesised molecules without undertaking calculations of very large molecules. The second is that understanding the nature of the bonding in these molecules might, as

suggested by Hay et al. give guidance as to whether they might be reasonable targets for synthetic investigations.

4.2 Computational details

4.2.1 Geometry Optimisation

The geometries of seven molecules were optimised in ADF 2008⁵³ using the PBE density functional. The geometries of HfCp₂O, ThCp₂O, CeCp₂O and CeCp₂NH were optimised in C_{2v} symmetry. CeCp₂F⁺ was not included as its geometry could not be optimised. Two geometries each were optimised for HfCp₂CH₂, ThCp₂CH₂ and CeCp₂CH₂, one with the methylene hydrogens parallel to cyclopentadienyl rings and one with the methylene hydrogens perpendicular to the cyclopentadienyl rings (shown in figure 4.1). All of the methylene structures were optimised in C_s symmetry. Frequency calculations were carried out on these structures and imaginary frequencies identified. These are discussed further in 4.3.1. The basis sets used were the ADF relativistic TZP bases for all atoms. Relativity was included using ZORA.

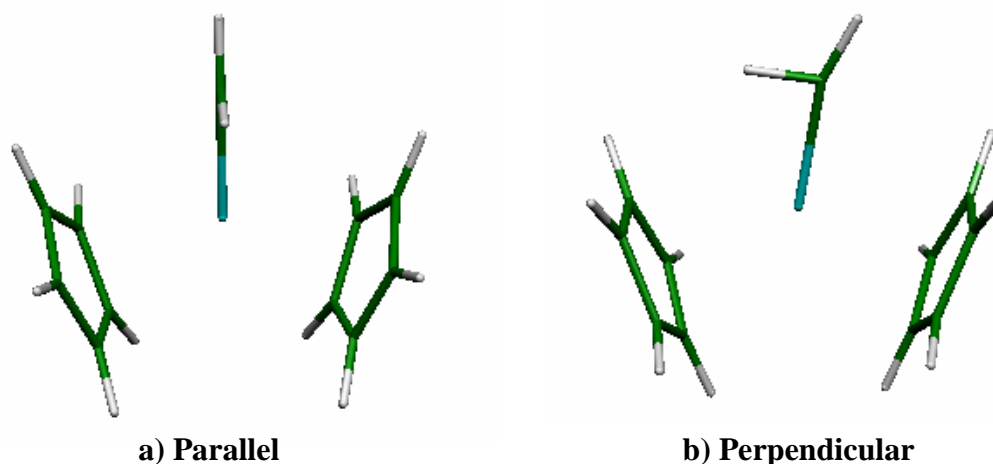


Figure 4.1- PBE optimised C_s geometries of CeCp₂CH₂

Gaussian03⁵¹ was also used to carry out constrained geometry scans of the methylene structures, with the PBE density functional, using the ADF geometry for CeCp₂CH₂ with the methylene hydrogens parallel to the cyclopentadienyl rings as a starting point. The basis sets used in this calculation were cc-pVDZ for carbon and hydrogen and the

RECP of the Stuttgart-Dresden group for Ce, together with the valence basis sets of Cao and Dolg in the segmented contraction with the g-functions removed. Relativity was included by means of the RECP for cerium.

4.2.2 Electronic Structure

CASPT2 (14,14) calculations were carried out in Molcas 6.4⁵² for all the structures, including the highest lying seven occupied orbitals for each structure and seven correlating orbitals of appropriate symmetry at the ADF PBE optimised geometries. The orbitals included in the active space were chosen on energetic grounds, a clear band of seven occupied orbitals having been identified from the HOMO to HOMO-6 using the IVO method⁷¹. Calculations were performed in C_{2v} or C_s symmetry, as appropriate. The basis sets used were relativistic ANOs: Ce(25,22,15,11/9,8,5,4); Hf(24,21,15,11/9,8,6,4); Th(27,24,28,14/9,8,6,4); O,N,C(14,9,4/3,2,1); H(8,4/2,1). Relativity was included using the Douglas-Kroll Hamiltonian.

The multiconfigurational wavefunctions were analysed in terms of natural orbitals and their occupancies and the calculated values of the total number of f electrons (n_f), calculated using the same method as in chapters 2 and 3. Atomic contributions were calculated from the square of the coefficients of the atomic contributions to the natural orbitals.

4.3 Results

4.3.1 Geometry Optimisations

The most important geometric parameter in the molecules investigated in terms of understanding the bonding is the metal-heteroatom distance (M-X), as this gives an idea of whether this distance is consistent with an ionic, single covalent or double covalent M-X interaction. The distances obtained from the PBE optimisation are compared with the B3LYP results from the earlier study¹⁵ in table 4.1, below.

Molecule	PBE M-X (Å)	B3LYP M-X (Å)
CeCp₂O	1.825	1.814
CeCp₂NH	1.941	1.925
CeCp₂CH₂ Perpendicular	2.892	2.127
CeCp₂CH₂ Parallel	2.129	
HfCp₂O	1.796	1.798
HfCp₂CH₂ Perpendicular	2.542	-
HfCp₂CH₂ Parallel	2.185	-
ThCp₂O	2.011	-
ThCp₂CH₂ Perpendicular	2.975	-
ThCp₂CH₂ Parallel	2.173	-

Table 4.1- Comparison of M-X distances for geometries optimised using PBE and B3LYP functionals. (B3LYP data from Clark et al.¹⁵ for which CeCp₂CH₂ molecule has C₁ symmetry, C_s for PBE determined geometries)

Table 4.1 shows very good agreement between the geometries obtained using the two different functionals for CeCp₂O, CeCp₂NH and HfCp₂O. The lanthanide contraction observed in reference¹⁵ is also seen in the PBE geometries where Hf-O < Ce-O. Other corroboration with the B3LYP study is observed in terms of the variation of Ce-X bond distance with X. In both studies this varies in the order O < NH < CH₂ as would be expected if these bonds involved a covalent interaction. Further, the M-X distances obtained are smaller than would be expected by consideration of the ionic radii of M and X only, again indicating some covalent interaction.

Fig. 4.1, above, shows the CeCp₂CH₂ parallel and perpendicular geometries. The geometry obtained in the B3LYP calculations was without geometry constraints and showed an agostic interaction¹⁵, as did a CASPT2 study on the CeCH₂⁺ species⁷⁷. Table 4.1 shows that the closest match to this geometry was obtained with the parallel methylene, as this yields a Ce-C(methylene) distance very close to that obtained in the unconstrained B3LYP optimisation. Furthermore, the perpendicular methylene M-X distances suggest a weaker M-X interaction for all M than the parallel methylene structures.

However, the PBE energy of the perpendicular structures is lower in all cases than the parallel structures. An important caveat to this is that the parallel structures all have one large imaginary frequency, as shown below, table 4.2.

Molecule	PBE energy (eV)	Imaginary Frequencies (cm⁻¹)
CeCp₂O	-141.116	45.3i, 32.2i
CeCp₂NH	-144.857	-
CeCp₂CH₂ Perpendicular	-147.444	30.1i
CeCp₂CH₂ Parallel	-147.343	215.5i, 27.8i
HfCp₂O	-140.852	40.6i, 21.6i
HfCp₂CH₂ Perpendicular	-148.381	-
HfCp₂CH₂ Parallel	-147.214	451.3i, 26.2i
ThCp₂O	-142.169	-
ThCp₂CH₂ Perpendicular	-148.425	40.9i, 38.3i, 5.3i
ThCp₂CH₂ Parallel	-148.203	300.4i, 11.9i

Table 4.2-Comparison of energies and imaginary frequencies of PBE optimised geometries.

All of the small imaginary frequencies arise from vibrations of the cyclopentadienyl rings. This can be seen from the images of the imaginary frequencies below, figure 4.2.

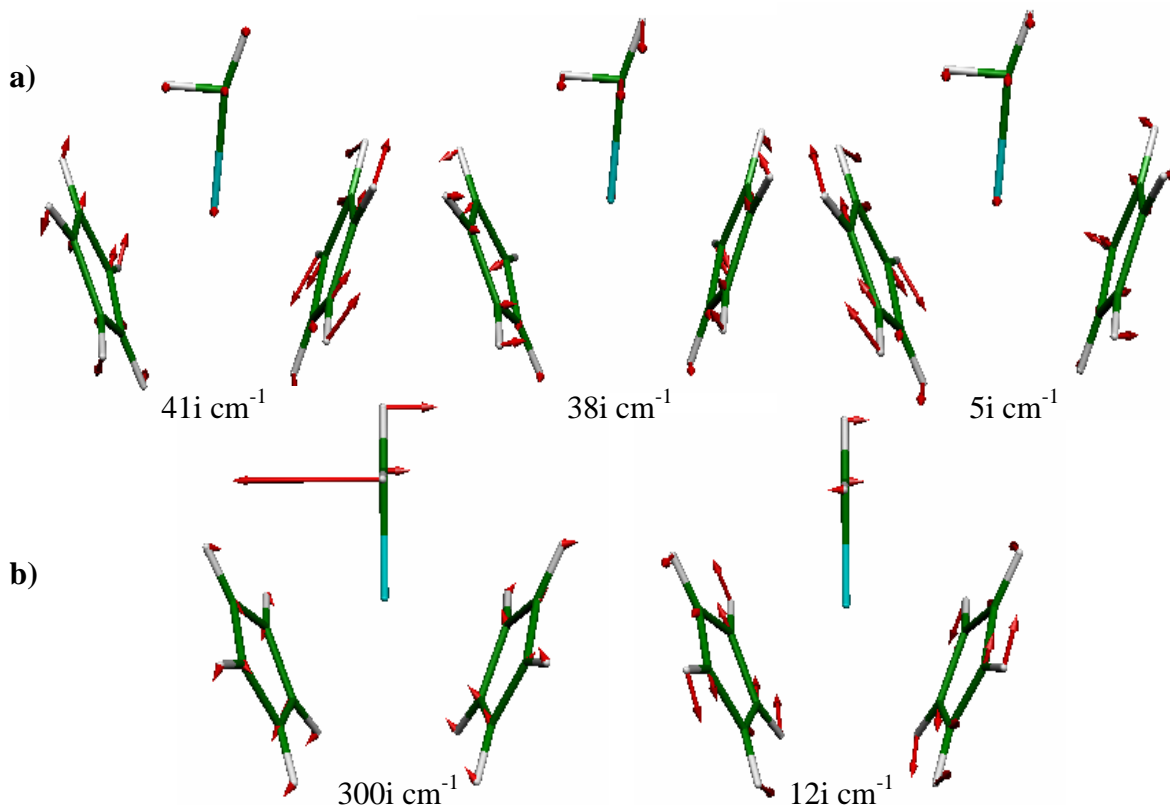


Figure 4.2- Displacement vectors of imaginary frequencies of a) perpendicular and b) parallel ThCp_2CH_2 with associated wavenumbers.

It can be seen from the displacement vectors in fig. 4.2 that the imaginary frequencies of the perpendicular structure are very small and correspond in the main to a slight twisting of the cyclopentadienyl rings away from the eclipsed conformation imposed by the C_s symmetry. This is also the case for the smaller imaginary frequency of the parallel structure. However, the large imaginary frequency of the parallel structure corresponds to a twisting of the methylene group and has a very large displacement vector.

The large MCp_2CH_2 parallel imaginary frequencies arise from a twist of the methylene group, due to a driving force for an agostic interaction, as shown in fig. 4.2 b). Therefore a constrained geometry optimisation was carried out based on the CeCp_2CH_2 parallel methylene geometry using Gaussian03 'scan' option, twisting the methylene group through 360° . The effect of this twisting on the energy of the molecule is shown in figure 4.3, below.

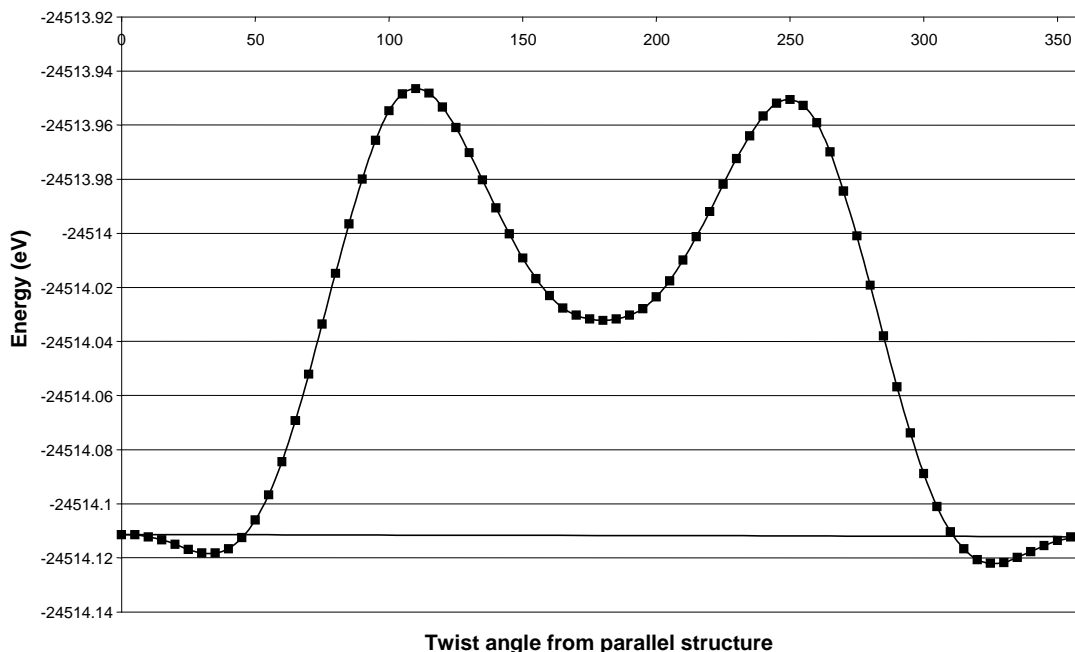


Figure 4.3- Effect on PBE energy of CeCp_2CH_2 of twisting the methylene group relative to cyclopentadienyl rings.

Figure 4.3 shows that the parallel structure (twist angle 0°) is a low energy transition state, just 0.01 eV above the two minima either side, at twist angles of 30° and 330° , the lowest at 330° . The B3LYP optimisation found a twist angle of 49.31° with a Ce-C- H_{eq} angle of 94.4° in comparison with 85.7° in this work, Ce-C- H_{ax} angle of 150° in comparison with 165° in this work. In both studies the C- H_{eq} distance is larger than the C- H_{ax} distance due to the interaction with of H_{eq} with the Ce atom, which leads to Ce- H_{eq} distances of 2.481 Å in the B3LYP optimisation and 2.339 Å in the constrained PBE calculation. This comparison shows that the PBE constrained result matches the B3LYP full optimisation well.

Despite the large imaginary frequency, the C_s parallel methylene structure seems a better C_s symmetry representation of the structure than the C_s perpendicular methylene structure as the minimum established in the scan is a very small twist relative to this geometry. Not only this, but the perpendicular C_s structure has a very large Ce- CH_2 distance, which is not supported by the work of Hay et al.¹⁵. It is necessary to make this approximation in order to impose symmetry which will enable the electronic structure to be probed using a high level method. However, this assumption will be further

investigated in the natural orbital analysis section for CeCp₂CH₂, **4.3.2.3**, where both the parallel and perpendicular structures are analysed.

The comparable large imaginary frequencies for the parallel ThCp₂CH₂ and HfCp₂CH₂ structures suggests that the lowest energy geometries for these systems also involve an agostic interaction, causing a twisting of the methylene group relative to the parallel C_s geometry. This is corroborated by a CASPT2 study⁹² on H₂MCH₂ systems with M=Zr, Nb, Mo, Ru, Th and U, which found such an agostic interaction, though smaller than in the CeCH₂⁺ study⁷⁷.

4.3.2 Natural Orbital Analysis

All natural orbital analysis is carried out on the natural orbitals from the CAS part of CASPT2 calculations.

4.3.2.1 CeCp₂O

The ground state of CeCp₂O was found to be ¹A₁. The natural occupancies from the (14,14) CASPT2 calculation in C_{2v} symmetry, are shown below, table 4.3. This shows that there is very little multiconfigurational character to the wavefunction of CeCp₂O as there is very little deviation in the natural occupancies from integer values.

Orbital Symmetry	Orbital Number	Natural Occupancy	Orbital Symmetry	Orbital Number	Natural Occupancy
a₁	26	1.967	b₂	17	1.956
	27	1.957		18	1.961
	28	0.042		19	0.013
b₁	13	1.956		20	0.043
	14	1.983	a₂	9	1.981
	15	0.051		10	0.043
	16	0.040		11	0.007

Table 4.3- Natural occupancies of natural orbitals of CeCp₂O from CASPT2(14,14) C_{2v} calculation

Those orbitals with significant oxygen character are shown in table 4.4, along with their orbital breakdown in terms of atomic character.

Natural Orbital	27a₁	13b₁	17b₂
Ce <i>m</i>	9.15	2.20	0.92
Ce <i>d</i>	8.64	8.85	4.45
Ce <i>f</i>	7.10	3.61	5.78
O π	-	84.15	65.18
O <i>o</i>	62.85	0.10	0.05
C <i>c</i>	11.96	1.07	23.52
H <i>H</i>	0.36	0.00	0.10

Table 4.4- Percentage atomic orbital character of natural orbitals of CeCp₂O with significant O-character, where O_o indicates non- π oxygen character and C_c indicates cyclopentadienyl carbon character.

Table 4.4 shows three orbitals involved in Ce-O bonding. This concurs with the results from the DFT study of 2005¹⁵ and is consistent with the presence of both a σ and two π interactions. Both works indicate that the bonds have largely O character with approximately 20% Ce character. However, the current work shows very slightly greater f-contributions.

The total n_f from all of the active space orbitals is 0.390 ± 0.003 . This small and delocalised f electron character indicates a close to Ce 4f⁰ system, as would be expected from the 4+ oxidation state.

Those orbitals which are involved in the Ce-O bond, those of table 4.4, are shown below, along with their natural occupancies, figure 4.4. These show clearly the σ bond and the two π bonds, one of which includes some bonding to the cyclopentadienyl rings.

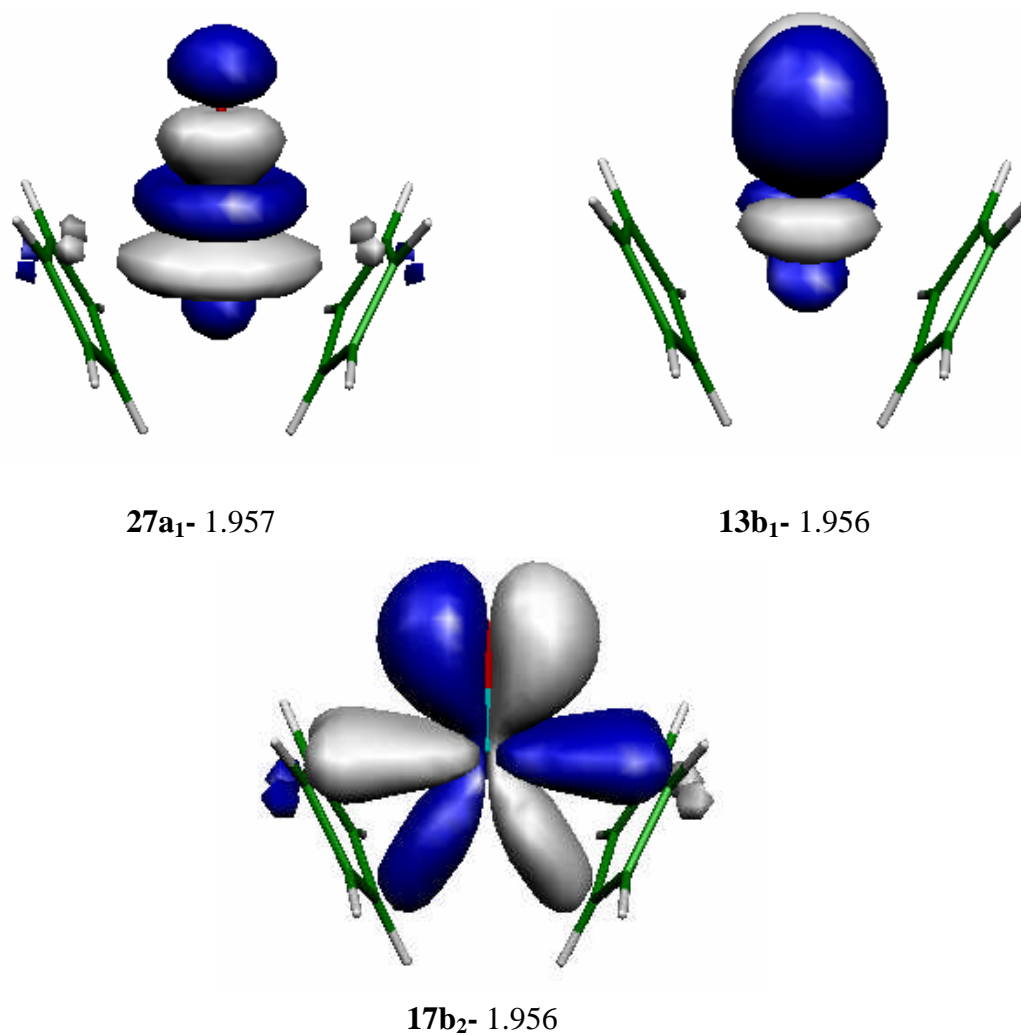


Figure 4.4- Natural orbitals 27a₁, 13b₁ and 17b₂ and their natural occupancies of CeCp₂O structure

4.3.2.2 CeCp₂NH

The ground state of CeCp₂NH was found to be ¹A₁. The natural occupancies from the (14,14) CASPT2 calculation in C_{2v} symmetry, are shown below, table 4.5. This shows that there is very little multiconfigurational character to the ground state wavefunction of CeCp₂NH as there is very little deviation in the natural occupancies from integer values.

Orbital Symmetry	Orbital Number	Natural Occupancy	Orbital Symmetry	Orbital Number	Natural Occupancy
a₁	26	1.975	b₂	17	1.962
	27	1.965		18	1.949
	28	0.025		19	0.050
b₁	13	1.949		20	0.015
	14	1.983	a₂	9	1.981
	15	0.041		10	0.007
	16	0.056		11	0.044

Table 4.5- Natural occupancies of natural orbitals of CeCp₂NH from CASPT2(14,14) C_{2v} calculation

Those orbitals with significant nitrogen character are shown in table 4.6, along with their orbital breakdown in terms of atomic character.

Natural Orbital	26a ₁	13b ₁	18b ₂
Ce m	9.47	2.31	0.47
Ce d	11.22	18.01	8.64
Ce f	2.35	5.16	9.47
N π	-	72.11	63.95
N_N	68.55	0.02	0.02
C_C	0.78	1.16	17.08
H_H	7.61	0.23	0.37

Table 4.6- Percentage atomic orbital character of natural orbitals of CeCp₂NH with significant N-character

Table 4.6 shows three orbitals involved in Ce-N bonding. This concurs with the results from the DFT study of 2005¹⁵, suggesting the presence of both a σ and two π interactions. Both works indicate that the bonds have largely N character with approximately 20% Ce character, arising from both d and f contributions.

The total n_f determined from all the active space orbitals is 0.400 ± 0.005 , this is very close to that obtained for the oxo molecule and again, does not indicate a Ce 4f¹ state and is thus consistent with the formal 4+ oxidation state of the metal.

Those orbitals which are involved in the Ce-N bond, from table 4.6, are shown along with their natural occupancies in figure 4.5. These show clearly one σ bond and two π bonds, one of which includes some bonding to the cyclopentadienyl rings.

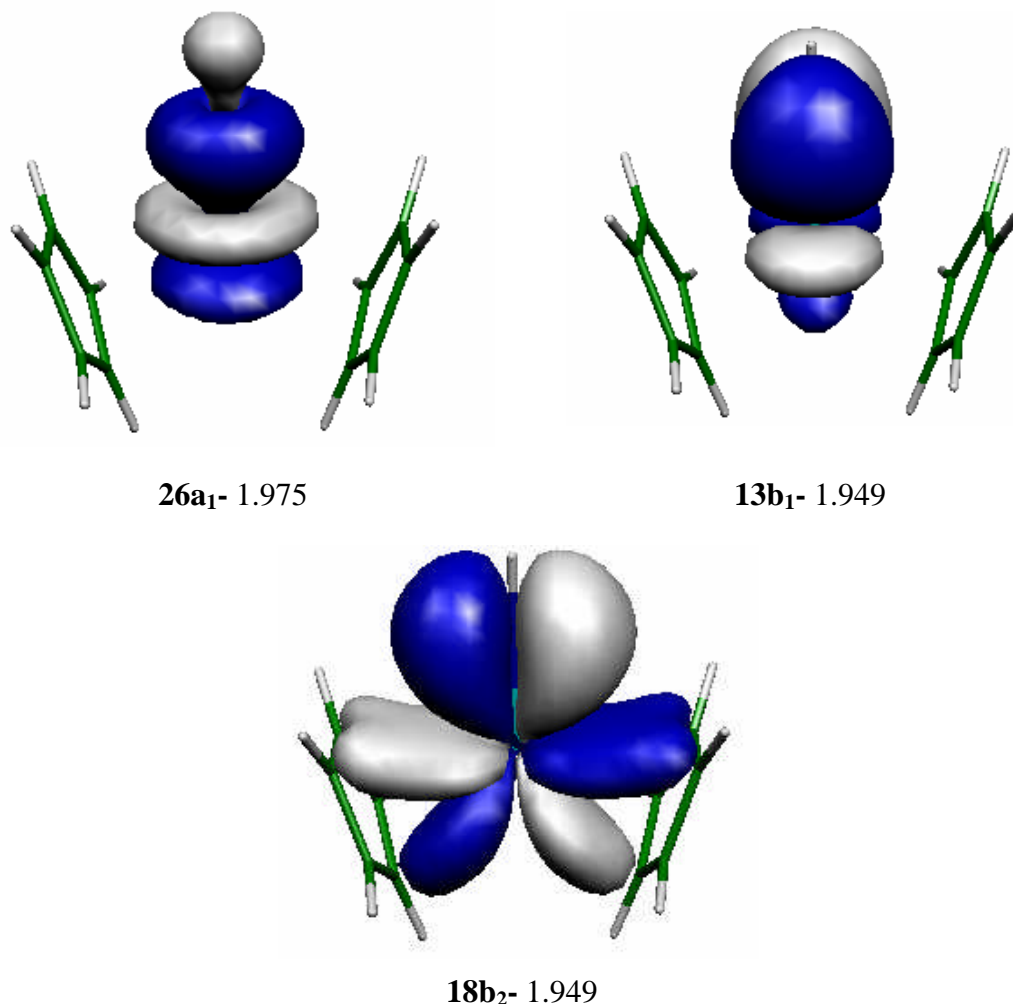


Figure 4.5- Natural orbitals 26a₁, 13b₁ and 18b₂ and their natural occupancies of CeCp₂NH structure

4.3.2.3 CeCp₂CH₂

In order for a calculation with the same size active space to be used for CeCp₂CH₂ as for CeCp₂O and CeCp₂NH, (14,14) CASPT2 calculations were carried out at the two C_s geometries, with methylene hydrogens parallel and perpendicular to the Cp rings. As was shown in figure 4.3, the parallel structure is a transition state. The perpendicular structure was shown to be lower in energy at the PBE level, however, this may, in part be due to the fact that the C_s constraint places the parallel structure at a transition state. The long Ce-C(methylene) bond for the perpendicular structure (relative to the previous

B3LYP study, with no symmetry constraints) indicates that this structure is not the optimum. Also, the CASPT2 calculations place the parallel structure 0.094 eV lower in energy than the perpendicular structure. Therefore results for both are presented here.

4.3.2.3.1 Perpendicular Methylene Results

The ground state of perpendicular CeCp_2CH_2 was found to be $^1\text{A}'$. Natural occupancies of the (14,14) CASPT2 calculation in C_s symmetry, are shown below, table 4.7. This shows that there is very little multiconfigurational character to the ground state wavefunction as there is very little deviation in the natural occupancies from integer values.

Orbital Symmetry	Orbital Number	Natural Occupancy	Orbital Symmetry	Orbital Number	Natural Occupancy
a'	42	1.979	a''	21	1.965
	43	1.959		22	1.961
	44	1.954		23	1.920
	45	1.947		24	0.048
	46	0.007		25	0.078
	47	0.047		26	0.050
	48	0.031			
	49	0.052			

Table 4.7- Natural occupancies of natural orbitals of CeCp_2CH_2 with methylene hydrogens perpendicular to cyclopentadienyl rings from CASPT2(14,14) C_s calculation

Those orbitals with significant methylene carbon character are shown in table 4.7, along with their orbital breakdown in terms of atomic character.

Natural Orbital	44a'	45a'	23a''
Ce <i>m</i>	6.61	3.50	2.34
Ce <i>d</i>	4.23	7.57	28.26
Ce <i>f</i>	1.03	7.19	10.25
Cmethylene π	0.05	0.02	56.90
Cmethylene σ	14.94	32.56	-
C <i>c</i>	71.33	44.40	1.92
H <i>H</i>	1.80	4.78	0.35

Table 4.8- Percentage atomic orbital character of natural orbitals of CeCp₂CH₂ perpendicular with significant C-character

Table 4.8 shows three orbitals involved in Ce-C bonding. These do not corroborate the results from the DFT study of 2005¹⁵ for CeCp₂CH⁻ (this study did not analyse the molecular orbitals of the CeCp₂CH₂ system) as there appear to be two σ and just one π interactions. There is also less Ce f-character in the π interaction in this calculation than in the DFT study, but comparable d-character.

Those orbitals which are involved in the Ce-C(methylene) bond, from table 4.8, are shown, along with their natural occupancies in figure 4.6.

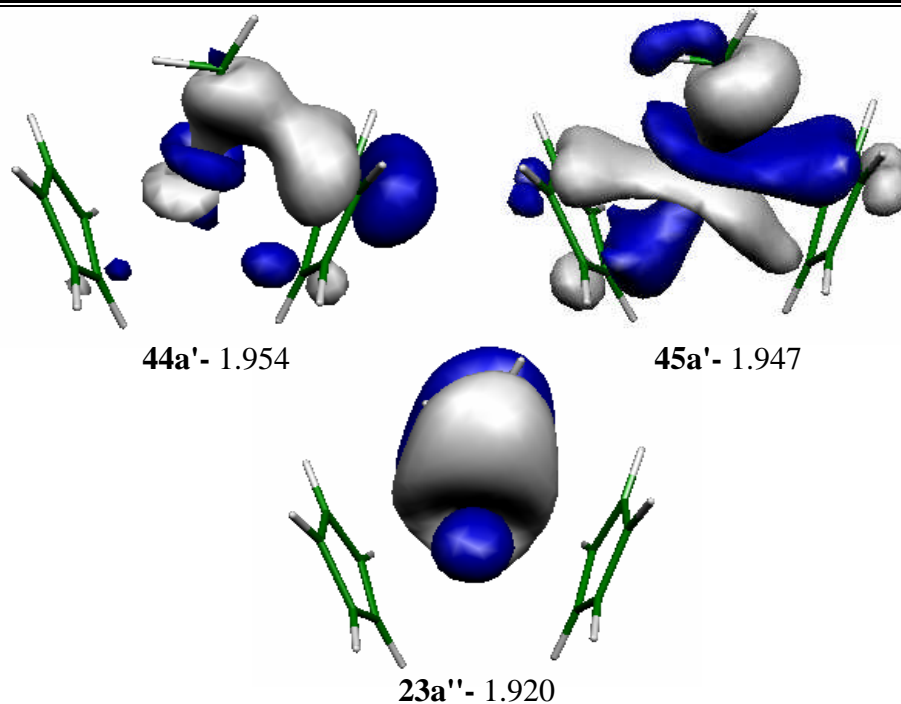


Figure 4.6- Natural orbitals 44 and 45 a' and 23a'' and their natural occupancies of perpendicular CeCp_2CH_2 structure

Orbital 23a'' is clearly a π bond between the Ce and methylene group, with little Cp ring involvement. Orbitals 44 and 45a' both show much more σ than π character.

4.3.2.3.2 Parallel Methylene Results

The ground state of parallel CeCp_2CH_2 was found to be $^1A'$. Natural occupancies of the (14,14) CASPT2 calculation in C_s symmetry, are shown below, table 4.9. This shows that there is significant multiconfigurational character to the ground state wavefunction as there is a large deviation in the natural occupancies from integer values in orbitals 27 and 28a''.

Orbital Symmetry	Orbital Number	Natural Occupancy	Orbital Symmetry	Orbital Number	Natural Occupancy
a'	38	1.981	a''	25	1.962
	39	1.972		26	1.953
	40	1.961		27	1.495
	41	1.953		28	0.505
	42	0.026		29	0.034
	43	0.020		30	0.052
	44	0.051			
	45	0.035			

Table 4.9- Natural occupancies of natural orbitals of CeCp₂CH₂ with methylene hydrogens perpendicular to cyclopentadienyl rings from CASPT2(14,14) C_s calculation

Those orbitals with significant methylene carbon character are shown in table 4.10, along with their orbital breakdown in terms of atomic character.

Natural Orbital	38a'	39a'	27a''	28a''
Ce <i>m</i>	10.31	4.68	0.57	0.63
Ce <i>d</i>	5.96	10.92	3.56	0.06
Ce <i>f</i>	0.61	1.17	51.18	52.55
Cmethylene π	8.12	21.63	42.38	43.94
Cmethylene σ	50.25	35.87	-	-
C <i>C</i>	0.42	5.60	2.10	2.75
H <i>H</i>	24.24	25.18	0.22	0.65

Table 4.10- Percentage atomic orbital character of natural orbitals of CeCp₂CH₂ parallel with significant C-character

Table 4.10 shows four orbitals involved in Ce-C bonding. However, in agreement with the results from the DFT study of 2005¹⁵ for CeCp₂CH⁻, these indicate the presence of both a σ and two π interactions. Orbital 28 a'' is a π -antibonding orbital. The DFT study showed approximately 30% Ce f-character to one of the π interactions, whilst the proportion here, in orbitals 27 and 28 a'', is somewhat larger.

The total n_f determined from all active space orbitals is 1.10 ± 0.006 , indicating a Ce $4f^1$ state, which is unexpected given the formal 4+ oxidation state of the metal.

Those orbitals which are involved in the Ce-C(methylene) bond are shown below, along with their natural occupancies, figure 4.7.

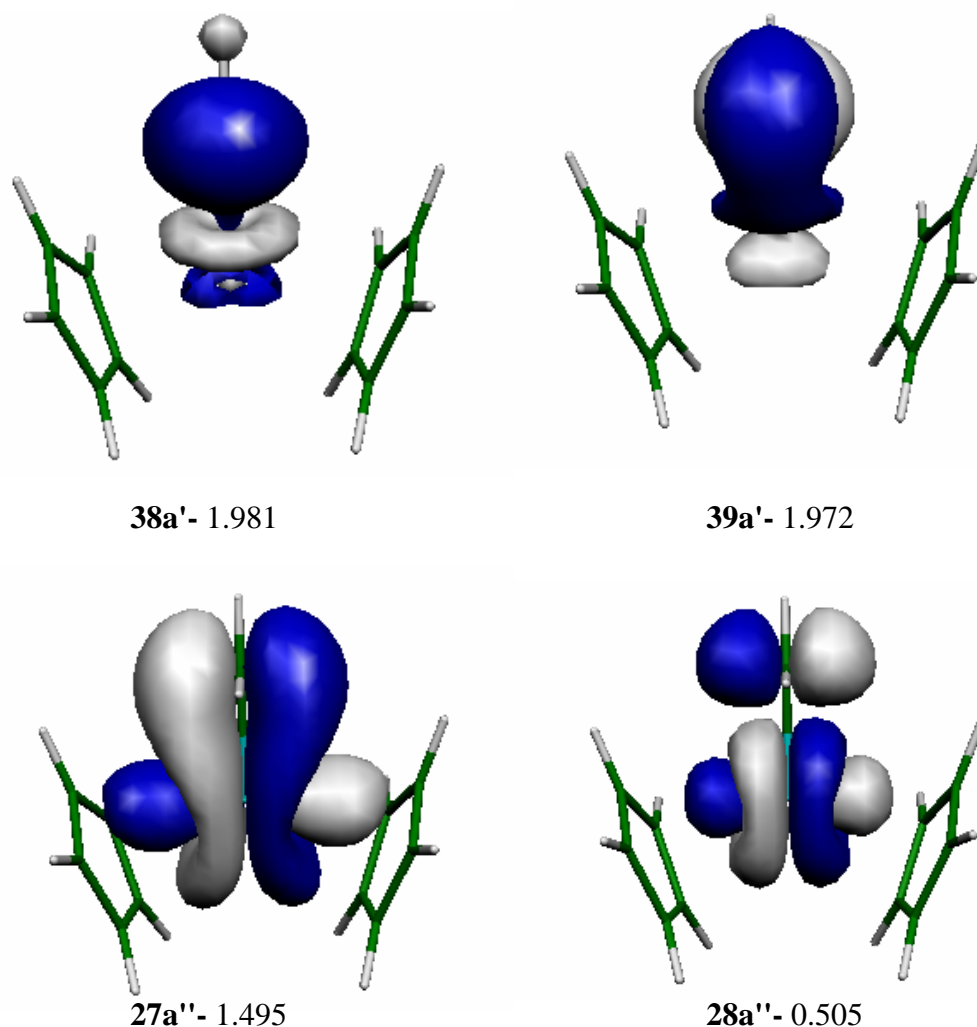


Figure 4.7- Natural orbitals 38 and 39 a' and 27 and 28 a'' and their natural occupancies of parallel CeCp₂CH₂ structure

These orbital pictures clearly show one σ bond and two π bonds, one involving a bonding and correlating orbital. The pictures of orbitals 27 and 28a'' also show that the parallel alignment of the methylene group allows overlap of the Ce f_π orbital with the methylene C_π orbital. The other two lobes of the f orbital are also aligned with the Cp rings. Conversely, in the case of the perpendicular methylene, there will be no alignment with the π -bonding f-orbital and the Cp rings.

The most pronounced differences between the perpendicular methylene structure and the parallel structure are:

- a) The much shorter Ce-C(methylene) distance in the parallel structure.
- b) The multiconfigurational character to the wavefunction of the parallel methylene structure.
- c) The presence of one σ and two π bonds in the parallel case and two σ -type and only one π bond in the perpendicular methylene case.

Another interesting point to note is the very large value of n_f (1.10 ± 0.006) in the parallel methylene case, arising from orbitals 27 and 28 a", in contrast to $n_f = 0.44 \pm 0.009$ in the perpendicular methylene case.

4.3.2.3.3 Twisted Methylene Results

The C_s constrained geometries calculations show very different results for the perpendicular and parallel structures. Therefore a no-symmetry CASPT2 calculation was performed on the 330° twisted methylene structure, which was shown to be a minimum in the PBE scan (figure 4.3). The lack of symmetry in this calculation makes a (14,14) active space an extremely large calculation, as described in **1.2.1.5.2** therefore a smaller active space was used, (6,6). There is a gap in energy of 0.36 eV between the SCF HOMO-2 and HOMO-3 orbitals of the molecule and therefore, this smaller active space does not seem unreasonable, and should include all of the bonding Ce-C(methylene) bonding orbitals identified in the C_s structure. The CASPT2 energy obtained from this calculation is 0.23 eV lower than the parallel C_s structure and 0.33 eV lower than the perpendicular C_s structure. Table 4.11 shows the natural occupancies of the active space orbitals.

Orbital Number	Natural Occupancy
66	1.482
67	1.972
68	1.981
69	0.027
70	0.021
71	0.518

Table 4.11- Natural occupancies of CeCp₂CH₂, twisted methylene active space orbitals

Those orbitals with significant methylene carbon character are shown in table 4.12, along with their orbital breakdown in terms of atomic character.

Natural Orbital	66	67	68	71
Ce <i>m</i>	0.67	3.91	10.40	0.97
Ce <i>d</i>	3.44	9.43	6.01	0.39
Ce <i>f</i>	50.42	0.96	0.61	51.53
Cmethylene π	42.65	25.11	4.85	44.01
Cmethylene <i>Cmeth</i>	0.47	25.41	53.72	0.58
C <i>c</i>	1.82	0.51	0.45	2.12
H <i>H</i>	0.54	3.45	23.98	0.39

Table 4.12- Percentage atomic orbital character of natural orbitals of CeCp₂CH₂ twisted methylene with significant C(methylene) character

Figure 4.8 shows the natural orbitals with significant natural occupancies (>0.2) along with their natural occupancies.

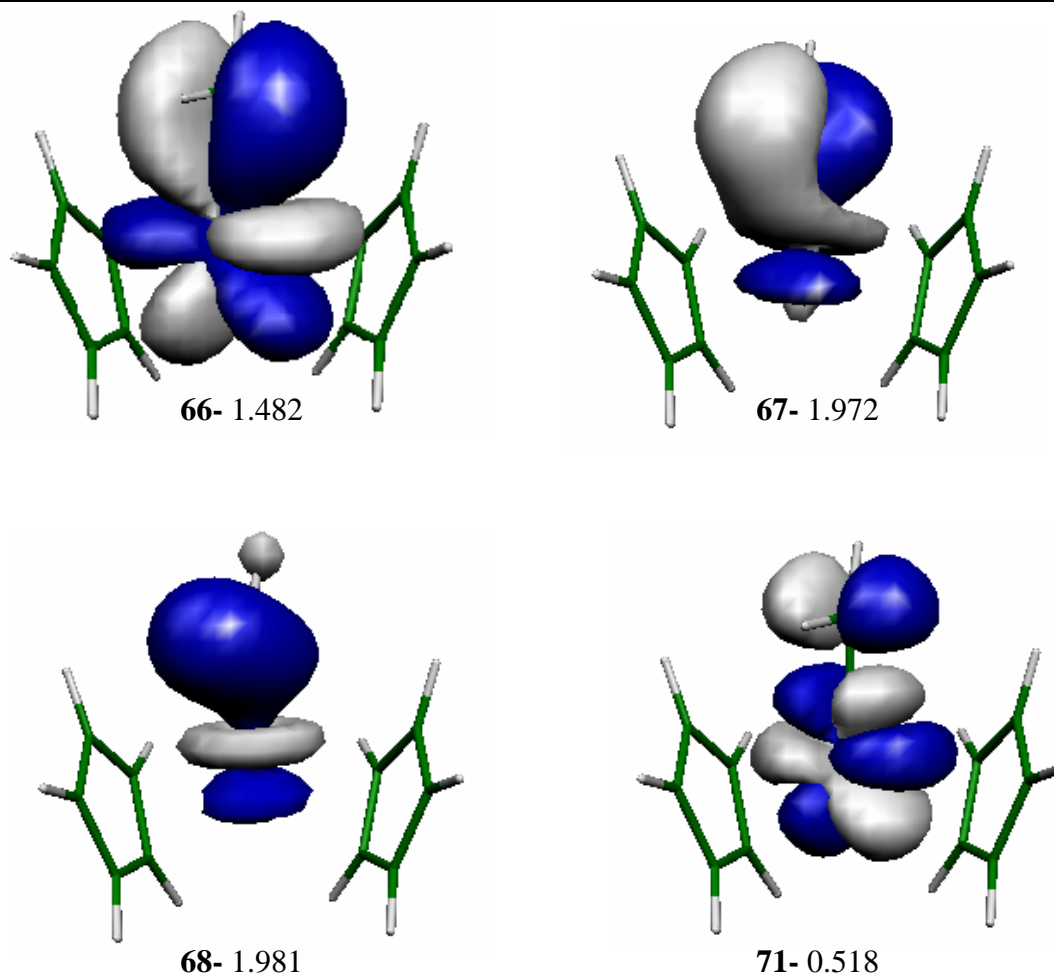


Figure 4.8- Natural orbitals of nosymmetry 330° twist methylene CeCp_2CH_2 with their natural occupancies

Table 4.11 shows that the twisted geometry of CeCp_2CH_2 has a multiconfigurational wavefunction. The natural orbitals, their natural occupancies and the atomic components of these orbitals, table 4.12 are very similar to that obtained for the C_s parallel geometry. Three bonding orbitals are found, one σ , one π and one part σ , part π orbital. The π -bonding orbital has a natural occupancy deviating significantly from an integer value with a correlating (antibonding) orbital. This orbital has largely Ce 4f and C(methylene) π -character, as shown in table 4.12. Similar to the parallel C_s CeCp_2CH_2 case, the n_f value is 1.05 ± 0.005 .

4.3.2.3.4 Summary

The results for the three CeCp_2X molecules show that there are three bonds between the Ce and heteroatom, one σ and two π bond. For $\text{X}=\text{O}$, NH there is very little Ce character to these bonds, and this component is largely Ce d. However, for the $\text{X}=\text{CH}_2$ molecule, one of the π bonds is found to have a large Ce f component. The electronic structure of this molecule should be determined with a multiconfigurational method, the natural occupancies of two of the active space orbitals indicating that a single determinant method will not model the electronic structure accurately. The n_f for Ce in the CeCp_2CH_2 molecule is ~ 1 , indicating that there is significant ligand to metal charge transfer via the Ce 4f orbital interacting with the methylene group in a π fashion.

The calculations performed suggest a Ce oxidation state in the oxo and imido molecules is very close to the formal 4+ oxidation state, whilst in the methylene molecule it is much closer to 3+. The delocalised nature of the Ce 4f electron density is very similar to that observed in both cerocene and CeCp_3^+ , chapters 2 and 3.

It is now interesting to observe whether similar changes in metal involvement in the M-X bond occur when moving from the more electronegative O to CH_2 groups in the transition metal and actinide analogues, Hf and Th.

4.3.2.4 HfCp₂O

The ground state of HfCp_2O was found to be $^1\text{A}_1$. The natural occupancies of the active space orbitals for HfCp_2O in C_{2v} symmetry are shown below, table 4.13.

Orbital Symmetry	Orbital Number	Natural Occupancy	Orbital Symmetry	Orbital Number	Natural Occupancy
a₁	28	1.968	b₂	15	1.950
	29	1.966		16	1.985
	30	0.034		17	0.037
b₁	19	1.966		28	0.060
	20	1.954	a₂	10	1.980
	21	0.013		11	0.008
	22	0.040		12	0.042

Table 4.13- Natural occupancies of active space orbitals for HfCp₂O

There is very little multiconfigurational character to the ground state wavefunction of HfCp₂O. The atomic breakdown for the orbitals with significant O character are shown below, table 4.14.

Natural Orbital	28a ₁	29a ₁	19b ₁	20b ₁	15b ₂
Hf <i>m</i>	1.37	9.21	3.81	0.10	2.00
Hf <i>d</i>	16.06	4.78	9.92	2.51	15.28
Hf <i>f</i>	0.10	0.10	0.05	0.67	0.36
O <i>π</i>	-	-	45.98	42.84	81.33
O <i>o</i>	31.81	55.14	0.05	0.00	0.10
C <i>c</i>	50.51	30.67	40.03	53.58	0.72
H <i>H</i>	0.20	0.10	0.15	0.20	0.26

Table 4.14- Percentage atomic orbital character of natural orbitals with significant O character for HfCp₂O

It can be seen that there appear to be five orbitals involved in the Hf-O bond. Two σ -type bonds and three π -type bonds, although 20b₁ has very little Hf character, and might better be viewed as bonds between O and the cyclopentadienyl rings. The DFT study of Clark et al.¹⁵ found just three bonds, as for CeCp₂O. The Hf contribution to these bonds was also somewhat higher than found here, 20-28% rather than the 3-18% found here.

4.3.2.5 HfCp₂CH₂

The C_s optimised geometry with the methylene hydrogens parallel to the cyclopentadienyl rings was used, as this was shown to be the most reasonable structure in the CeCp₂CH₂ case. The C_s structure for Hf is likely to be even less of a deviation from the nosymmetry minimum, the agostic interaction in Hf being expected to be less than that for Ce⁹² due to less accessible valence d orbitals, as a result of the lanthanide contraction.

The ground state of HfCp₂CH₂ with parallel methylene hydrogens was found to be ¹A'. The natural occupancies for the active space orbitals are shown below, table 4.15.

Orbital Symmetry	Orbital Number	Natural Occupancy	Orbital Symmetry	Orbital Number	Natural Occupancy
a'	42	1.980	a''	28	1.963
	43	1.966		29	1.956
	44	1.955		30	1.934
	45	1.962		31	0.058
	46	0.022		32	0.031
	47	0.037		33	0.052
	48	0.054			
	49	0.031			

Table 4.15- Natural occupancies of active space orbitals of parallel HfCp₂CH₂

There is very little multiconfigurational character to the ground state wavefunction of HfCp₂CH₂. The atomic breakdown for the orbitals with significant methylene C character are shown below, table 4.16.

Natural Orbital	42a'	43a'	29a''	30a''
Hf <i>m</i>	9.44	10.78	0.51	1.34
Hf <i>d</i>	6.62	12.00	28.99	6.51
Hf <i>f</i>	0.10	0.20	0.05	0.47
Cmethylene π	12.42	10.78	30.57	26.58
Cmethylene σ	31.31	30.56	-	-
C <i>C</i>	1.01	15.82	39.47	64.79
H <i>H</i>	39.14	19.79	0.46	0.31

Table 4.16- Percentage atomic orbital character of natural orbitals with significant methylene C character for parallel methylene HfCp₂CH₂

In this case there appear to be two largely σ bonds between Hf and the methylene group and two largely π bonds. In both σ bonds there is a total metal character of approximately 15-20% but this involves the s and p orbitals as well as the d orbitals. The 29a'' π bond, on the other hand, is ~30% Hf d character. The 30a'' π bond has close to 6% Hf d character, indicating a much more polarised π bond.

The increase in metal character in the bonding orbitals with the X group observed moving from X=O to X=CH₂ for M=Ce is not repeated for M=Hf. Although there is a slight increase in the metal character to these bonds, it is far less pronounced than for the corresponding Ce systems.

4.3.2.6 ThCp₂O

The ground state of ThCp₂O was found to be ¹A₁. The natural occupancies of the active space orbitals for ThCp₂O in C_{2v} symmetry are shown below, table 4.17.

Orbital Symmetry	Orbital Number	Natural Occupancy	Orbital Symmetry	Orbital Number	Natural Occupancy
a₁	32	1.972	b₂	21	1.963
	33	1.964		22	1.959
	34	0.029		23	0.014
b₁	17	1.960		24	0.038
	18	1.983	a₂	11	1.982
	19	0.038		12	0.005
	20	0.049		13	0.044

Table 4.17- Natural occupancies of active space orbitals for ThCp₂O

There is very little multiconfigurational character to the ground state wavefunction of ThCp₂O. The atomic breakdown of the orbitals with significant O character are shown below, table 4.18.

Natural Orbital	32a ₁	17b ₁	21b ₂
Th <i>m</i>	7.00	2.04	4.33
Th <i>d</i>	10.95	8.42	7.13
Th <i>f</i>	3.65	3.52	2.04
O <i>π</i>	-	84.34	68.62
O <i>o</i>	68.81	0.10	0.05
C <i>c</i>	9.53	1.53	17.73
H <i>H</i>	0.05	0.10	0.05

Table 4.18- Percentage atomic orbital character of natural orbitals with significant O character for ThCp₂O

It can be seen that there are three orbitals involved in the Th-O bond, one σ -type bond and two π -type bonds. These bonds are all highly polarised towards the O, with 70-80% O character and only 15-20% Th character, in comparison with 10-25% metal character for CeCp₂O. This is not unsurprising as the valence orbitals of Th would be expected to be more diffuse and hence more polarisable by an electronegative ligand such as O than their lanthanide counterpart, Ce.

4.3.2.7 ThCp₂CH₂

The C_s optimised geometry with the methylene hydrogens parallel to the cyclopentadienyl rings was used, as this was shown to be the most reasonable structure in the CeCp₂CH₂ case. The C_s structure for Th is likely to be even less of a deviation from the nosymmetry minimum, the agostic interaction in Th having been found to be less than that for Ce⁹².

The ground state of ThCp₂CH₂ with parallel methylene hydrogens was found to be ¹A'. The natural occupancies for the active space orbitals are shown below, table 4.19.

Orbital Symmetry	Orbital Number	Natural Occupancy	Orbital Symmetry	Orbital Number	Natural Occupancy
a'	48	1.980	a''	31	1.960
	49	1.969		32	1.963
	50	1.961		33	1.949
	51	1.954		34	0.031
	52	0.035		35	0.045
	53	0.052		36	0.051
	54	0.021			
	55	0.030			

Table 4.19- Natural occupancies of active space orbitals of parallel ThCp₂CH₂

There is very little multiconfigurational character to the ground state wavefunction of ThCp₂CH₂. The atomic breakdown for the orbitals with significant methylene C character are shown below, table 4.20.

Natural Orbital	48a'	49a'
Th <i>m</i>	9.70	3.35
Th <i>d</i>	8.08	18.74
Th <i>f</i>	1.41	7.11
Cmethylene π	7.78	19.55
Cmethylene σ	36.72	25.39
C <i>c</i>	0.66	2.95
H <i>H</i>	35.61	22.96

Figure 4.20- Percentage atomic orbital character of natural orbitals with significant methylene C character for parallel methylene ThCp₂CH₂

In this case there appear to be two largely σ bonds between Th and the methylene group, one with rather more methylene π character (49a"). There is more Th character in the latter bond, and this is comprised of both d and f character. However, the large ligand to metal charge transfer observed for CeCp₂CH₂ is absent.

There is very little change in the metal character to the Th-X bonds when X is changed from the very electronegative oxo group to the much less electron-withdrawing methylene group.

4.4 Conclusions

The multiconfigurational calculations performed on the series of MCp₂X species can offer illumination on both some computational and, possibly, synthetic questions. Let us first consider the computational points.

In common with other multiconfigurational^{15, 77, 92} and single determinant studies, the geometry of the Cp₂M-CH₂ bond was found to involve an agostic interaction and therefore to be of C₁ symmetry. This is also consistent with experimental and computational data on unsaturated d-block transition metals, as noted in reference¹⁵ and arises as a result of empty and low-energy d-orbitals on the metal⁷⁷. For the molecules

previously studied using B3LYP¹⁵ very similar M-X bond lengths were determined using the PBE functional.

The ground state wavefunction of all the molecules studied, apart from CeCp₂CH₂, was found to be largely single configurational, and thus DFT can reasonably be used to study these. The wavefunction of CeCp₂CH₂, by contrast, was found to be highly multiconfigurational and is therefore, like the other two formally Ce(IV) systems studied in chapters 2 and 3, not a suitable target for a DFT study.

A large ligand to metal charge transfer was found for the CeCp₂CH₂ molecule, reducing its formal 4+ oxidation state to closer to 3+. However, similar to both cerocene and CeCp₃, this 4f charge density was found to be delocalised and thus the formal oxidation state Ce(IV) remains a reasonable one.

This has implications in terms of potential synthetic targets. It appears that a low electronegativity ligand such as methylene, can result in significant ligand to metal charge transfer which may stabilise the high formal oxidation state of the cerium. However, the twisted structure found (due to an agostic interaction) provides guidance for the necessary characteristics of a stable synthetic molecule. Often a lanthanide centre will be stabilised using highly substituted ligands^{93, 94}. This may not be the best approach for this target or at least care should be taken to avoid large steric hindrance between the cyclopentadienyl rings and the methylene group as this could prevent the optimum geometry for ligand to metal charge transfer being obtained. The potential energy surface for the twisting of the methylene group has been shown to have several minima, fig. 4.3 and the perpendicular methylene group, which does not allow significant ligand to metal charge transfer is a minimum at long Ce-C(methylene) distances. Therefore sterically bulky cyclopentadienyl rings may prevent the stabilising ligand to metal charge transfer from occurring.

Hafnium and thorium, in contrast to cerium, show only a very slight increase in the metal character of the M-X bonds in moving from X=O to X=CH₂. The large ligand to metal charge transfer observed for CeCp₂CH₂, stabilising the high Ce oxidation state, was absent for both the Hf and Th analogues.

5. General Conclusions

The detailed conclusions from each of the results chapters are included within each, however, the systems studied are closely linked and the aim of this section is thus to draw together some of the linking themes identified.

Five formally Ce(IV) molecules have been studied, those with electron-rich, carbon-based ligands have been found to involve significant ligand to metal charge transfer to the 4f orbitals. This results in values of n_f for these molecules of close to 1. However, this electron density is highly delocalised. It is therefore suggested that the formal oxidation state label of Ce(IV) is still a reasonable one for these systems but that this high oxidation state is stabilised by the observed ligand to metal charge transfer.

Some interesting aspects of the behaviour of these molecules have been discussed with reference to this large, delocalised 4f density, namely the magnetic properties of cerocene, the photoelectron spectrum of CeCp₃ and the possibility of synthesising CeCp₂CH₂, or a substituted analogue. In particular it is interesting to note that different experimental methods for determining oxidation state may yield different results for cerium in these systems depending on whether they determine oxidation state in terms of oxidation/reduction potential of the metal or electron density around the metal. This goes some way to explain the previous experimental controversy surrounding the determination of the oxidation state of the metal in cerocene where cyclic voltammetry (measuring the oxidation potential of the metal) found Ce(IV) whilst XANES (a measure of electron density around the metal) found Ce(III).

Computationally, it has been found that the wavefunctions of these systems are highly multiconfigurational and it is therefore suggested that DFT, whilst describing geometries well, cannot properly describe the bonding in these molecules. Hence, a reasonable approach would be to avoid DFT, or other single configurational methods when investigating Ce(IV) systems with electron-rich ligands. Importantly, this work also adds to the body of knowledge which shows that analysis of the multiconfigurational wavefunction in terms of configurational weights is not stable to

state average size and that the more reliable natural orbitals and their occupancies is therefore a better choice.

6. Bibliography

1. N.N.Greenwood; A.Earnshaw, *Chemistry of the Elements*. Pergamon Press: Oxford, 1990; p 1424-1425.
2. W.G.Richards; H.P.Trivedi; D.L.Cooper, *Spin-orbit coupling in molecules*. Clarendon Press: Oxford, 1981; p 2.
3. N.Kaltsyannis; P.Scott, *The f elements*. Oxford University Press: Oxford, 1999; p 24.
4. B.T.Kilbourn, *Cerium: A guide to its role in Chemical Technology*. Molycorp: New York, 1992.
5. A.Greco; S.Cesca; G.Bertolini, *Journal of Organometallic Chemistry* **1976**, 113, 321.
6. A.Streitwieser; S.A.Kinsley; J.T.Rigsbee; I.L.Fragala; E.Ciliberto; N.Rösch, *Journal of the American Chemical Society* **1985**, 107, 7786-7788.
7. A.Ashley; G.Balazs; A.Cowley; J.Green; C.H.Booth; D.O'Hare, *Chemical Communications* **2007**, 1515-1517.
8. M.Dolg; P.Fulde; W.Kuchle; C.S.Neumann; H.Stoll, *Journal of Chemical Physics* **1991**, 94, 3011-3017.
9. M.Dolg; P.Fulde; H.Stoll; H.Preuss; A.Chang; R.M.Pitzer, *Chemical Physics* **1995**, 195, 71-82.
10. N.M.Edelstein; P.G.Allen; J.J.Bucher; D.K.Shuh; C.D.Sofield; N.Kaltsyannis; G.H.Mauder; M.R.Russo; A.Sella, *Journal of the American Chemical Society* **1996**, 118, 13115-13116.
11. C.H.Booth; M.D.Walter; N.Daniel; W.W.Lukens; R.A.Andersen, *Physical Review Letters* **2005**, 95, 267202-267205.
12. M.Dolg; P.Fulde, *Chemistry a European Journal* **1998**, 4, 200-204.
13. A.Streitwieser; S.A.Kinsley; C.H.Jenson; J.T.Rigsbee, *Organometallics* **2004**, 23, 5169-5175.
14. M.Coreno; M.de Simone; J.C.Green; N.Kaltsyannis; N.Narband; A.Sella, *Chemical Physical Letters* **2006**, 432, 17-21.
15. D.L.Clark; J.C.Gordon; P.J.Hay; R.Poli, *Organometallics* **2005**, 24, 98.
16. E.Schrödinger, *Physical Review* **1926**, 28, 1049-1070.

-
17. F.Jensen, *Introduction to Computational Chemistry*. John Wiley & Sons Ltd.: Chichester, 2003; p 98.
 18. B.O.Roos; P.O.Widmark, Multiconfigurational Self-Consistent Theory. In *European Summerschool in Quantum Chemistry II*, Chemical Centre Printshop: Lund, 2007; p 306.
 19. B.O.Roos; K.Andersson, *Chemical Physical Letters* **1995**, 245, 215-223.
 20. F.Hausdorff, *Ber Verh Saechs Akad Wiss Leipzig* **1906**, 58, 19-48.
 21. T.J.Lee; P.R.Taylor, *International Journal of Quantum Chemistry* **1989**, S23, 199.
 22. P.Hohenberg; W.Kohn, *Physical Review* **1964**, 136, B864.
 23. E.Bright Wilson; A.Rich; N.Davidson, In *Structural Chemistry and Biology*, W.H. Freeman: San Francisco, 1968; p 753.
 24. L.H.Thomas, *Proceedings of the Cambridge Philosophical Society* **1927**, 5, 542-548.
 25. E.Fermi, *Rend.Accademia Nazionale dei Lincei* **1927**, 6, 602-607.
 26. W.Kohn; L.J.Sham, *Physical Review* **1965**, 140, A1133.
 27. T.A.Koopmans, *Physica* **1933**, 1, 104.
 28. J.F.Janak, *Physical Review B* **1978**, 18, 7165.
 29. J.Slater, *Advances in Quantum Chemistry* **1972**, 6, 1.
 30. J.P.Perdew; K.Schmidt In AIP Conference Proceedings, 2001, 2001; 2001; p 1.
 31. J.P.Perdew; Y.Wang, *Physical Review B* **1991**, 45, 13244.
 32. A.D.Becke, *Physical Review A* **1988**, 38, 3098.
 33. J.P.Perdew; K.Burke; M.Ernzerhof, *Physical Review Letters* **1996**, 77, 3865.
 34. J.P.Perdew; K.Burke; M.Ernzerhof, *Physical Review Letters* **1997**, 78, 1396.
 35. C.Lee; W.Yang; R.G.Parr, *Physical Review B* **1988**, 37, 785.
 36. J.Tao; J.P.Perdew; V.N.Staroverov; G.E.Scuseria, *Physical Review Letters* **2003**, 91, 146401.
 37. E.Runge; E.K.U.Gross, *Physical Review Letters* **1984**, 52, 997.
 38. P.O.Widmark, P-Ö.Malmqvist; B.O.Roos, *Theoretica Chimica Acta* **1990**, 77, 291.
 39. M.A.L.Marques; E.K.U.Gross, *Annual Review of Physical Chemistry* **2004**, 55, 427.
 40. P.R.T.Schipper; O.V.Gritsenko; S.J.A.van Gisbergen; E.J.Baerends, *Journal of Chemical Physics* **2000**, 112, 1344.

-
41. P.A.M.Dirac, *Proceedings of the Royal Society of London* **1928**, A117, 610.
 42. K.G.Dyall; K.Faegri, *Introduction to Relativistic Quantum Chemistry*. Oxford University Press: Oxford, 2007; p 277.
 43. L.L.Foldy; S.A.Wouthuysen, *Physical Review* **1950**, 78, 29.
 44. M.Douglas; N.M.Kroll, *Annals of Physics (New York)* **1974**, 82, 89.
 45. B.A.Hess, *Physical Review A* **1985**, 32, 756.
 46. B.A.Hess, *Physical Review A* **1986**, 33, 3742.
 47. C.Chang; N.Pelissier; M.Durand, *Physica Scripta* **1986**, 34, 294.
 48. S.Faas; J.G.Snijder; J.H.van Lenthe; E.van Lenthe; E.J.Baerends, *Chemical Physical Letters* **1995**, 246, 632.
 49. H.Stoll; B.Metz; M.Dolg, *Journal of Computational Chemistry* **2002**, 23, 767.
 50. P.O.Widmark, *European Summerschool in Quantum Chemistry, II*. Chemical Centre Printshop: Lund, 2007.
 51. M.J.Frisch; G.W.Trucks; H.B.Schlegel; G.E.Scuseria; M.A.Robb; J.R.Cheeseman; J.A.Montgomery, Jr.; T.Vreven; K.N.Kudin; J.C.Burant; J.M.Millam; S.S.Iyengar; J.Tomasi; V.Barone; B.Mennucci; M.Cossi; G.Scalmani; N.Regia; G.A.Petersson; H.Nakatsuji; M.Hada; M.Ehara; K.Toyota; R.Fukuda; J.Hasegawa; M.Ishida; T.Nakajima; T.Honda; O.Kitao; H.Nakai; M.Klene; X.Li; J.E.Knox; H.P.Hratchian; J.B.Cross; V.Bakken; C.Adamo; J.Jaramillo; R.Gomperts; R.E.Stratmann; O.Yazyev; A.J.Austin; R.Cammi; C.Pomelli; J.W.Ochterski; P.Y.Ayala; K.Morokuma; G.A.Voth; P.Salvador; J.J.Dannenberg; V.G.Zakrzewski; S.Dapprich; A.D.Daniels; M.C.Strain; O.Farkas; D.K.Malick; A.D.Rabuck; K.Raghavachari; J.B.Foresman; J.V.Ortiz; Q.Cui; A.G.Baboul; S.Clifford; J.Cioslowski; B.B.Stefanov; G.Liu; A.Liashenko; P.Piskorz; I.Komaromi; R.L.Martin; D.J.Fox; T.Keith; Laham, M. A. A.; C.Y.Peng; A.Nanyakkara; M.Challacombe; P.M.W.Gill; B.Johnson; W.Chen; M.W.Wong; C.Gonzalez; J.A.Pople *Gaussian 03, Revision D.01*, Gaussian, Inc.: Wallingford CT, 2004.
 52. G.Karlström; R.Lindh; P-Ö.Malmqvist; B.O.Roos; U.Ryde; V.Veryazov; P.O.Widmark; M.Cossi; B.Schimmelpfennig; P.Neogady; L.Seijo, *Computational Material Science* **2003**, 28, 222. The following persons have contributed to the development of the MOLCAS software: K. Andersson, M. Barysz, A. Bernhardsson, M. R. A. Blomberg, Y. Carissan, D. L. Cooper, M. Cossi, A. Devarajan, M. P. Fu Ischer, A. Gaenko, L. Gagliardi, C. de Graaf, B. A. Hess, D. Hagberg, G. Karlström, J. W. Krogh, R. Lindh, P.- A. Malmqvist, T. Nakajima, P. Neogady, J. Olsen, T. B. Pedersen, J. Raab, B. O. Roos, U. Ryde, B. Schimmelpfennig, M. Schütz, L. Seijo, L. Serrano-Andres, P. E. M. Siegbahn, J. Stalring, T. Thorsteinsson, V. Veryazov, P.-O. Widmark.

-
53. E.J.Baerends; J.Autschbach; A.B.rces In *SDF 2008.01, SCM, Theoretical Chemistry*, 2008.
 54. P-Ö.Malmqvist, *International Journal of Quantum Chemistry* **1986**, 30, 479.
 55. A. Kerridge; R.Coates; N.Kaltsoyannis, *Journal of Physical Chemistry A* **2009**, 113, 2896.
 56. J.C.Green, *Accounts of Chemical Research* **1994**, 27, 131-137.
 57. M.Newville, University of Chicago: Chicago, 2004.
 58. C-S.Neumann; P.Fulde, *Zeitschrifte für Physik B* **1989**, 74, 277-278.
 59. J.Kondo, *Progress in Theoretical Physics* **1964**, 32, 37-49.
 60. B.R.Bulka; S.Lipinski, *Physical Review B* **2003**, 67, 24404.
 61. S.N.Mishra; P.Taneja; P.Ayyub; A.A.Tulapurkar, *Physica B* **2002**, 312, 162-164.
 62. Y.Y.Chen; Y.D.Yao; C.R.Wang; W.H.Li; C.L.Chang; T.K.Lee; T.M.Hong; J.C.Ho; S.F.Pan, *Physical Review Letters* **2000**, 84, 4990.
 63. S-W.Han; C.H.Booth; E.D.Bauer; P.H.Huang; Y.Y.Chen; J.M.Lawrence, *Journal of Magnetism and Magnetic Materials* **2004**, 272-276.
 64. F.E.Senftle; A.N.Thorpe, *Physical Review* **1968**, 175, 1144-1146.
 65. T.H.Dunning, *Journal of Chemical Physics* **1989**, 90, 1007.
 66. X.Cao; M.Dolg, *Journal of Molecular Structure (Theochem)* **2002**, 581, 139.
 67. B.O.Roos, *Molcas 6.4*: 2003.
 68. B.O.Roos; R.Lindh; P-O.Malmqvist; V.Veryazov; P.O.Widmark, *Journal of Physical Chemistry A* **2005**, 108, 2851.
 69. E.Kurras, *Private Communication* In M.Dolg; P.Fulde; H.Stoll; H.Preuss; A.Chang; R.M.Pitzer, (*ref 9*) 1995.
 70. S.L.Altmann; P.Herzig, *Point-Group Theory Tables*. Oxford Science Publications: Oxford, 1994.
 71. W.J.Hunt; W.A.Goddard, *Chemical Physical Letters* **1969**, 3, 414.
 72. J. Dominikowska; M.Palusiak, *New Journal of Chemistry* **2010**, 34.
 73. B.O.Roos, *Theoretical Chemistry Accounts* **2000**, 103, 228-230.
 74. P.O.Löwdin, *Physical Review* **1955**, 97, 1474-1520.
 75. M.W.Schmidt; M.S.Gordon, *Annual RReview of Physical Chemistry* **1998**, 49, 233-266.
 76. S.F.Boys; P-O.Löwdin, In *Quantum Theory of Atoms, Molecules and the Solid State*, Academic: New York, 1966; pp 263-280.

-
77. B.O.Roos; P.Pyykko, *Chemistry a European Journal* **2010**, 16, 270.
78. Z.Azizi; B.O.Roos; V.Veryazov, *Physical Chemistry Chemical Physics* **2006**, 8, 2727.
79. M.D.Walter; R.Fandos; R.A.Andersen, *New Journal of Chemistry* **2006**, 30, 1065-1070.
80. C.H.Booth; M.D.Walter; D.Kazhdan; Y-J.Hu; W.W.Lukens; E.D.Bauer; L.Maron; O.Eisenstein; R.A.Andersen, *Journal of the American Chemical Society* **2009**, 131, 6480.
81. G.Balazs; F.G.N.Cloke; J.C.Green; R.M.Harkar; A.Harrison; P.B.Hitchcock; C.N.Jardine; R.Walton, *Organometallics* **2007**, 26, 3111-3119.
82. S.A.Kozimor; B.M.Bartlet; J.D.Rinehart; J.R.Long, *Journal of American Chemical Society* **2007**, 129, 10672.
83. N.Rösch; A.Streitweiser, *Journal of the American Chemical Society* **1983**, 105, 7237.
84. E.I.Solomon; L.Basumallik; P.Chen; P.Kennepohl, *Coordination Chemistry Reviews* **2006**, 249, 229.
85. J.H.D.Eland, *Photoelectron Spectroscopy*. Butterworth & Co: London, 1984; p 36.
86. A.Einstein, *Annals of Physics* **1905**, 17, 132.
87. B.Penc; A.Szytula; E.Wawrzyńska; A.Winiarski, *Physica Status Solidi (C)* **2006**, 3, 166.
88. R.Coates; M.Coreno; M.de Simone; J.C.Green; N.Kaltsyoyannis; A.Kerridge; N.Narband; A.Sella, *Dalton Transactions* **2009**, 30, 5943-5953.
89. S.D.Stults; R.A.Andersen; A.Zalkin, *Organometallics* **1990**, 9, 115.
90. P.B.Hitchcock; M.F.Lappert; L.Maron; A.V.Protchenko, *Angew. Chem. Int. Ed.* **2008**, 47, 1488.
91. Y.Bian; J.Jiang; Y.Tao; M.T.M.Choi; R.Li; A.C.H.Ng; P.Zhu; N.Pan; X.Sun; D.P.Arnold; Z-Y.Zhou; H-W.Li; T.C.W.Mak; D.K.P.Ng, *Journal of the American Chemical Society* **2003**, 125, 12257.
92. B.O.Roos; R.Lindh; H-G.Cho; L.Andrews, *Journal of Physical Chemistry A* **2007**, 111, 6420.
93. A.Sella; S.E.Brown; J.W.Steed; D.A.Tocher, *Inorganic Chemistry* **2007**, 46, 1856.

-
94. M.G.B.Drew; O.W.Howarth; C.J.Harding; N.Martin; J.Nelson, *Journal of Chemical Society, Chemical Communications* **1995**, 8, 903.